Titre: Title:	Optimal control of induction heating for semi-solid alloy forming
Auteur: Author:	Hui Jiang
Date:	2006
Type:	Mémoire ou thèse / Dissertation or Thesis
Référence: Citation:	Jiang, H. (2006). Optimal control of induction heating for semi-solid alloy forming [Thèse de doctorat, École Polytechnique de Montréal]. PolyPublie. https://publications.polymtl.ca/7769/

UNIVERSITÉ DE MONTRÉAL

OPTIMAL CONTROL OF INDUCTION HEATING FOR SEMI-SOLID ALLOY FORMING

HUI JIANG
DÉPARTEMENT DE GÉNIE MÉCANIQUE
ÉCOLE POLYTECHNIQUE DE MONTRÉAL

THÈSE PRÉSENTÉE EN VUE DE L'OBTENTION
DU DIPLÔME DE PHILOSOPHIAE DOCTOR
(GÉNIE MÉCANIQUE)
AOÛT 2006

Your file Votre référence
ISBN: 978-0-494-20831-1
Our file Notre référence
ISBN: 978-0-494-20831-1

UNIVERSITÉ DE MONTRÉAL

ÉCOLE POLYTECHNIQUE DE MONTRÉAL

Cette thèse intitulée:

OPTIMAL CONTROL OF INDUCTION HEATING FOR SEMI-SOLID ALLOY FORMING

présentée par: JIANG Hui

en vue de l'obtention du diplôme de: Philosophiae Doctor

a été dûment acceptée par le jury d'examen constitué de:

M. VASSEUR Patrick, Ph.D., président

M. NGUYEN The Hung, Ph.D., membre et directeur de recherche

M. PRUD'HOMME Michel, Ph.D., membre et codirecteur de recherche

M. VO Huu Duc, Ph.D., membre

M. LOONG Chee-Ang, Ph.D., membre

DÉDICACE

À ma femme Hui Liu

À mon père Prof. Ke-guo Jiang et ma mère Prof. Yi-ping Huang

À mes sœurs: Yun et Ning

À mon beau frère Prof. Yin Chen

À tous ceux qui me sont chers

ACKNOWLEDGEMENTS

First of all, I would like to express my greatest appreciation to my supervisor, Prof. The Hung Nguyen, for his wise guidance, encouragement and continuous support in all phase of my studies in the department of mechanical engineering of École Polytechnique in the past three years. I have learned so much about research work under his supervision. The opportunity to be one of his students is my forever pleasure.

I am very indebted to Prof. Michel Prud'homme, my co-supervisor, for his invaluable help in many ways. I am very pleased to have the opportunity to work under his supervision and consultant since the year of 2001 when I was a master student. His patience, humor and wisdom have been permanently branded on my memory.

I would also like to thanks my wife and my parents for their love, support and help. I can not imagine having enough courage and power to conquer various difficulties without their encouragements.

Special thanks go to Dr. S. Jasmin and Dr. H. Bougherara, who were Ph.D students of the department of engineering at École Polythechnique, and other friends for many useful discussions and suggestions.

Finally, I owe a debt of gratitude to the Ministère de l'Éducation du Québec for the exemption of the foreign student tuition fees for the first year, and to the Natural Sciences and Engineering Research Council of Canada for its financial support during my studies at École Polythechnique de Montréal.

RÉSUMÉ

La technique de *thixoforming* exige un chauffage de la matière de base jusqu'à l'état semi-solide en un temps relativement court avec une distribution uniforme de la température aussi bien qu'une fraction liquide optimale pour réaliser une microstructure globulaire satisfaisante. *L'effet de peau* du chauffage d'induction a comme conséquence de produire un profil exponentiel de distribution de densité de puissance (source de chaleur) le long du rayon des matériaux cylindriques et un profil de température inégal en profondeur. Notre objectif principal de cette étude est de chercher une stratégie optimale de chauffage d'induction en utilisant des méthodes d'optimisation pour obtenir la valeur exigée de la température sans gradient thermique dans les matériaux à la fin du traitement.

Ce problème d'optimisation est essentiellement un problème inverse de transfert thermique. Nous commençons notre étude à partir du problème inverse de détermination du flux dépendant du temps de la chaleur imposée à la frontière d'une plaque à partir de la distribution finale de la température au temps final en employant la méthode du gradient conjugué (CGM) et la méthode de la décomposition en valeurs singulières (SVD) séparément. La possibilité de récupérer le flux de frontière s'avère dépendre de toute la période du processus de chauffage/refroidissement. Le flux exact de la chaleur peut être reconstruit seulement dans une gamme non-dimensionnelle de temps [t_f-0.1, t_f], au-delà de laquelle nous obtenons seulement la moyenne. Cependant, en employant une méthode modifiée de gradient conjuguée, nous pouvons reconstruire le flux de chaleur à la frontière pendant des périodes plus grandes si sa valeur initiale est connue. Ce problème inverse est alors considéré dans un système bidimensionnel de convection naturelle dans le milieu poreux. Le flux de chaleur dépendant du temps et de la position peut être récupéré avec succès dans un intervalle non-dimensionnel de temps de l'ordre de 0.1 pour un nombre de Rayleigh allant jusqu'à 1000. La sensibilité de ce problème inverse est considérablement réduite à mesure que le temps total ou le nombre de

Rayleigh augmente. En outre, les solutions numériques obtenues à partir des données bruyantes de mesure sont également présentées pour montrer la puissance de régularisation de la méthode du gradient conjuguée.

Basé sur l'étude précédente, la méthode du gradient conjuguée en même temps que la méthode d'équation adjoint est implantée à un problème de contrôle optimal d'estimation de la source de chaleur (densité de puissance) pour réaliser une distribution uniforme de la température au temps final. Les modèles physiques et mathématiques tiennent compte des propriétés thermo-physiques dépendantes de la température et la formulation est donnée dans le système de coordonnées cylindriques. Des pertes de chaleur par convection et radiation sont également considérées. Le processus de changement de phase dans la région mixte est simulé en appliquant la méthode de chaleur massique apparent. Un tel modèle de système de chauffage d'induction s'avère raisonnable en comparant les solutions numériques aux données expérimentales. Les stratégies optimales de chauffage estimées par CGM régulier peuvent réaliser une distribution plus uniforme de la température au temps final que les méthodes empiriques obtenues à partir des expériences. Un CGM modifié peut être une meilleure approche pour résoudre ce problème de contrôle optimal parce que moins d'itérations sont nécessaires et une uniformité plus parfaite de la température pourrait être réalisée.

On pourrait conclure qu'un algorithme numérique général a été appliqué avec succès au contrôle de chauffage optimal de la formation d'alliage à l'état semi-solide. Cette méthode d'optimisation peut fournir une stratégie raisonnable de chauffage en quelques minutes pour n'importe quel genre de matériaux d'alliage en n'importe quelle taille à n'importe quelle fréquence de fonctionnement du chauffeur par induction.

ABSTRACT

Thixoforming technique requires reheating the feedstock to a semi-solid state in relatively short time with a uniform temperature distribution as well as an optimum liquid fraction to achieve a satisfactory globular microstructure. The skin effect of induction heating results in an exponential profile of power density (heat source) distribution along the radius of the cylindrical materials and an uneven temperature profile from surface to core. Our main objective of this study is to seek an optimal induction heating strategy by utilizing optimization methods to obtain the required temperature value without thermal gradient within the materials at the end of the process. This optimization problem is essentially an inverse heat transfer problem.

We start our study by investigating the inverse problem of determining the time-dependent heat flux imposed on the boundary of a solid slab from the final temperature distribution by using the conjugate gradient (CG) and the truncated singular value decomposition (TSVD) methods separately. The feasibility of recovering the boundary flux is found to depend on the total time of the heating/cooling process: the exact heat flux can be reconstructed only in a non-dimensional time range $[t_f\text{-}0.1, t_f]$, beyond which we obtain only the time-averaged values. However, by using a modified conjugate gradient method, we may reconstruct the boundary heat flux for much larger times if its initial value is known. This kind of inverse problem is then extended to a two-dimensional system of natural convection in porous medium. The time and position dependent heat flux can be recovered with success in a non-dimensional time interval of the order of 0.1 for a Rayleigh number up to 1000. The sensitivity of this inverse problem is significantly reduced as the final time or Rayleigh number increases. In addition, the numerical solutions obtained from the noisy measurement data are also presented to show the regularization power of the conjugate gradient method.

Based on the previous study, the conjugate gradient method in conjunction with the adjoint method is implanted into an optimal control problem of estimating the timewise-varying strength of heat source (power density) with exponential profile along the radius of a cylinder to achieve a uniform temperature distribution at the final time. The physical and mathematical models take into account the temperature-dependent thermo-physical properties and the formulation is performed in cylindrical coordinates system. Radiative and convective heat losses are also considered. The phase change process in the mushy region is simulated by applying the *apparent heat capacity method.* Such a model of induction heating system is proved to be reasonable by comparing the numerical solutions with experimental data. The optimal heating strategies estimated by regular CGM may achieve more uniform temperature distribution at the final time than the empirical methods obtained from experiments. A modified CGM may be a better approach to solve this optimal control problem because less iterations are needed and more perfect temperature uniformity could be achieved.

One might conclude that a general numerical algorithm has been successfully applied to the optimal heating control of semi-solid metal forming. This optimization method may provide a reasonable heating strategy in a few minutes for any kind of alloy materials of any size under any operating frequency of an induction heater.

CONDENSÉ EN FRANÇAIS

La fonte ou le forgeage d'un métal à l'état semi solide (SSM) est devenu une technique concurrentielle dans le domaine du traitement et de la fabrication d'alliages, particulièrement l'industrie automobile depuis la fin du 20ème siècle. Cette technique a été développée à l'origine par le professeur Merton C. Flemings au MIT dans les années 70. Elle est appliquée couramment en industrie de nos jours. Comparée aux méthodes conventionnelles comme le moulage sous pression qui présentent divers problèmes tels que les enflures, la ségrégation, et les défauts thermiques de la matrice etc., la technique de SSM travaille à partir des alliages de métaux à l'état partiellement liquide et solide. En augmentant la viscosité de l'écoulement et diminuer la température de traitement pendant le processus de la fonte, elle conduit à un écoulement laminaire et diminue le rétrécissement de solidification et donne donc des pièces de plus haute qualité en évitant l'occlusion de gaz. Ses avantages incluent également une excellente qualité de surface, le respect de tolérances sévères, un haut niveau de résistance et une basse porosité, une microstructure fine, l'économie d'énergie, etc.

Une des techniques de formation semi-solides, le *thixoforming*, exige habituellement de réchauffer la matière de base prétraitée en une structure fine et non-dendritique d'une fraction liquide de 40%~50% environ. Parce que les propriétés rhéologiques des alliages semi-solides sont très sensibles aux variations dans la partie liquide, le processus de chauffage doit être exactement contrôlé pour obtenir une distribution uniforme de la température dans le matériau et la fraction liquide requise. D'autre part, le processus de chauffage doit être relativement rapide afin de préserver la microstructure globulaire initiale. Autrement, les alliages semi-solides ne montreront pas de comportements thixotropiques sous le cisaillement et ne rempliraient pas ainsi la cavité du moule correctement.

De nos jours, le chauffage par induction est la méthode la plus utilisée dans les applications commerciales de production, particulièrement pour traiter les métaux semi

solides, parce que c'est une méthode rapide, non intrusive, propre, et la puissance requise peut être contrôlée facilement avec précision Les composants principales d'un système de chauffage par induction incluent une source de courant alternatif, les bobines d'induction, et le matériau à chauffer. L'alimentation envoie un courant alternatif dans les bobines, produisant un champ magnétique. Quand le matériau d'alliage est placé dans l'enroulement, le champ magnétique induit un courant de circulation dans l'objet. Selon la loi de Joule, soit $Q = I^2R$, le courant peut ainsi générer de la chaleur sans contact physique entre l'enroulement et le métal.

Le chauffage par induction a comme inconvénient de provoquer une non uniformité thermique en raison de l'effet de peau, de l'effet de bout et de l'effet électromagnétique transverse de bord. À cause de l'effet de peau, la plupart de la densité de courant - source de chaleur- se concentre à la surface, et décroît exponentiellement vers le centre. Pour cette raison, l'extérieur se réchauffera plus rapidement que l'intérieur. Ainsi de 80 à 86% de la chaleur est produite dans une couche extérieure appelée "profondeur de pénétration". Cette profondeur est une fonction de la fréquence et des propriétés des matériaux. Elle diminue quand la fréquence augmente.

Les chercheurs et les ingénieurs travaillant en SSF (semi-solid forming) se préoccupent de l'irrégularité de la température dans les matériaux métalliques, qui constitue l'un des problèmes les plus difficiles de SSF utilisant la technique de chauffage par induction. Le but de la présente étude est d'arriver à déterminer une stratégie optimale de chauffage, en employant un algorithme d'optimisation, pour réaliser une distribution uniforme de la température dans le matériau à la fin du traitement dans une période courte. En fait, ce problème de contrôle optimal est essentiellement un problème de transfert thermique inverse visant à déterminer la source de chaleur transitoire nécessaire pour obtenir une distribution de température désirée.

Dans cette thèse, on considère le problème de chauffage optimal de l'alliage d'aluminium (A356/A357). On suppose qu'un lingot d'un diamètre de 76mm et d'une

hauteur de 152mm est placé verticalement dans un réchauffeur par induction. L'alimentation électrique produit du courant alternatif à 10KHz. Afin d'obtenir une fraction liquide uniforme et une bonne viscosité, la température du lingot devrait se situer autour de 585℃ avant que la matière coule dans la cavité du moule sous pression. L'effet de bord ne sera pas considéré en raison de la géométrie cylindrique de l'objet. Si le réchauffeur par induction est bien conçu et qu'il n'y a aucun surplus d'enroulement, les effets de bout peuvent être ignorés. Le modèle physique/mathématique peut donc se simplifier au cas unidimensionnel.

Le but principal de cette recherche est de proposer une stratégie optimale de contrôle de chauffage pour l'alliage semi solide en utilisant des techniques inverses. Les objectifs détaillés sont comme suit:

1) Résoudre un problème inverse de conduction de la chaleur unidimensionnel du deuxième type pour reconstituer les flux de la chaleur à la frontière à partir des mesures de la température au temps final. Analyser l'existence, l'unicité et la stabilité de la solution, mettre en évidence les caractéristiques essentielles de ce genre de problème inverse et puis confirmer la possibilité de résoudre le problème optimal réel de contrôle du chauffage par induction.
2) Étendre ce genre de problème inverse à un système bidimensionnel en convection naturelle dans le milieu poreux. Le but de cet exercice est d'examiner l'adaptabilité de l'algorithme inverse dans des systèmes plus compliqués.
3) Reconstruire la source de chaleur dépendant de la position radiale dans le matériau cylindrique à partir des mesures de la température en supposant que toutes les conditions limites sont connues, ce qui fournit une méthode pour estimer la distribution de la source de chaleur dans le matériau quand la mesure directe n'est pas réalisable.
4) Trouver un flux de refroidissement de frontière pour obtenir une distribution uniforme de la température dans le domaine au temps final pendant le processus de chauffage en supposant que la source de chaleur est donnée. Étudier la possibilité de

contrôler l'uniformité de la température par le refroidissement à la surface. C'est l'un des objectifs les plus importants de cette thèse.

5) Déterminer une stratégie optimale de contrôle de la puissance à fournir pour obtenir une distribution uniforme de la température au temps final en supposant que le flux de la chaleur est connu à la frontière. Le transfert de chaleur avec changement de phase est également considéré. C'est l'objectif ultime de ce projet de recherche.

Nous commençons notre recherche par les caractéristiques essentielles du problème inverse du deuxième type en étudiant un problème de condition limite. La recherche actuelle indique qu'un flux continu de chaleur à la frontière peut être reconstruit de la distribution finale de la température seulement pendant un temps non-dimensionnel de l'ordre de 0.1. La méthode de décomposition en valeurs singulières (SVD) et la méthode du gradient conjugué (CGM) pourraient être employée pour résoudre ce problème inverse du deuxième type. La méthode SVD donne de meilleurs résultats et requiert moins de temps de calcul. Pour de plus longs intervalles, la solution n'est pas uniformément valide, à moins que le flux ait une forme plutôt spécifique. Un effet de moyenne dans le temps se manifeste alors. Le problème devient plus gravement mal posé quand le temps final augmente, ce qui a été confirmé par l'analyse de conditionnement discret de Picard. Si le flux de frontière est connu à $t = 0$, cependant, une méthode de gradient conjugué modifiée peut être employée avec succès pour reconstruire le flux de chaleur sur une période plus longue, tant que le profil demeure monotone ou présente seulement un ou deux minimum/maximum. Si un certain bruit aléatoire est présent dans les mesures de la température, la régularisation de Tikhonov semble efficace pour stabiliser les solutions inverses obtenues par la méthode du gradient conjugué ou de la décomposition en valeurs singulières quand le paramètre de régularisation est déterminé selon le critère de courbe L.

L'étude se poursuit au chapitre II. On présente une formulation du problème inverse de convection du deuxième type bidimensionnel en milieu poreux, conduisant à un

algorithme itératif de solution par la méthode du gradient conjugué avec équations adjointes, qui est valide pour une géométrie arbitraire du domaine. Les calculs pour la détermination des flux de chaleur inconnus à la frontière à partir de la distribution finale de la température sont exécutés dans une cavité carrée. La méthode actuelle peut prévoir un flux non-uniforme de la chaleur dépendant de la position imposé à la frontière active pour un nombre de Rayleigh allant jusqu'à 1000. Pour des profils dépendant du temps, de nombreuses itérations doivent être prévues. La sensibilité de la méthode chute de manière significative quand la période de chauffage augmente, car la distribution finale de la température ne dépend plus des détails de l'évolution antérieure du flux. Des solutions raisonnables peuvent être obtenues pour un intervalle non-dimensionnel de l'ordre de 0.1, au delà duquel la solution inverse a tendance à converger vers une valeur moyenne. Des résultats provenant de données bruyantes peuvent être régularisés efficacement par l'algorithme de CG et le principe d'anomalie.

Afin de résoudre finalement le problème de contrôle du chauffage par induction, nous devons premièrement estimer la distribution de source de chaleur dans le matériau. On sait que le réchauffeur par induction peut produire une distribution exponentielle de la source de chaleur le long du rayon du lingot cylindrique. Généralement la source de chaleur est difficile à mesurer avec une précision satisfaisante, particulièrement pour des profils exponentiels. Cependant, la mesure de la température est relativement plus facile en utilisant des thermocouples, des thermomètres infrarouges ou d'autres dispositifs. La distribution du terme source peut être aussi calculée à partir d'une formule semi-empirique. Toutefois, nous la déterminons plutôt en utilisant des techniques inverses au chapitre III. La méthode du gradient conjugué est appliquée pour récupérer la distribution de source de chaleur de deux manières : 1) en mesurant l'histoire de la température à la surface du matériau; 2) en mesurant la distribution de la température dans le lingot au temps final. Pour les profils exponentiels, la distribution de la source peut être récupérée avec précision en adoptant la méthode 1 même si les mesures de température contiennent une erreur relative allant jusqu'à 5%, mais la durée totale de

l'expérience doit se limiter à 5 secondes. Les solutions reconstruites peuvent ne pas être fiables pour les profils non exponentiels. D'une part, la méthode 2 est adaptable à un profil arbitraire du terme source, mais il faut compter des centaines d'itérations. En outre, la méthode 2 est beaucoup plus sensible à l'erreur contenue dans des données. Les solutions reconstituées peuvent dévier plus ou moins selon les profils des données exactes à cause des bruits de faible intensité. Généralement l'erreur relative de mesure devrait être contrôlée en dedans de 1%.

Au dernier chapitre, nous construisons un modèle physique et mathématique selon la méthode de chaleur massique apparente pour simuler le processus de chauffage d'induction à l'état semi-solide. On prend en compte les variations des propriétés thermo physiques avec la température, et on inclut également les pertes de chaleur par convection et par rayonnement dans l'analyse. Le modèle est validé par comparaison des solutions numériques avec les données expérimentales dans la région solide et dans la région semi-solide. Une approche d'optimisation basée sur la méthode CGM est appliquée pour résoudre un problème optimal de chauffage ou de refroidissement pour thixoforming d'alliage semi-solide. Les stratégies de chauffage optimales estimées par le CGM régulier produisent une distribution plus uniforme de la température au temps final que les méthodes empiriques. Un algorithme CGM modifié pourrait être mieux adapté pour résoudre ce problème de contrôle optimal parce qu'il requiert moins de calculs itératifs et qu'on obtient une meilleure uniformité de la température en fin de compte. Cependant, une unité de chauffage par induction de plus grande puissance pourrait être requise. L'optimisation du chauffage d'un alliage semi solide est plus difficile à réaliser que celle du chauffage dans un solide, parce que l'irrégularité de la température dans la région biphasique est beaucoup plus importante: la différence de température maximale peut être deux fois celle qu'on retrouve dans la phase solide avec un chauffage constant. Les expériences numériques suggèrent qu'une évolution sinusoïdale à décroissance monotone pourrait être le profil de chauffage idéal pour assurer l'uniformité de la température à la fin du traitement thermique.

D'une part, une fois que la procédure de chauffage est établie, on peut également obtenir une stratégie optimale de refroidissement à la surface par la méthode CGM pour éliminer les gradients thermiques et les non-uniformités dans la distribution finale de la température. Le refroidissement à la surface peut avoir un effet équivalent à celui de la stratégie de chauffage, mais il pourrait être beaucoup plus simple à appliquer en refroidissant seulement la surface avec un flux constant dans la dernière douzaine de secondes selon la durée totale du traitement thermique.

En principe, le problème de contrôle optimal du chauffage par induction pour la formation semi-solide a été résolu. Bien que seulement un matériau spécifique, une taille, et une fréquence de courant aient été considérés, le modèle mathématique et l'algorithme d'optimisation développé dans cette thèse sont adaptables à tous les alliages métalliques de toutes dimensions à n'importe quelle fréquence.

Sur la base du présent travail, nous pouvons émettre les recommandations suivantes pour la recherche à venir:

1) Toutes les stratégies de chauffage ou de refroidissement obtenues par l'algorithme d'optimisation devraient être validées par des expériences;
2) Le modèle physique devrait être poussé plus loin pour décrire l'effet de bout et/ou l'effet de bord, et le modèle mathématique devrait être étendu au cas bidimensionnel et/ou tridimensionnel en conséquence;
3) Considérer les écarts possibles entre les résultats numériques et les données, une unité de PID pourrait être incluse dans le système de contrôle pour modifier la stratégie de chauffage prévue.

TABLE OF CONTENTS

DÉDICACE iv

ACKNOWLEDGEMENTS v

RÉSUMÉ vi

ABSTRACT viii

CONDENSÉ EN FRANÇAIS x

TABLE OF CONTENTS xvii

LIST OF TABLES xx

LIST OF FIGURES xxi

LIST OF SYMBOLS xxvii

INTRODUCTION 1

0.1 Background of the Research Project 1

0.2 Inverse Problems 4

0.3 Review of Literature 7

0.4 Objectives and Contents of this Thesis 11

CHAPTER I INVERSE BOUNDARY HEAT FLUX PROBLEM OF HEAT CONDUCTION 14

1.1 Problem Definition 14

1.1.1 Direct Problem 14

1.1.2 Inverse Problem 15

1.2 Conjugate Gradient Method 15

1.2.1 Sensitivity Equation 16

1.2.2 Adjoint Equation 16

1.2.3 Solution Algorithm 18
1.3 Fredholm Equation and SVD method 19
1.4 Components of Inverse Solution By CGM 23
1.5 Degree of Ill-Posedness 28
1.6 Modified CGM 32
1.7 Numerical Solutions by CGM and TSVD 33
1.7.1 Typical Profiles 33
1.7.2 Effect of Noisy Input Data 37
1.7.3 Constrained and Unconstrained Problem 40
1.8 Numerical Solutions by Modified CGM 41
1.8.1 Typical Profiles 41
1.8.2 Effect of Noisy Input Data 44
1.8.3 Optimal Control Problem 44
1.9 Influence of Heat Flux Profiles 48

CHAPTER II: INVERSE BOUNDARY HEAT FLUX PROBLEM OF NATURAL CONVECTION IN A POROUS MEDIUM 50
2.1 Problem Definition and Formulation 50
2.1.1 Sensitivity Equations 52
2.1.2 Adjoint Equations 52
2.2 Results and discussion 55
2.2.1 The effect of Rayleigh number 55
2.2.2 The influence of final time 60
2.2.3 The influence of noisy data 64

CHAPTER III: HEAT SOURCE RECONSTRUCTION PROBLEM 66
3.1 General Inverse Heat Source Problem 66
3.1.1 Sensitivity Equation 66
3.1.2 Adjoint Equation 67

3.2 Reconstruction of the Heat Source Distribution 68
3.3 Results and Discussion 70
3.3.1 Results by Method1 70
3.3.2 Results by Method2 74

CHAPTER IV: OPTIMALCONTROLOF INDUCTION HEATING FOR SEMI-SOLID FORMING 82
4.1 Problem description 82
4.2 Mathematical model 83
4.3 Heat source distribution 84
4.4 Phase change and apparent heat capacity method 85
4.5 Optimal heating control problem 88
4.5.1 Sensitivity equation 89
4.5.2 Adjointe quation 89
4.5.3 Regular conjugate gradient method 90
4.5.4 Modified conjugate gradient method 90
4.6 Optimal cooling control problem 92
4.7 Results and discussion 93
4.7.1 Optimal heating problem 94
4.7.2 Optimal cooling problem 117

CONCLUSION 124

REFERENCES 128

LIST OF TABLES

Table 1.1 Fitting Coefficients of Least Square, Exact $q(t) = \sin(10\pi t)$, $t \in [0, 0.1]$ 25

Table 1.2 Fitting Coefficients of Least Square, Exact $q(t) = \sin(5\pi t)$, $t \in [0, 0.2]$ 25

Table 1.3 Fitting Coefficients of Least Square, Exact $q(t) = \sin(\pi t)$, $t \in [0, 1]$ 25

Table 1.4 Influence of Extreme Points 48

Table 4.1 Chemical composition of A356/A357 alloy 93

Table 4.2 Thermo-physical and electromagnetic properties of A356/A357 93

Table 4.3 Parameters in calculations 94

LIST OF FIGURES

Figure 1.1 Geometry and boundary conditions 14

Figure 1.2a Fitting curve by LS, $t_f = 0.1$ 25

Figure 1.2b Fitting curve by LS, $t_f = 0.2$ 26

Figure 1.2c Fitting curve by LS, $t_f = 1.0$ 26

Figure 1.3a Inverse solution by CGM, $q(t) = \sin(10\pi t)$, $t_f = 0.1$, $\xi = 0$ 27

Figure 1.3b Inverse solution by CGM, $q(t) = \sin(\pi t)$, $t_f = 1.0$, $\xi = 0$ 27

Figure 1.4 Decay rate of singular values, L=1.0, imax=100 29

Figure 1.5a Discrete Picard Condition, $q(t) = \sin(\pi t)$, $t_f = 1$, imax = 100 29

Figure 1.5b Discrete Picard Condition, $q(t) = \sin(10\pi t)$, $t_f = 0.1$, imax = 100 30

Figure 1.6a Solution of inverse problem, $q(t) = \sin(\pi t)$, k = 11, imax = 100 30

Figure 1.6b Solution of inverse problem, $q(t) = \sin(\pi t)$, k = 13, imax = 100 31

Figure 1.7 Inverse solution by TSVD, $q(t) = \sin(10\pi t)$, $t_f = 0.1$, k = 20, imax = 100 31

Figure 1.8a Inverse solution by CGM, $q(t) = 10t$, $\xi = 0$, $S(x,t) = 0$ 34

Figure 1.8b Inverse solution by TSVD, $q(t) = 10t$, $k = 20$, $S(x,t) = 0$ 34

Figure 1.9a Inverse solution by CGM, triangular heat flux profile, $\xi = 10^{-7}$, $S(x,t) = 0$ 35

Figure 1.9b Inverse solution by TSVD, triangular heat flux profile, $k = 20$, $S(x,t) = 0$ 35

Figure 1.10a Inverse solution by CGM, long pulse heat flux, $\xi = 10^{-7}$, $S(x, t) = 0$ 36

Figure 1.10b Inverse solution by TSVD, long pulse exact heat flux, $k = 20$, $S(x,t) = 0$ 36

Figure 1.11a Discrete Picard Condition, $q(t) = \exp[\pi^2 (t - t_f)]$, $t_f = 1.0$, $\sigma = 0$, imax = 100 37

Figure 1.11b Discrete Picard Condition, $q(t) = \exp[\pi^2 (t - t_f)]$, $t_f = 1.0$, $\sigma = 0.001$, imax = 100 38

Figure 1.12 L-Curve for SVD, $q(t) = 10t$, Noise level $\sigma = 0.01$ 39
Figure 1.13 Inverse solution by SVD, $q(t) = 10t$, $\sigma = 0.01$, $\xi = 0.001$ 39
Figure 1.14 Optimal solution for unconstrained problem by regular CGM 40
Figure 1.15 Optimal solution for constrained problem by regular CGM 40
Figure 1.16 Inverse solution by MCGM, linear heat flux profile 41
Figure 1.17 Inverse solution by MCGM, sinusoidal heat flux profile 41
Figure 1.18 Inverse solution by MCGM, triangular heat flux profile 42
Figure 1.19 Inverse solution by MCGM, trapezoidal heat flux profile 42
Figure 1.20 Inverse solution by MCGM, $q(t) = 1\text{-}t$, $t_f = 1.0$, initial guess = 0 42
Figure 1.21 Inverse solution by MCGM, $q(t) = 1\text{-}t$, $t_f = 1.0$, initial guess = 1.0 42
Figure 1.22a Inverse solution by MCGM, sinusoidal profile 43
Figure 1.22b Final temperature distribution with relative error $\sigma = 5\%$ 43
Figure 1.23a Inverse solution by MCGM, linear profile 43
Figure 1.23b Final temperature distribution with relative error $\sigma = 5\%$ 43
Figure 1.24a Inverse solution by MCGM, trapezoidal profile 43
Figure 1.24b Final temperature distribution with absolute error $\sigma = 0.05$, Tmax = 1.2 43
Figure 1.25 Optimal solution by modified CGM, initial guess = 0 45
Figure 1.26 Optimal solution by modified CGM, initial guess = 1.75 45
Figure 1.27 Relative error vs dimensionless final time 46
Figure 1.28a Optimal solution by regular CGM 47
Figure 1.28b Evolution of temperature distribution, regular CGM 47
Figure 1.29a Optimal solution by modified CGM 47
Figure 1.29b Evolution of temperature distribution, modified CGM 47
Figure 1.30 Inverse solution by MCGM, $q(t) = \sin(0.05\pi t)$ 49
Figure 1.31 Inverse solution by MCGM $q(t) = \sin(\pi t) + \cos(\pi t) - 1.0$ 49
Figure 1.32 Inverse solution by MCGM, $q(t) = \sin(5\pi t)$, $t_f = 0.4$ 49
Figure 1.33 Inverse solution by MCGM $q(t) = \sin(20\pi t)$, $t_f = 0.15$ 49

Figure 1.34 Inverse solution by MCGM, $q(t) = \sin(58\pi t)$, $t_f = 0.07$ 49
Figure 1.35 Inverse solution by MCGM, $q(t) = \sin(100\pi t)$, $t_f = 0.05$ 49
Figure 2.1 Geometry and boundary conditions 50
Figure 2.2 Inverse solutions, $q = \sin(\pi y)$, $t_f = 1$ 56
Figure 2.3 Inverse solutions, $q = y$, $t_f = 1$ 57
Figure 2.4a Temperature Distribution at $t = t_f = 1.0$, $q = \sin(\pi y)$, $Ra = 10^4$ 57
Figure 2.4b Temperature Distribution at $t = tf = 1.0$, $q = 0.64$, $Ra = 10^4$ 58
Figure 2.5 Inverse solutions, triangular profile, $t_f = 1$ 58
Figure 2.6 Inverse solutions, rectangular profile, $t_f = 1$ 59
Figure 2.7 Inverse solutions, $q = \sin(8\pi y)$, $t_f = 1$ 59
Figure 2.8 Inverse solutions, $q = -\sin(\pi y) - \sin(8\pi y)$, $t_f = 1$ 60
Figure 2.9 Inverse solution, $q = 10t$, $Ra = 500$, $t_f = 0.1$ 62
Figure 2.10 Inverse solution, $q = 10t$, $Ra = 500$, $t_f = 0.2$ 62
Figure 2.11a Exact $q(y,t) = 10\cos(\pi y)t$ 63
Figure 2.11b Inverse Solution, $Ra = 500$ 63
Figure 2.12 Convergence Performance, $Ra = 500$ 63
Figure 2.13 Inverse solutions, $q(y) = y$, $\sigma = 0.05$ 64
Figure 2.14 Inverse solutions, $q(y) = \cos(2\pi y)$, $\sigma = 0.05$ 65
Figure 3.1a Inverse solution by method 1, $g(x) = \exp(10(x-1.0))$, $t_f = 0.05$ 71
Figure 3.1b Surface temperature evolution, $\sigma = 0.05$, $t_f = 0.05$ 72
Figure 3.2 Inverse solutions by method 1, $g(x) = \exp(5(x-1.0))$, $\sigma = 0.05$ 72
Figure 3.3a Inverse solutions by method 1, $g(x) = \sin(\pi x)$ 73
Figure 3.3b Surface temperature evolution, $g(x) = \sin(\pi x)$ 74
Figure 3.4a Inverse solution by method 2, $g(x) = \exp(5(x-1.0))$, $\sigma = 0$ 76
Figure 3.4b Inverse solutions by method 2, $g(x) = \exp(5(x-1.0))$, $\sigma = 0.02$ 76
Figure 3.4c Final temperature distribution, $g(x) = \exp(5(x-1.0))$ 77
Figure 3.5a Inverse solutions by method 2, sinusoidal profile 77

Figure 3.5b Final temperature distribution, $g(x) = \sin(\pi x)$ 78
Figure 3.6a Inverse solutions by method 2, rectangular profile 78
Figure 3.6b Final temperature distribution, rectangular profile 79
Figure 3.7a Inverse solutions by method 2, triangular profile 79
Figure 3.7b Final temperature distribution, triangular profile 80
Figure 3.8a Inverse solutions by method 2, $g(x) = \sin(\pi x) - \sin(8\pi x) + 1.0$ 80
Figure 3.8b Final temperature distribution, heat source distribution with high frequency components 81
Figure 4.1 Schematic of Induction Heating Coil and Slug 83
Figure 4.2 Heat Source Distribution of A356 85
Figure 4.3a Normal distribution model, A357 alloy, $\varepsilon = 0.045$ 87
Figure 4.3b Liquid fraction vs temperature, A357 alloy, $\varepsilon = 0.045$ 88
Figure 4.4a Temperature Evolution, $q(t) = 0$, $f = 10$KHz, $t_f = 240$s 97
Figure 4.4b Surface-to-Core temperature profile, $q(t) = 0$, $f = 10$KHz, $t_f = 240$s 97
Figure 4.5 Temperature difference vs frequency, $q(t) = 0$, $t_f = 240$s 98
Figure 4.6 Temperature difference vs heating time, $q(t) = 0$, $f = 10$KHz 98
Figure 4.7a Temperature Evolution, q(t) =-100KW/m2 (t>220s), f = 10KHz 99
Figure 4.7b Surface-to-Core temperature profile, $q(t) = -100\text{KW/m}^2$ ($t > 220$s), $t_f = 240$s 99
Figure 4.8a Optimal heating strategy by CGM, initial guess = 0, $q(t) = 0$, $f = 10$KHz, $t_f = 240$s 101
Figure 4.8b Temperature distribution at final time, $q(t) = 0$, $f = 10$KHz, $t_f = 240$s . 101
Figure 4.8c Surface and center temperature evolution, $f = 10$KHz, $t_f = 240$s 102
Figure 4.8d Evolution of maximum temperature difference, $f = 10$KHz, $t_f = 240$s . 102
Figure 4.9a Optimal heating strategy by CGM, initial guess=strategy B, $t_f = 240$s 103
Figure 4.9b Temperature distribution at final time, $q(t) = 0$, $f = 10$KHz, $t_f = 240$s . 104
Figure 4.10a Optimal heating strategy by MCGM, initial guess $G^0 = 168\%$Gmax... 104
Figure 4.10b Temperature distribution at final time, $q(t) = 0$, $f = 10$KHz, $t_f = 240$s . 105
Figure 4.10c Temperature evolution, $q(t) = 0$, $f = 10$KHz, $t_f = 240$s 105

Figure 4.10d Evolution of maximum temperature difference, q(t) = 0, f = 10KHz, t_f = 240s 106

Figure 4.11a Four-stage heating strategy, maximum power = 5.7KW, η_E = 80% ... 108

Figure 4.11b Temperature evolution in the mushy region 109

Figure 4.12a Optimal heating strategy by CGM, initial guess = 0, f = 10KHz, t_f = 490s 110

Figure 4.12b Temperature distribution at final time, f = 10KHz, t_f = 490s 111

Figure 4.13 Maximum temperature difference at final time, initial guess = 0..... 111

Figure 4.14a Optimal solution by CGM, t_f = 490s, initial guess $G^0 = 65\%P_{max}\sin(0.5\pi(t_f - t)/t_f)$ 112

Figure 4.14b Temperature distribution at final time, t_f = 490s, initial guess $G^0 = 65\%P_{max}\sin(0.5\pi(t_f - t)/t_f)$ 113

Figure 4.14c Evolution temperature difference, t_f = 490s, initial guess $G^0 = 65\%P_{max}\sin(0.5\pi(t_f - t)/t_f)$ 113

Figure 4.15 Optimal solution by CGM, t_f = 300s, initial guess $G^0 = 120\%P_{max}\sin(0.5\pi(t_f - t)/t_f)$ 114

Figure 4.16a Optimal solution by modified CGM, t_f = 490s, initial guess $G^0 = 65\%P_{max}\sin(0.5\pi(t_f - t)/t_f)$ 115

Figure 4.16b Final temperature distribution, t_f = 490s, initial guess $G^0 = 65\%P_{max}\sin(0.5\pi(t_f - t)/t_f)$ 115

Figure 4.17 Optimal solution by modified CGM, t_f =300s, initial guess $G^0 = 120\%P_{max}\sin(0.5\pi(t_f - t)/t_f)$ 116

Figure 4.18a Optimal cooling strategy, f = 10KHz, t_f = 240s 118

Figure 4.18b Temperature distribution at final time, f = 10KHz, t_f = 240s 118

Figure 4.19 Evolution of temperature difference, P(t) = 50%Pmax, t_f = 490s..... 120

Figure 4.20a Optimal cooling strategy, P(t) = 50%Pmax, t_f = 490s 121

Figure 4.20b Temperature distribution at the final time, t_f = 490s, P(t) = 50%Pmax 121

Figure 4.21 Evolution of temperature difference, P(t) = 80%Pmax, t_f = 300s..... 122
Figure 4.22a Optimal cooling strategy, P(t) = 80%Pmax, t_f = 300s 122
Figure 4.22b Temperature distribution at the final time, t_f = 300s, P(t) = 80%Pmax 123

LIST OF SYMBOLS

b	source term
c	thermal capacity
C_a	active boundary
C_p	thermal capacity at constant pressure
E	error functional
f	current frequency
g	gradient function
H	height of the system
I	current density
k	thermal conductivity, $W/(m \cdot K)$
L	length of the system
P	search direction
q	heat flux
Ra	Rayleigh number
S	heat source
t	time
t_f	final time
T	temperature
u, v	scalar velocity
x, y	coordinates

Greek symbols

α	step size
β	conjugate coefficient
σ	error level, Stefan-Boltzmann constant
Ω	system surface

ψ	stream function
ε	convergent criterion or arbitrary tiny real number
τ	time variable
ξ	regularization parameter
χ	load resistivity
μ	load magnetic permeability
δ	skin depth
Δ	increment
ρ	mass density
∇	gradient operator
∇^2	Laplacian operator

Superscripts

$-$	adjoint variables
$\sim$	sensitivity variables
*	dimensionless variables
k	iteration number

Subscripts

0	reference state
E	expected value
l	liquid
m	measured value
max	maximum value
min	minimum value
r	relative value

ref	reference state
s	solid

Other symbols

$\langle \cdot \vert \cdot \rangle$	inner product
$\Vert \cdot \Vert$	norm
$\vert \cdot \vert$	modulus

Abbreviations

CGM:	conjugate gradient method
DPC:	discrete Picard condition
IHCP:	inverse heat conduction problem
IHTP:	inverse heat transfer problem
MCGM:	modified conjugate gradient method
SVD:	singular value decomposition
TSVD:	truncated singular value decomposition

INTRODUCTION

0.1 Background of the Research Project

Semi-solid metal (SSM) forming has become a competitive technique in the treatment and manufacture of metal alloys especially for the automotive industry since the end of the 20th century. This technique was originally developed by Prof. Merton C. Flemings [1-3] at MIT in the 1970's, and is being practiced commercially in industries nowadays. Compared to conventional methods such as gravity die-casting and squeeze casting which have various problems such as blowholes, segregation, and thermal defects of the die etc., the SSM technique requires casting the metal alloys when they are partially solid. This increases flow viscosity and decreases the processing temperature during the casting process, leading to laminar flow and lower solidification shrinkage, and therefore a higher quality of cast products by preventing the entrapment of gas. Its advantages also include excellent surface quality, tight tolerances, high strength, low level of porosity, fine microstructure, energy saving, etc.[4-14]. Several metal alloys including copper, magnesium, nickel and ductile iron have been used for SSM casting.

One of the semi-solid forming techniques, thixoforming, usually requires reheating pre-processed feedstock with a fine and non-dendritic structure to a liquid fraction of about 40%~50%. At such a liquid fraction, the rheological properties of the semi-solid alloys are very sensitive to variations in the liquid fraction. So the heating process must be accurately controlled to achieve a uniform temperature distribution in the material and necessary liquid fraction. On the other hand, the heating process is required to be relatively rapid in order to maintain the initial globular microstructure. Otherwise, the semi-solid alloys will not display thixotropic behaviors under shear and thus would not fill the die cavity properly [5, 15].

The traditional heating technique in the metallurgical industries is related to the gas-fired furnace because of its low cost. However, a gas-fired furnace requires a very long

heating tunnel to create the temperature uniformity, and this technique results in poor surface quality due to scaling, decarburization, oxidation, coursing of grains etc. Nowadays induction heating is one of the most commonly used methods in commercial production applications in semi-solid metal processing because that it is a non-contact, clean, compact and fast method and the input power can be easily, precisely and timely controlled.

The basic components of an induction heating system include an AC power supply, induction coils (single or multiple), and workpiece (material to be heated). The power supply sends alternating current through the coil, generating a magnetic field. When the workpiece is placed in the coil, the magnetic field induces the circulating current named *eddy current* in the workpiece. According to the Joule's law namely $Q = I^2R$, the eddy current may generate heat without any physical contact between the coil and the workpiece.

However, the induced eddy currents are not uniformly distributed within the workpiece. The maximum value of the current density is located on the surface. Current density then decreases rapidly from the surface towards the center. This phenomenon of non-uniform current distribution is called the *skin effect*. In addition, there exists another type of temperature non-uniformity along the length of the material due to the *electromagnetic end effect*, usually it is called *nose-to-tail temperature profile.* In commercial operation, the workpieces are sometimes required to be sent into the horizontal induction heating machine continuously. If they travel end-to-end through the heating line, nose-to-tail profile is not a serious problem. Unfortunately an air gap of 5 to 10 inches is present between the leading and following bars in most cases. These air gaps may result in an overheating of the front end, while overhang of the bar results in an underheating of the back end because of the distortion of electromagnetic field around these areas, and then it creates unacceptable temperature non-uniformity along the length of the bar. Besides that, non-cylinder shaped workpieces may distort the electromagnetic fields in their edgy areas. It creates a non-uniform temperature profile

within the transverse cross-section of the material. This phenomenon is called *electromagnetic transverse edgy effect* [16-21]. In order to avoid a more complicated situation, the workpieces under treatment are normally cylindrical.

Induction heating has its inherent drawback of non-uniformity of heating due to the skin effect, end effect and electromagnetic transverse edge effect. Because of the *skin effect*, most power density (heat source) is concentrated on the surface, and decays exponentially below the surface. Then the outside will heat more quickly than the inside; 80%~86% of the heat is produced in the surface layer called *current penetration depth*. The non-uniform temperature distribution along the radius of the material is called *surface- to-core temperature profile*. The skin depth is a function of frequency and material properties, it decreases when frequency increases. So the low frequencies of 5 to 30kHz are effective for thicker materials requiring deep heat penetration, while higher frequencies of 100 to 400kHz are effective for smaller parts or shallow penetration. Considering the maximum electrical efficiency and minimum electromagnetic forces, the commercial machines often work at a frequency of more than 10kHz. Such a frequency also makes the system more compact [20].

The researchers and engineers working on SSF are puzzled by the temperature non-uniformity of metal materials which is one of the most difficult problems in semi-solid metal forming process while employing the induction heating technique. In order to achieve a uniform temperature, at least three heating methods have been frequently applied SSF: (1) Single coil: a billet is heated in the same coil, input power varies according to the temperature values measured by the sensors embedded within the material; (2) Multi-coils: a billet passes through a series of coils sequentially and reaches semi-solid state in the last coil. A rotation disk induction heater obtained the patent of semi-solid metal heating (American Patent 4,569,218) in 1986; (3) Hybrid method: The researchers at Materials Research Laboratory of Taiwan combined these two methods and modified the electrical and temperature control circuit. These approaches essentially are similar: when the temperature reaches a pre-determined value,

the input power is cut off or decreased. The heating procedure is determined by empirical data from experiments. However, the drawback is also obvious: the strategy may not be the "best", the heating time may not be short, and if the size of material or material itself or the operating frequency of induction heater changes, the experiments must be repeated.

How to determine an optimal heating strategy by using a numerical method to achieve a uniform temperature distribution in the material at the end of processing within as short a time as possible is the main objective of this research. In fact, this optimal control problem is essentially an inverse heat transfer problem of determining the time-dependent heat source (power density) to obtain the targeted temperature distribution. Then let us review the basic concepts of inverse problem.

0.2 Inverse Problems

What is the inverse problem? J.B. Keller [22] defined the inverse problem as follows: two problems are inverse to each other if the formulation of one problem involves the other one. Usually the simpler one or the one which was studied earlier is called direct problem, the other one is the inverse problem. Thus one might say that inverse problems are concerned with determining causes for a desired or an observed effect [23]. O. M. Alifanov [24], the Russian proponent of inverse methods, probably said it best: solution of an inverse problem entails determining unknown causes based on observation of their effects. This is in contrast to the corresponding direct problem, whose solution involves finding effects based on a complete description of their causes.

In the last twenty years, the research on inverse problems has undergone rapid development because of the needs of applications both in science and industry. In various fields, such as heat transfer, the earth science, aeronautics, metallurgy, energy engineering, chemical engineering, signal and image processing, medical machines,

bioelectric technique etc., the inverse problems are attracting extensive attention.

If the geometric shape of the system boundary, boundary conditions, initial conditions, thermo-physical properties etc. are given, to determine the temperature (or the other parameters) distribution within the domain is the direct problem; on the other hand, if the temperature (or the other parameters) of one point or some points within a system or on a part of the bounding surface is known, to estimate the boundary conditions, inner heat source, or initial conditions etc. is the inverse problem.

One might classify the inverse problems according to their practical purpose such as diagnostic problems, process control problems, optimal design problems and so on. Another means of classification is by the type of information that is being sought in the solution procedure: backward or retrospective problems, coefficient estimation problems, and boundary value problems etc.

Inverse heat transfer problems might be encountered in many situations where the direct measurement of boundary conditions or the determination of thermo-physical properties of a system is impractical. One typical example is related to the determination of the heat flux on the surface of a spacecraft or a missile. When the spacecraft reenters the atmosphere, the heat flux to be imposed on the surface is too high to be measured directly due to aerodynamic effects. Researchers had to estimate the timewise-varying surface flux by the inverse method, through the temperature values measured by the sensors embedded in the heat protective materials.

Normally the inverse problems are thought to be much more difficult than the direct problems because:

1) The solutions of the inverse problems are unstable, i.e., very sensitive to the errors of measurements. A small error in input data can produce a physically unacceptable error in the solutions;

2) The response of the inner points to the variation of boundary conditions is attenuated

and delayed.

Inverse problems are mathematically regarded as ill-posed problems, in the sense of Hadamard [25]. That means, they may have no solution, or if a solution exits, it might not be unique or not continuous with respect to the given data. Therefore they were thought to be unsolvable and of no practical or physical meanings. This was wrong, since the developments of applied mathematics and modern computer technology have made it possible to obtain meaningful solutions.

One may clearly observe the ill-posedness of inverse problems from the point of view of linear algebra. If a direct problem can be described by a matrix equation $[A]\{X\} = \{F\}$, and [A] and {F} are known, to determine the unknown vector {X} is an inverse problem. Let us repeat a simple example which was put forth by Hensel [26]:

$$\begin{bmatrix} 1 & 1 \\ 1 & 1.01 \end{bmatrix} \begin{Bmatrix} x_1 \\ x_2 \end{Bmatrix} = \begin{Bmatrix} 1 \\ 1 \end{Bmatrix}$$

The exact solution to this problem is x_1=1 and x_2=0. Suppose there exists a one percent of perturbation in the input data vector {F}, and the problem is modified as:

$$\begin{bmatrix} 1 & 1 \\ 1 & 1.01 \end{bmatrix} \begin{Bmatrix} x_1 \\ x_2 \end{Bmatrix} = \begin{Bmatrix} 1 \\ 1.01 \end{Bmatrix}$$

The solution accordingly becomes x_1=0 and x_2=1. This example demonstrates how a slight change in the input data leads to a big change in the solution. In fact, for most inverse problems, the coefficient matrix [A] is singular (the determinant of $|A| = 0$) or highly ill-conditioned in general. Most matrix solvers such as Gaussian elimination and *LU* decomposition will fail to produce a correct solution. Then in an algebraic system, ill-posedness may be interpreted as *ill-conditionedness*. Any $M \times N$ matrix [A] can be written as the product of a $M \times N$ column-orthogonal matrix [U], a $N \times N$ diagonal matrix [W] with positive or zero elements (the singular values), and the transpose of an $N \times N$ orthogonal matrix [V]. The singular values $\{w_1, w_2, \cdots, w_N\}$ are the eigenvalues of

the square matrix $[A]^T[A]$, they are non-negative and they can always be ordered in non-increasing order such that $w_1 \geq w_2 \geq w_3 \cdots \geq 0$. The decay rate of the singular value w_i is fundamental for describing the behavior of ill-posed problem and can be used to characterize the degree of ill-posedness. On the other hand, for a well conditioned matrix, singular values will be roughly of the same order of magnitude. As the matrix becomes more ill conditioned, they will become more dispersed. Formally, the *condition number* is defined as the natural logarithm of the ratio of the largest singular value to the minimum, namely $N_C = \log_{10}\left(\frac{w_{max}}{w_{min}}\right)$. The condition number also ascribes the degree of ill-posedness: the larger the condition number, the more ill-conditioned is the coefficient matrix, then the more ill-posed is the problem.

0.3 Review of Literature

The earliest works on inverse problems are concerned with the determination of the historical climate and thermal conductivity of the earth's ground layer over a century ago. In 1890 Stefan obtained the first exact solution of the one-dimensional inverse heat conduction problem. Tyomkin and Burggraf got similar results in 1961 and 1964 for a series of linear problems [24]. Even though the work of constructing solutions of inverse problems had already started since the end of nineteenth century, the rapid growth happened only during the last two decades. The enormous increase in computing power and the development of mathematical algorithms made it possible to consider the various real problems and apply the techniques of inverse problem to more complicated systems.

For a long time researchers estimated parameters using optimization techniques. Some methods known two centuries ago, for example, the least squares criterion introduced by Legendre (1801) and Gauss (1809) are still used at present [27, 28, 29]. The late 1960s and early 1970s were a golden age for the theory of inverse problems, a lot of modern

methods and algorithms appeared during this period. Tikhonov [30] proposed the well-known *regularization* method based on a modification to the objective function using priori information as a regularization term in 1963. Nowadays Tikhonov regularization has been developed into an important direction of mathematics. And it is considered as a milestone of inverse problem: *opening a fruitful direction in mathematical physics and computing mathematics, and considerably broadening the bounds of effective practical use of ill-posed problems in various fields of science and technology* [24]. The process of converting an ill-posed problem to a well-posed one is termed *regularization* which is an effective technique to conquer the ill-posedness. Tikhonov regularization, the maximum entropy regularization [31], truncated total least squares, least squares with a quadratic constraint [32] and others can be classified as *direct regularization methods*. Along this direction, Alifanov [24] developed a so-called *iterative regularization* by conjugate gradient method. The *v*-method and bidiagonalization with regularization are also the typical iterative regularization methods. Beck [33] presented a fast algorithm namely *future times*, which is essentially an extension of Stoltz's method [34], but the objective function corresponding to the current time is determined by the measured data from several future times steps. If the number of future times r is 1, these two methods have exactly the same scheme. Recently, Murio [35] proposed a regularization method which is called *mollification* based on data smoothing techniques; Martin and Dulikravich [36] implemented the boundary element formulation into steady IHCP, this technique has good adaptability for complex geometries. A good review can be found in Woodbury [37].

Besides the above regularizing techniques, there exists an important probabilistic approach frequently applied to inverse problems in geophysics. Purely probabilistic formulations of inverse theory appeared around 1970. Keilis-Borok and Yanovskaya founded earth model based on the Monte Carlo theory in 1967 [38]. Backus and Gilbert obtained the unknown function from discrete data in the years 1967-1970 [39-41]. Recently, the interest in Monte Carlo methods for the solution of inverse problems has

been increasing. Mosegaard and Tarantola proposed a generalization of the Metropolis algorithm in 1995 [42]. A good review of this probabilistic method may be seen in references [43] and [44]. Recently Monte Carlo based inverse technique has also been applied to inverse heat transfer problems [45-47].

The most common inverse heat transfer problems (IHTP) are related to the determination of the objective variables (function or parameters) according to the temperature history or evolution of one point or some points within the domain. A much less studied IHTP is to estimate the boundary or initial conditions from the temperature distribution *at the final time*. For example, a retrospective convection problem was solved by Nguyen and Zhang [48] to trace back the initial temperature field. This kind of problem may be referred to as IHTP of the second kind while the former may be called IHTP of the first kind [49].

Recently, heating control problems which belong to the class of inverse problems of the second kind have been considered in various engineering fields. For example, in order to obtain a high quality steel production, one needs to reduce the temperature uniformly during the cooling process [50]. The semi-solid forming technology also requires a uniform temperature of the heated material at the final time to obtain a desired globular microstructure [51]. During the rapid thermal processing of a 12-inch silicon wafer, uniformity of surface temperature is also necessary [52]. This kind of optimal heating control problem in distributed-parameter system was first proposed by Butkovskii and Lerner [53] in 1960. Sakawa [54-55] used a variational method, Cavin and Tandon [56] applied a finite element method, Meric[57-58] adopted conjugate gradient method to solve the linear and nonlinear boundary control problems.

In the last two decades, the solution algorithms were further improved due to the fast development of optimization and inverse problem techniques. To achieve a uniform final temperature field under a Stefan-Boltzmann boundary condition, Kelley and Sachs [59] developed a Steihaug trust-region-conjugate-gradient method with a smoothing step

at each iteration. It appears that the Steihaug trust-region-conjugate-gradient method has stronger convergence properties than the non-linear conjugate gradient method, especially for constrained problems. The numerical tests show that the error functional is about 10^{-3} after only one iteration. Huang [60] solved a similar 1-D control problem by the conjugate gradient method to obtain a targeted temperature at the final time. Two values of final times were considered. The numerical results showed that the estimated boundary heat fluxes change steeply near the final time. The author concluded that the standard CGM can be successfully applied to solve the nonlinear control problem but the estimated solution is difficult to realize in practice. More recently, the same control problem was extended to 3-D geometries by Huang and Li [61]. Numerical tests were performed for rectangular and irregular domains. It was found that, as in the 1-D problem, the estimated boundary heat flux tends to a constant value, and changes just before the final time.

In addition, Krengel et al. [62] developed a method of feasible directions, Tröltzsch and Unger [63] adopted a suboptimal solution method, to the similar control problems. Landl and Engl [64], Engl, Langthaler and Mansellio [65], Grever [66], Leibfritz and Sachs [67], and other European researchers also made the important investigation on this issue.

On the other hand, the control of induction heating for semi-solid metal forming has been investigated in recent years by using the experimental approaches. Ono et al. [12] found that the imp edance of the heating coil is very sensitive to the billet (A357) state such as temperature, deformation and solid/liquid fraction, and could be used as a parameter to monitor and control the heating process. Bendada et al. [68] proposed a two-stage heating strategy for A356 alloy casting and recovered the temperature distribution along the radius of material with surface infrared measurements using conjugate gradient method. Kim et al. [69] applied the Taguchi method, regression analysis and neural network technique to analyze the relationship between thermal processing conditions and solid fraction. The learning data were extracted from the

experiments on A356 alloy based on a multi-step heating method. Jung and Kang [70], and Kang [71] et al. adopted the similar multi-step strategy to heat the Al-Si alloys for experimental research on semi-solid die casting and microstructure of the materials.

In summary, although the IHTPs of the second kind have been considered within the framework of optimal control by using various methods, this domain is still open because the reconstruction problems have never been examined so far. The control and reconstruction problems are basically different: there may be no exact solution to a control problem, while an exact solution must *de facto* exist in a reconstruction problem. More importantly, optimization techniques have not been applied to the induction heating control for semi-solid metal forming. Empirically heating control strategies have been proposed based on many experiments and data comparison. Although they are reliable, they may not be the "best".

0.4 Objectives and Contents of this Thesis

The main purpose of this research is to propose an optimal heating control strategy for semi-solid alloy forming by utilizing inverse techniques. The detailed objectives are as follows:

1) Solve a one dimensional inverse heat conduction problem of the second kind, recover the boundary heat fluxes from the temperature measurements at the final time. The main task is to analyze the existence, uniqueness and stability of the solution, reveal the essential character of this kind of inverse problem and then confirm the feasibility of solving the real optimal induction heating control problem.
2) Extend this kind of inverse problem to a two-dimensional system of natural convection in porous medium. The purpose of this work is to examine the adaptability of present inverse algorithm to more complicated systems.
3) Reconstruct the position-dependent heat source along the radius of the metal cylinder from the temperature measurements, supposing that all the boundary conditions are known. It provides a possible method to estimate the distribution of power density within the material when the direct measurement is not applicable.

4) Find an optimal heat flux of boundary cooling to obtain the desired temperature distribution within the domain at the final time during a heat conduction process, supposing that the heat source (power density) is given. This work studies the possibility of controlling the temperature uniformity by surface cooling. It is one of the most important objectives of this thesis.
5) Determine an optimal input power control strategy to obtain the desired temperature distribution at the final time, supposing that the boundary heat flux is known, and considering also the two-phase heat transfer. It is the ultimate target of this research project.

The contents of this thesis contain the following parts:

First of all, we introduce the basic concept of semi-solid metal forming, induction heating and inverse transfer problem. The history and typical methods of inverse problem, the development of optimal control problem, and the present situation of induction heating control for semi-solid metal forming are presented on the basis of literature review. In addition, the objectives of this thesis are also given.

In Chapter I, we firstly adopt conjugate gradient method (CGM) in conjunction with adjoint equation to solve a 1-D IHCP of the second kind. Then we convert an inverse problem with a partial differential parabolic equation into a problem with an integral equation—Fredholm equation of the first kind which is solved by truncated singular value decomposition (TSVD) and CGM. Both reconstruction problem and optimal control strategy problem are investigated.

In chapter II, the same inverse problem is considered in a two-dimensional domain with natural convection in a porous medium. The conjugate gradient method (CGM) and a modified CGM are applied to determine the time and position dependent heat fluxes for different cases subjected to the influence of Rayleigh number, error level of temperature measurements, final time and heat flux profiles.

In chapter III, the heat source distributions along the radius of a metal cylinder are reconstructed by utilizing CGM from the temperature measurements at the final time or the surface temperature history. The numerical tests are performed for various profiles of heat source distributions with different noise levels in the input temperature data.

In chapter IV, the optimal heating strategies for semi-solid alloy forming are estimated by utilizing CGM and modified CGM to achieve a uniformly distributed target temperature at the end of heat treatment. The model based on the apparent heat capacity method is adopted to describe the phase change process in mushy region and is validated by comparison of the numerical solutions with experimental data. In addition, the boundary cooling strategies are also studied, supposing that the input heating power is fixed.

CHAPTER I
INVERSE BOUNDARY HEAT FLUX PROBLEM OF HEAT CONDUCTION

We started our research by investigating a boundary control problem to reveal the essential character of this kind of inverse problem and then confirmed the feasibility of solving the real optimal induction heating control problem.

1.1 Problem Definition

Suppose a metal bar is heated or cooled from the right side, and its left side is adiabatic. The initial temperature field is assumed to be known: $T(x, 0) = f(x)$. A heat source which is a function of position and time may exist within the system. The geometry of the system and boundary conditions are also summarized in Fig.1.1. Our objective is to seek the unknown heat flux q(t) at the right boundary during the period $0 \le t \le t_f$ from the expected temperature distribution $T(x, t_f) = T_E(x)$ at final time.

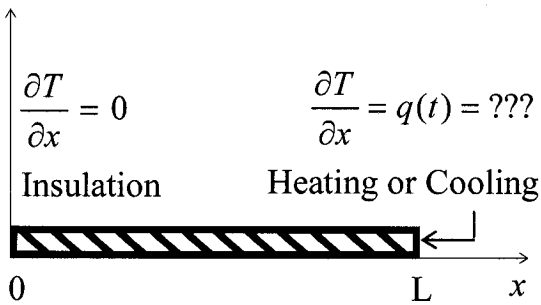

Figure1.1: Geometry and boundary conditions

1.1.1 Direct Problem

Generally a physical phenomenon in nature can always be described with the aid of the laws of physics in terms of algebraic, differential or integral equations. This 1-D heat conduction problem is governed by a parabolic equation:

$$\rho c \frac{\partial T}{\partial t} = k \frac{\partial^2 T}{\partial x^2} + S \tag{1.1}$$

where $S = S(x,t)$ denotes inner heat source; ρ is density; c is specific heat and k is

thermal conductivity. At the reference temperature $T_0 = T_\infty$ the dimensionless temperature, length, time and heat source are defined as follows:

$$T^* = \frac{T - T_\infty}{\Delta T},\ x^* = \frac{x}{L},\ t^* = \frac{tk}{\rho c L^2},\ S^* = \frac{SL^2}{k\Delta T} \tag{1.2}$$

here $\Delta T = \frac{Q_{ref} L}{k}$ is a temperature scale. Omitting the superscript "*", and substituting Eq.(1.2) into Eq.(1.1), we may easily obtain the non-dimensional heat equation:

$$\frac{\partial T}{\partial t} = \frac{\partial^2 T}{\partial x^2} + S \tag{1.3}$$

The boundary and initial conditions are as follows:

$$\left.\frac{\partial T}{\partial x}\right|_{x=0} = 0,\ \left.\frac{\partial T}{\partial x}\right|_{x=1} = q(t),\ T(x,0) = f(x) \tag{1.4}$$

1.1.2 Inverse Problem

Suppose the temperature distribution of the metal bar $T(x,t_f)$ at the final time and the heat source are known. Initial conditions and all the boundary conditions except the heat flux on active boundary are given. The purpose of the inverse problem is to seek the unknown heat flux q(t) during the time interval $0 \le t \le t_f$ from the following information:

$$\left.\frac{\partial T}{\partial x}\right|_{x=0} = 0,\ T(x,0) = f(x),\ T(x,t_f) = T_E(x),\ S = S(x,t)$$

1.2 Conjugate Gradient Method

The objective of this inverse problem is to find a boundary heat flux q(t) which would satisfy the expression $T(x,t_f) = T_E(x)$. Then the inverse problem may be converted to an optimization problem by minimizing the error function E. Based on the principle of Tikhonov regularization, the error function is defined here as:

$$E(q) = \frac{1}{2}\int_0^L [T(x,t_f) - T_E(x)]^2 dx + \frac{\xi}{2}\int_0^{t_f} q^2(t)dt \tag{1.5}$$

The symbol ξ is known as the regularization parameter. Among the various

optimization algorithms, the conjugate gradient method is frequently adopted by researchers not only owing to its powerful efficiency but also due to its self-regularizing character. For an iterative algorithm, the determination of the search direction and step size is the most important task. The search direction is related to the gradient of E which is obtained by solving the adjoint problem, while optimal step size may be determined by solving the sensitivity problem.

1.2.1 Sensitivity Equation

The temperature sensitivity $\tilde{T}$ is defined as the directional derivative of T at q in the direction Δq:

$$\tilde{T} = \lim_{\varepsilon \to 0} \frac{T(q + \varepsilon \Delta q) - T(q)}{\varepsilon} \tag{1.6}$$

Starting from Eq.(1.3), we must have

$$\lim_{\varepsilon \to 0} \frac{\partial}{\partial t}\left(\frac{T(q + \varepsilon \Delta q) - T(q)}{\varepsilon}\right) = \lim_{\varepsilon \to 0} \frac{\partial^2}{\partial x^2}\left(\frac{T(q + \varepsilon \Delta q) - T(q)}{\varepsilon}\right) + \lim_{\varepsilon \to 0}\left(\frac{S(q + \varepsilon \Delta q) - S(q)}{\varepsilon}\right)$$

The heat source is a given term and thus is not a function of q, so $\lim_{\varepsilon \to 0}\left(\frac{S(q + \varepsilon \Delta q) - S(q)}{\varepsilon}\right) = 0$. Then according to the definition of the sensitivity, the sensitivity equation is directly obtained:

$$\frac{\partial \tilde{T}}{\partial t} = \frac{\partial^2 \tilde{T}}{\partial x^2} \tag{1.7}$$

Similarly we may get the respective initial and boundary conditions:

$$\tilde{T}(x,0) = 0, \quad \left.\frac{\partial \tilde{T}}{\partial x}\right|_{x=0} = 0, \quad \left.\frac{\partial \tilde{T}}{\partial x}\right|_{x=L} = \Delta q(t) \tag{1.8}$$

1.2.2 Adjoint Equation

The key of CGM is the determination of the gradient of error functional namely ∇E,

which is related to the directional derivative of E in the direction Δq. Starting from the definition of error function and sensitivity, it leads to the following equation:

$$\begin{aligned} D_{\Delta q}E(q) &= \lim_{\varepsilon\to 0}\frac{E(q+\varepsilon\Delta q)-E(q)}{\varepsilon} \\ &= \frac{1}{2}\lim_{\varepsilon\to 0}\frac{\int_0^L[T(q+\varepsilon\Delta q)-T_E]^2dx+\xi\int_0^{t_f}(q+\varepsilon\Delta q)^2dt-\int_0^L[T(q)-T_E]^2dx-\xi\int_0^{t_f}q^2dt}{\varepsilon} \\ &= \int_0^L\{\tilde{T}(x,t_f)\cdot[T(x,t_f)-T_E]\}dx+\xi\int_0^{t_f}(q\cdot\Delta q)dt \\ &= \int_0^{t_f}(\nabla E\cdot\Delta q)dt \end{aligned} \tag{1.9}$$

If the adjoint temperature $\bar{T}$ and Eq.(1.7) are respectively treated as Lagrange multiplier and constraint, using Lagrange multiplier method we may rewrite Eq.(1.9):

$$D_{\Delta q}E(q)=\int_0^L\{[T(x,t_f)-T_E]\cdot\tilde{T}(x,t_f)\}dx+\xi\int_0^{t_f}(q\cdot\Delta q)dt+\int_0^{t_f}\int_0^L\bar{T}\left(\frac{\partial\tilde{T}}{\partial t}-\frac{\partial^2\tilde{T}}{\partial x^2}\right)\cdot dxdt \tag{1.10}$$

Considering the initial and boundary conditions of the sensitivity problem, we must have

$$\begin{aligned} D_{\Delta q}E(q) = &\int_0^L\{[(T-T_E)+\bar{T}]\tilde{T}\}_{t=t_f}dx-\int_0^{t_f}\int_0^L\tilde{T}\left(\frac{\partial\bar{T}}{\partial t}+\frac{\partial^2\bar{T}}{\partial x^2}\right)\cdot dxdt \\ &+\int_0^{t_f}\int_0^L\frac{\partial}{\partial x}\left(\tilde{T}\frac{\partial\bar{T}}{\partial x}\right)\cdot dxdt-\int_0^{t_f}[\bar{T}(1,t)\cdot\Delta q]dt+\xi\int_0^{t_f}(q\cdot\Delta q)dt \end{aligned} \tag{1.11}$$

If the adjoint temperature satisfies the following equation and the "initial" and boundary conditions:

$$\frac{\partial\bar{T}}{\partial t}+\frac{\partial^2\bar{T}}{\partial x^2}=0 \quad \text{or} \quad \frac{\partial\bar{T}}{\partial\tau}=\frac{\partial^2\bar{T}}{\partial x^2},\ \tau=t_f-t \tag{1.12}$$

$$\left.\frac{\partial\bar{T}}{\partial x}\right|_{x=0}=0,\ \left.\frac{\partial\bar{T}}{\partial x}\right|_{x=L}=0 \tag{1.13}$$

$$\bar{T}(x,\tau=0)=-[T(x,t_f)-T_E(x)] \tag{1.14}$$

then the first, second and third term of right hand side of Eq.(1.11) vanish. Then Eq.(1.11) becomes

$$D_{\Delta q}E(q) = \int_0^{t_f}\left\{\left[\xi q - \bar{T}(L,t)\right]\cdot \Delta q\right\}dt \tag{1.15}$$

Comparing Eq.(1.15) and Eq.(1.9), we may obtain the gradient of the error function

$$\nabla E = \xi q - \bar{T}(L,t) \tag{1.16}$$

1.2.3 Solution Algorithm

For the Polak-Ribiere version of CGM, the iterative equation and the searching direction may be expressed as:

$$q^{k+1} = q^k + \alpha^k P^k \tag{1.17}$$

$$P^k = -g^k + \beta^k P^{k-1},\ \beta^k = \frac{(g^k - g^{k-1})^T g^k}{(g^{k-1})^T g^{k-1}} \tag{1.18}$$

Here "g" stands as the gradient of the objective functional of the minimization problem. On the other hand, the optimal step size might be derived by seeking the value that will make the first-order derivative of E in the direction α^k equal to zero:

$$\begin{aligned}\frac{\partial E}{\partial \alpha^k} &= \int_0^L \left[T(q^k + \alpha^k P^k) - T_E\right]\tilde{T}dx + \xi\int_0^{t_f}(q^k + \alpha^k P^k)P^k dt \\ &\approx \int_0^L \left(T^k + \alpha^k \tilde{T}^k - T_E\right)\tilde{T}^k dx + \xi\int_0^{t_f} q^k P^k dt + \xi\int_0^{t_f}\alpha^k (P^k)^2 dt \\ &= \alpha^k\left[\int_0^L (\tilde{T}^k)^2 dx + \xi\int_0^{t_f}(P^k)^2 dt\right] + \int_0^L \left(T^k - T_E\right)\tilde{T}^k dx + \xi\int_0^{t_f} q^k P^k dt \\ &= 0\end{aligned} \tag{1.19}$$

Then we get

$$\alpha^k = -\frac{\int_0^L (T^k - T_E)\tilde{T}^k dx + \xi \int_0^{t_f} q^k P^k dt}{\int_0^L (\tilde{T}^k)^2 dx + \xi \int_0^{t_f} (P^k)^2 dt} \tag{1.20}$$

We note that the temperature is assumed to be linear to the heat flux q in (1.19). For heat conduction, this hypothesis is reasonable.

The overall CGM algorithm may be summarized as follows [24].

1. Set initial guess $q^0 = q_0(t)$, set iteration counter k = 0.

2. Solve the direct problem with q^k to obtain T^k.

3. Evaluate the difference $T^k(x, t_f) - T_E$.

4. Solve the adjoint problem backward in time for $\overline{T}^k$.

5. Evaluate the gradient according to Eq.(1.16) on the active boundary x = L.

6. Calculate the search direction P^k:

$$P^k = \begin{cases} -\nabla E^k & \text{if} \quad k = 0 \\ -\nabla E^k + \beta^k P^{k-1} & \text{if} \quad k > 0 \end{cases} \tag{1.21}$$

$$\beta^k = \frac{\int_0^{t_f} (\nabla E^k - \nabla E^{k-1}) \nabla E^k dt}{\int_0^{t_f} (\nabla E^{k-1})^2 dt} \tag{1.22}$$

7. Solve the sensitivity problem with $\Delta q = P^k$ at x = L to obtain $\tilde{T}^k$.

8. Calculate the step size α^k with Eq.(1.20).

9. Update to $q^{k+1} = q^k + \alpha^k P^k$.

10. Set k = k + 1, go back to step 2, repeat until convergence criterion $E^k < \varepsilon E^0$ is satisfied.

1.3 Fredholm Equation and SVD method

If source term S(x, t) = 0, we may get the exact solution of direct problem Eq.(1.3) and

(1.4):

$$T(x,t) = \int_0^L f(x)dx + \int_0^t q(\tau)d\tau + 2\sum_{n=1}^{\infty}\left(\int_0^L f(x)\cos(n\pi x)dx\right)e^{-n^2\pi^2 t}\cos(n\pi x) + 2\sum_{n=1}^{\infty}\left(\int_0^t e^{-n^2\pi^2(t-\tau)}(-1)^n q(\tau)d\tau\right)\cos(n\pi x) \tag{1.23}$$

The derivation can be found in [72] or other books of heat transfer or partial differential equations. If we set the initial temperature field T(x, 0) = f(x) = 0, the temperature distribution at the final time

$$\int_0^{t_f} G(x,t)q(t)dt = T(x,t_f) \tag{1.24}$$

$$G(x,t) = 1 + 2\sum_{n=1}^{\infty} e^{n^2\pi^2(t-t_f)}\cos(n\pi)\cos(n\pi x) \tag{1.25}$$

Eq.1.24 is known as *Fredholm equation* of the first kind. q(t) is the unknown function to be solved with T(x, t_f) which is known as "right-hand-side". G(x, t) is called the *kernel*. Eq.(1.24) may be analogous to a matrix equation:

$$[G]\cdot\{q\} = \{T\} \tag{1.26}$$

whose solution is $q = G^{-1}\cdot T$, where $[G]^{-1}$ is the matrix of inverse and [G] is a constant matrix. Matrix [G] and vector {T} can be easily obtained by various numerical techniques such as the trapezoidal method or the Simpson method. Unfortunately, in this problem, it appears that $\det G \approx 0$ and the condition number $N_C \to \infty$, so [G] is a singular matrix and classic techniques such as the Gaussian elimination and LU decomposition can not give a correct inverse of [G]. We then have to adopt the singular value decomposition (SVD) technique. The kernel [G] can be expressed in the following form:

$$[G] = [U]\begin{bmatrix} w_1 & 0 & \cdots & 0 \\ 0 & w_2 & \cdots & 0 \\ 0 & 0 & \ddots & \vdots \\ 0 & 0 & \cdots & w_n \end{bmatrix}[V]^T \tag{1.27}$$

The numbers w_i are the singular values of [G] while the components u_i and v_i are called the *left and right singular vectors* of [G]. And the solution of Fredholm equation is:

$$\{q\} = [V]\left[\text{diag}\left(\frac{1}{w_i}\right)\right]\left([U]^T\{T\}\right) \tag{1.28}$$

As the very small singular values will result in the oscillation of the solution due to the amplification effect of $\frac{1}{w_i}$, we may adopt a simple but effective regularization technique called *truncated singular value decomposition* (TSVD): if $w_i \le \tau$ (τ is an arbitrary small number), let $\frac{1}{w_i} = 0$. Suppose w_k is the first singular value which reaches τ, the integer k is called the truncation parameter. The choice of truncation index is very important: if k is too large, the solution will be too corrupted by noise; if it is too small, too much information about the solution will be lost. Tikhonov regularization is another well-known method: $\frac{1}{w_i}$ is replaced by $\frac{w_i^2}{w_i^2 + \xi^2}\frac{1}{w_i}$ for all the singular values. The regularization parameter (for example τ and ξ) may be chosen by various principles such as Picard condition, L-Curve, discrepancy principle or generalized cross validation (GCV).

It should be noted that the Fredholm equation can also be solved by the conjugate gradient method to minimize the error function E which is defined as follow:

$$E = \frac{1}{2}\left(\{T\} - \{T_E\}\right)^T\left(\{T\} - \{T_E\}\right) + \frac{\xi}{2}\{q\}^T\{q\} \tag{1.29}$$

$\{T_E\}$ is given temperature distribution at $t = t_f$, and $\{T\} = [G]\cdot\{q\}$. It appears that E is a quadratic function of q:

$$E = \frac{1}{2}\left([G]\cdot\{q\} - \{T_E\}\right)^T\left([G]\cdot\{q\} - \{T_E\}\right) + \frac{\xi}{2}\{q\}^T\{q\} \tag{1.30}$$

Let $[H] = [G]^T\cdot[G]$, the gradient of E in the direction of q is thus:

$$\{\nabla E\} = [G]^T\left([G]\cdot\{q\} - \{T_E\}\right) + \xi\{q\} = [H]\cdot\{q\} - [G]^T\{T_E\} + \xi\{q\} \tag{1.31}$$

The boundary heat flux is then determined iteratively by

$$\{q^{k+1}\} = \{q^k\} + \alpha^k \{P^k\} \tag{1.32}$$

with α and P being the step size and the conjugate search direction respectively.

Let $\left.\frac{\partial E}{\partial \alpha}\right|_{\alpha=\alpha^k} = 0$, we must have

$$\{\nabla E^{k+1}\}^T \{P^k\} = 0 \tag{1.33}$$

Substituting Eq.(1.31) and (1.32) into Eq.(1.33),

$$\begin{aligned} &\left([G]^T\left([G]\cdot\{q^{k+1}\} - \{T_E\}\right) + \xi\{q^{k+1}\}\right)^T \{P^k\} \\ &= \left([G]\cdot\{q^k\} + [G]\alpha^k\{P^k\} - \{T_E\}\right)^T [G]\{P^k\} \\ &\quad + \xi(\{q^k\} + \alpha^k\{P^k\})^T\{P^k\} = 0 \end{aligned} \tag{1.34}$$

Considering that α is a scalar, let $\{Q^k\} = [G]\{P^k\}$, we have

$$\begin{aligned} &\left([G]\{q^k\} + \alpha^k\{Q^k\} - \{T_E\}\right)^T \{Q^k\} + \xi(\{q^k\} + \alpha^k\{P^k\})^T\{P^k\} = 0 \\ &\Rightarrow \left([G]\{q^k\} - \{T_E\}\right)^T \{Q^k\} + \xi\{q^k\}^T\{P^k\} = -\alpha^k(\{Q^k\}^T\{Q^k\} + \xi\{P^k\}^T\{P^k\} \\ &\qquad = -\alpha^k(\|Q^k\|^2 + \xi\|P^k\|^2 \end{aligned}$$

Then we obtain the step size

$$\alpha^k = -\frac{\left([G]\{q^k\} - \{T_E\}\right)^T \{Q^k\} + \xi\{q^k\}^T\{P^k\}}{\|Q^k\|^2 + \xi\|P^k\|^2} \tag{1.35}$$

On the other hand, the search direction may be expressed as

$$\{P^k\} = -\{\nabla E^k\} + \beta^k\{P^{k-1}\} \tag{1.36}$$

For conjugate search direction, we must have

$$\{P^k\}^T[H]\{P^{k-1}\} = 0 \tag{1.37}$$

Substituting Eq.(1.36) into Eq.(1.37), we get

$$-\{\nabla E^k\}^T[H]\{P^{k-1}\} + \beta^k\{P^{k-1}\}^T[H]\{P^{k-1}\} = 0 \tag{1.38}$$

and

$$\{\nabla E^k\} - \{\nabla E^{k-1}\} = [H]\left(\{q^k\} - \{q^{k-1}\}\right) = \alpha^{k-1}[H]\{P^{k-1}\}$$

Then

$$\{\nabla E^k\}^T\left(\{\nabla E^k\}-\{\nabla E^{k-1}\}\right)=\beta^k\{P^{k-1}\}^T\left(\{\nabla E^k\}-\{\nabla E^{k-1}\}\right) \text{ or}$$

$$\left(\{\nabla E^k\}-\{\nabla E^{k-1}\}\right)^T\{\nabla E^k\}=\beta^k\left(\{\nabla E^k\}-\{\nabla E^{k-1}\}\right)^T\{P^{k-1}\} \tag{1.39}$$

Because of Eq.(1.33), we have

$$\left(\{\nabla E^k\}-\{\nabla E^{k-1}\}\right)^T\{\nabla E^k\}=-\beta^k\{\nabla E^{k-1}\}^T\{P^{k-1}\}=-\beta^k\{\nabla E^{k-1}\}^T\left(-\{\nabla E^{k-1}\}+\beta^{k-1}\{P^{k-2}\}\right)$$
$$=\beta^k\{\nabla E^{k-1}\}^T\{\nabla E^{k-1}\}=\beta^k\left\|\nabla E^{k-1}\right\|^2$$

The conjugate coefficient β^k is then expressed by the following equality

$$\beta^k=\frac{\left(\{\nabla E^k\}-\{\nabla E^{k-1}\}\right)^T\{\nabla E^k\}}{\left\|\nabla E^{k-1}\right\|^2} \tag{1.40}$$

1.4 Components of Inverse Solution By CGM

Let us set the initial guess $q^0 = 0$ and the regularization parameter $\xi=0$, we then have $\nabla E=-\overline{T}(L,t)$ which can be obtained by solving the adjoint problem (1.12~1.14):

$$\overline{T}^k(x,t)=C_0+\sum_{n=1}^{\infty}C_n e^{n^2\pi^2 t}\cdot\cos(n\pi x) \tag{1.41}$$

$$C_0=\int_0^L\psi(x)dx,\quad C_n=\frac{2\int_0^L\psi(x)\cos(n\pi x)dx}{e^{n^2\pi^2 t_f}}$$
$$\psi(x)=\overline{T}^k(x,t_f)=-\left(T^k(x,t_f)-T_E(x)\right)$$

The gradient of the error function can be expressed by a series of exponential functions:

$$\nabla E^k=b_0+\sum_{n=1}^{\infty}b_n e^{n^2\pi^2(t-t_f)}$$
$$b_0=-\int_0^L\psi(x)dx,\quad b_n=(-1)^{n+1}2\int_0^L\psi(x)\cos(n\pi x)dx \tag{1.42}$$

Since $\psi(x)$ may be an arbitrary continuous function, then b_0 and b_n must be arbitrary real numbers. We may rewrite (1.42) as

$$\nabla E^k = b_0 + b_1 \exp\left(\pi^2 (t - t_f)\right) + b_2 \exp\left(4\pi^2 (t - t_f)\right) + \cdots + b_n \exp(n^2 \pi^2 (t - t_f)) \quad (1.43)$$

Noting that the coefficient β^k that determines the conjugate direction is a constant in each iteration, it follows that the inverse solution obtained by CGM must be a series of exponential functions

$$q(t) = a_0 + a_1 \exp\left(\pi^2 (t - t_f)\right) + a_2 \exp\left(4\pi^2 (t - t_f)\right) + \cdots + a_n \exp(n^2 \pi^2 (t - t_f)) \quad (1.44)$$

here a_0 and a_n are real constants depending on T_E.

If the exact heat flux q(t) is known, and supposing that it could be expressed by an exponential series as (1.44), the coefficients a_0 and a_n may be obtained by least square method numerically. Tables 1.1~1.3 and Figures 1.2a~1.2c present the fitting results of sine profiles for $t_f = 0.1$, $t_f = 0.2$ and $t_f = 1.0$, respectively. It appears that series like Eq.(1.44) may express the sine function with good accuracy for $t_f = 0.1$. However, the fitting curves differ more and more from the exact data as the final time increases. It suggests that it is not possible to recover an arbitrary boundary flux numerically by using CGM for a longer final time than 0.1. This is confirmed by the further numerical tests shown in Figures 1.3a~1.3b. The reconstructed solution for $t_f = 1$ considerably deviates from the exact value, increasing the number of iteration does not improve the results. However, we must point out here that this inaccurate solution can make $\|T - T_E\|$ very small, with a relative error of about 0.01%.

Table 1.1: Fitting Coefficients of Least Square, Exact $q(t) = \sin(10\pi t)$, $t \in [0, 0.1]$

a_0	a_1	a_2	a_3	a_4	a_5	a_6	a_7
-0.0004	0.0013	-0.002	0.0039	-0.011	0.0392	-0.135	0.415
a_8	a_9	a_{10}	a_{11}	a_{12}	a_{13}	a_{14}	
-1.054	2.127	-3.270	3.654	-2.774	1.2686	-0.262	

Table 1.2: Fitting Coefficients of Least Square, Exact $q(t) = \sin(5\pi t)$, $t \in [0, 0.2]$

a_0	a_1	a_2	a_3	a_4	a_5	a_6	a_7
0.000	0.000	0.000	0.0002	-0.001	0.006	-0.033	0.1464
a_8	a_9	a_{10}	a_{11}	a_{12}	a_{13}	a_{14}	
-0.520	1.429	-2.918	4.1903	-3.917	2.1011	-0.484	

Table 1.3: Fitting Coefficients of Least Square, Exact $q(t) = \sin(\pi t)$, $t \in [0, 1]$

a_0	a_1	a_2	a_3	a_4	a_5	a_6	a_7
0.0007	-0.0008	-0.0033	0.0380	-0.2626	1.1110	-2.2427	1.3598

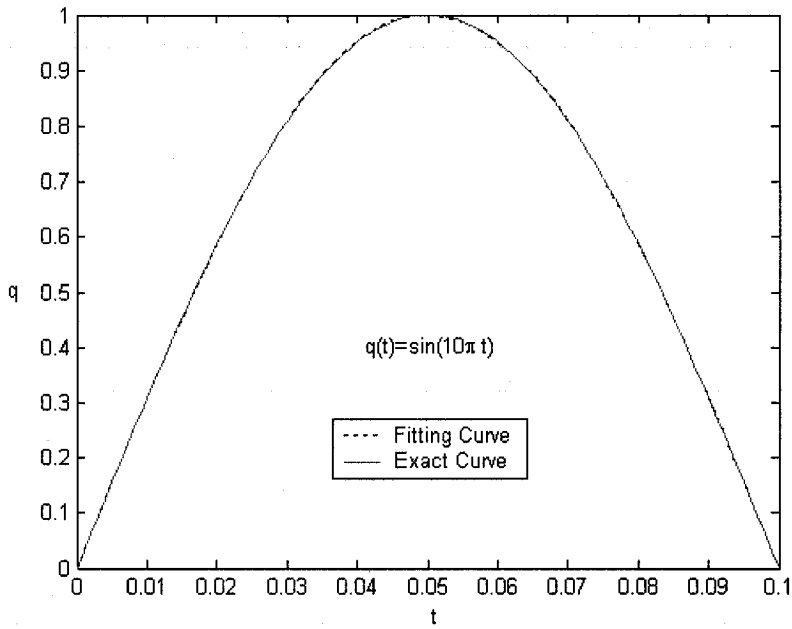

Figure 1.2a: Fitting Curve by LS, $t_f = 0.1$

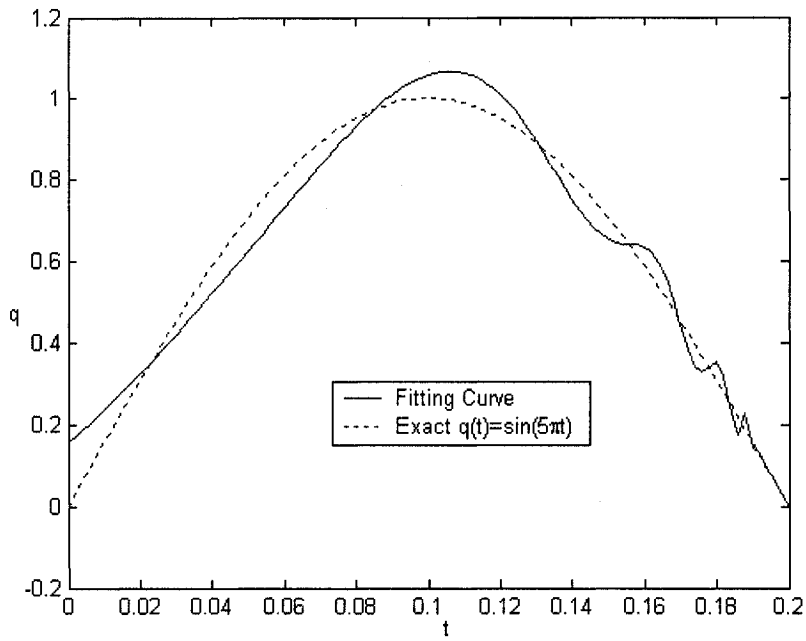

Figure 1.2b: Fitting Curve by LS, $t_f = 0.2$

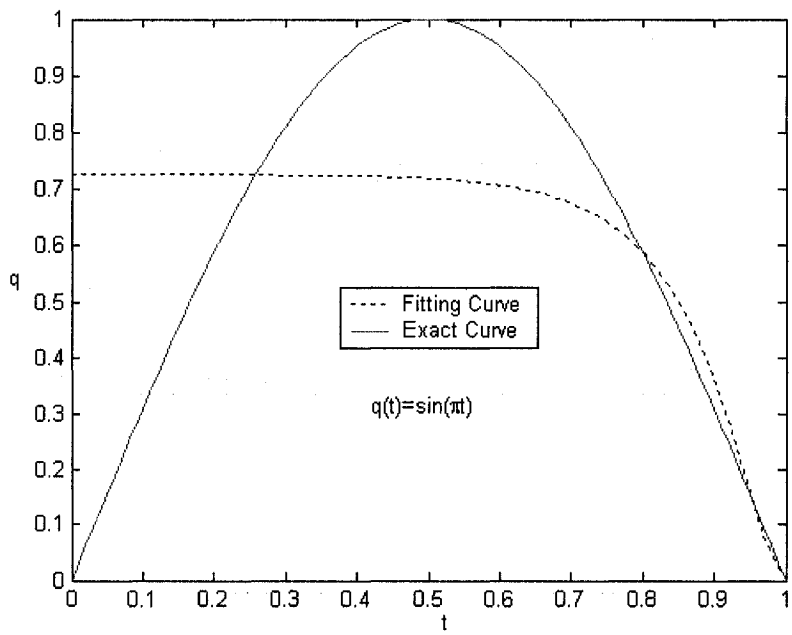

Figure 1.2c: Fitting Curve by LS, $t_f = 1.0$

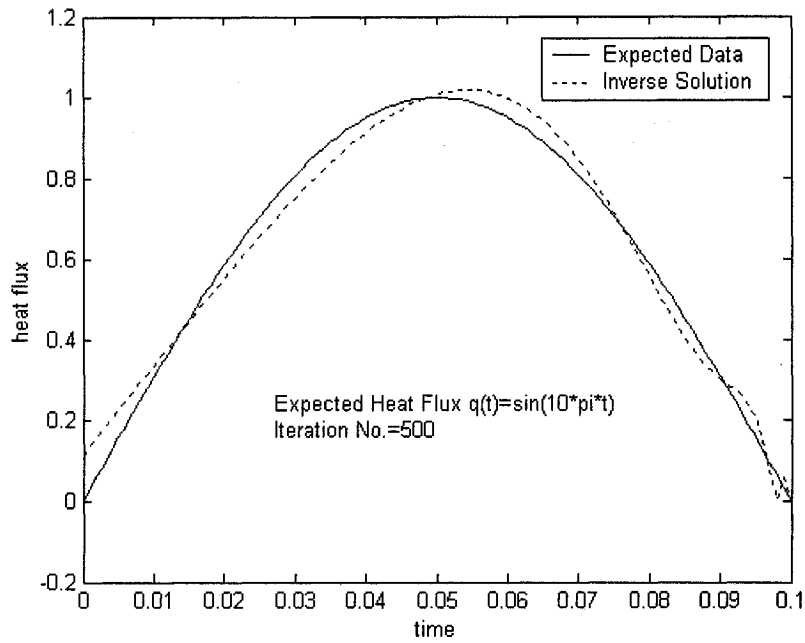

Figure 1.3a: Inverse Solution by CGM, $q(t) = \sin(10\pi t)$, $t_f = 0.1$, $\xi = 0$

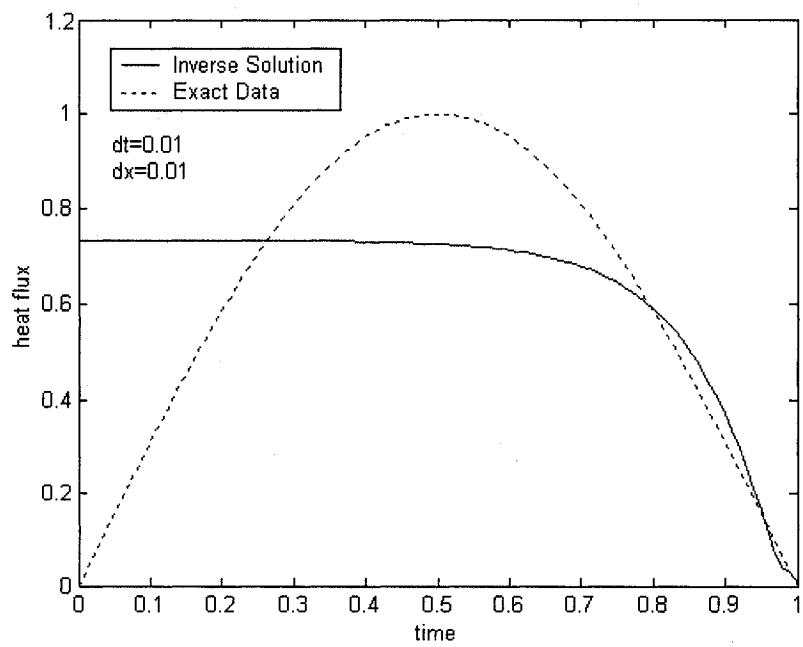

Figure 1.3b: Inverse Solution by CGM, $q(t) = \sin(\pi t)$, $t_f = 1.0$, $\xi = 0$

1.5 Degree of Ill-Posedness

The degree of ill-posedness is one of the most important features of inverse problems. It influences the stability and accuracy of the inverse (reconstructed) solution. Let us look at the Fredholm integral equation where the decay rate of the singular values w_i is an important factor: if it is very fast, the problem is severely ill-posed and vice versa. We may study the ill-posedness of the inverse problem through its kernel [G] which strongly depends on the upper limit of the integral, i.e., the final time t_f. For a "smooth" kernel [G], the decay rate of its singular values must be very fast. FIG.1.4 shows the decay of singular values for different final times. According to the definition of Hofmann [73, 74], it is found that the present inverse problem basically belongs to the severely ill-posed problem because that the decay rates of the singular values are faster than the function exp(-i) if $t_f > 0.1$. On the other hand, it also appears that the decay rate of singular values reduces obviously as the final time decreases. In other words, if the final time is shorter, the inverse problem becomes less ill-posed. This is in agreement with the *discrete Picard condition* (DPC). The DPC requires that the Fourier coefficients $|U^T T|$ decay to zero faster than the singular values w_i, otherwise the DPC is not satisfied and the lack of stability of the solution will make the problem ill-posed. From FIG.1.5a and 1.5b, we can see that DPC is satisfied only for $i < 12$ if $t_f = 1$, and SVD should be truncated at $k = 11$; but if $t_f = 0.1$, the truncation parameter k reaches 20. More tests indicate that if t_f is longer, k should be smaller, and the problem becomes more ill-posed since a too small truncation parameter will result in the loss of accuracy of solution. The concerned results of a numerical test are presented in Figs.1.6a and 1.6b. If k is chosen by DPC namely set $k = 11$, the smooth solution obtained by TSVD is very similar as that obtained by CGM (see FIG.1.3b). If k is set larger, for example at 13, the DPC is no longer satisfied, then the oscillation of solution occurs as expected. It suggests that both CGM and TSVD may pay the price of losing useful information for filtering out the noise. However, if final time is short, for example $t_f \leq 0.1$, it is believed that the problem is probably termed moderately or mildly ill-posed and is possible to be solved.

At $t_f = 0.1$, the heat flux with a classical profile of sine is perfectly reconstructed by utilizing TSVD (see FIG.1.7).

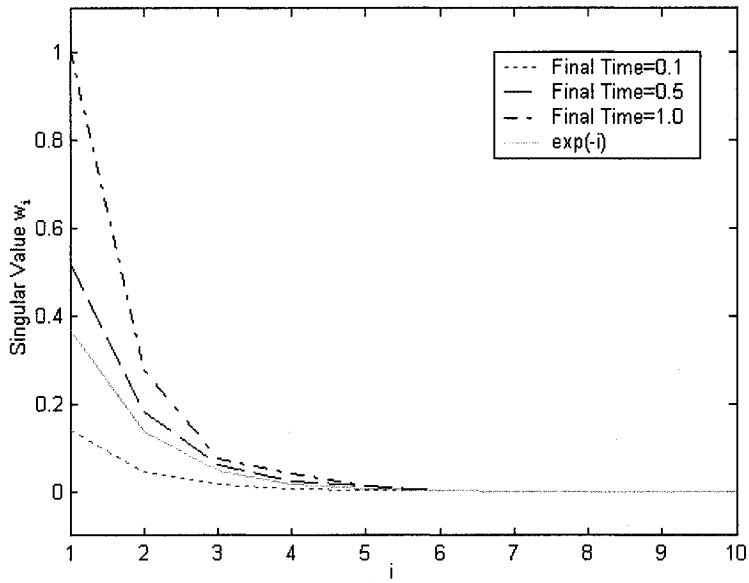

Figure 1.4: Decay Rate of Singular Values, L = 1.0, imax = 100

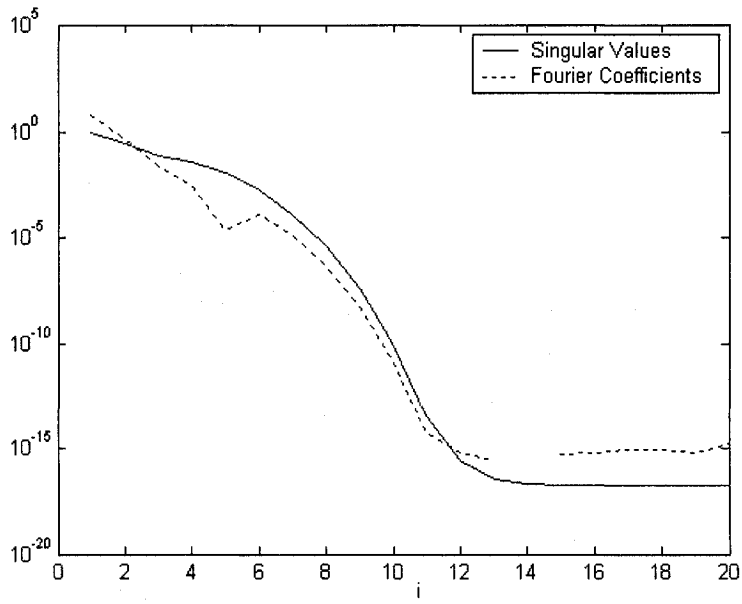

Figure 1.5a: Discrete Picard Condition, $q(t) = \sin(\pi t)$, $t_f = 1$, imax = 100

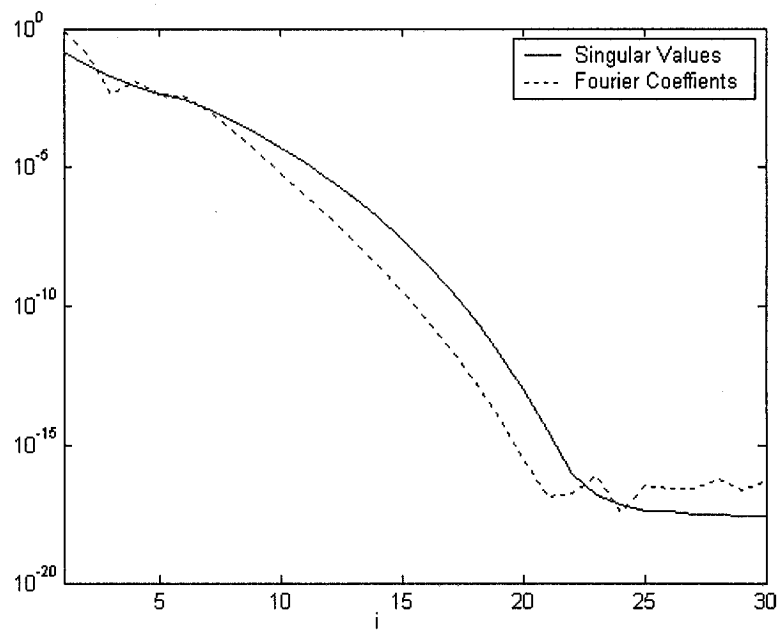

Figure 1.5b: Discrete Picard Condition, $q(t) = \sin(10\pi t)$, $t_f = 0.1$, $i_{max} = 100$

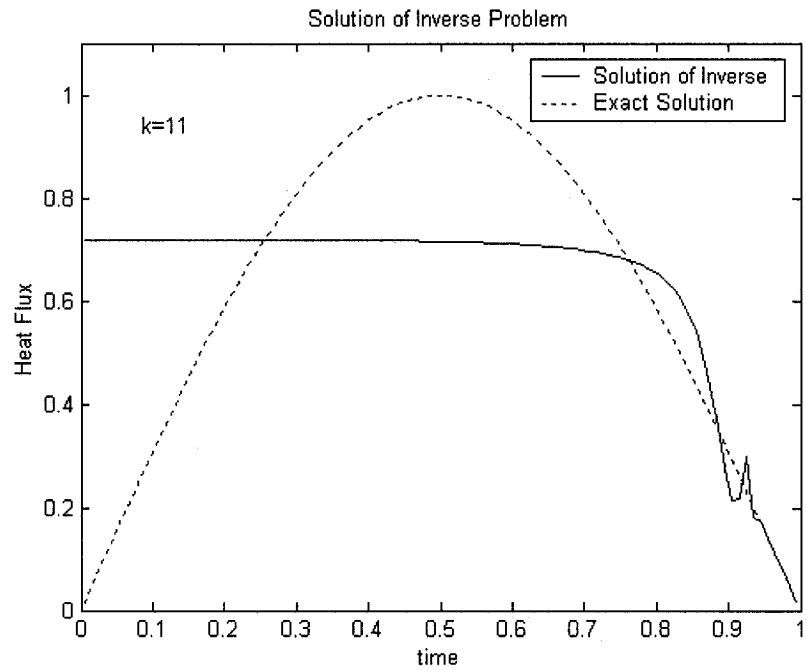

Figure 1.6a: Solution of Inverse Problem, $q(t) = \sin(\pi t)$, $k = 11$, $i_{max} = 100$

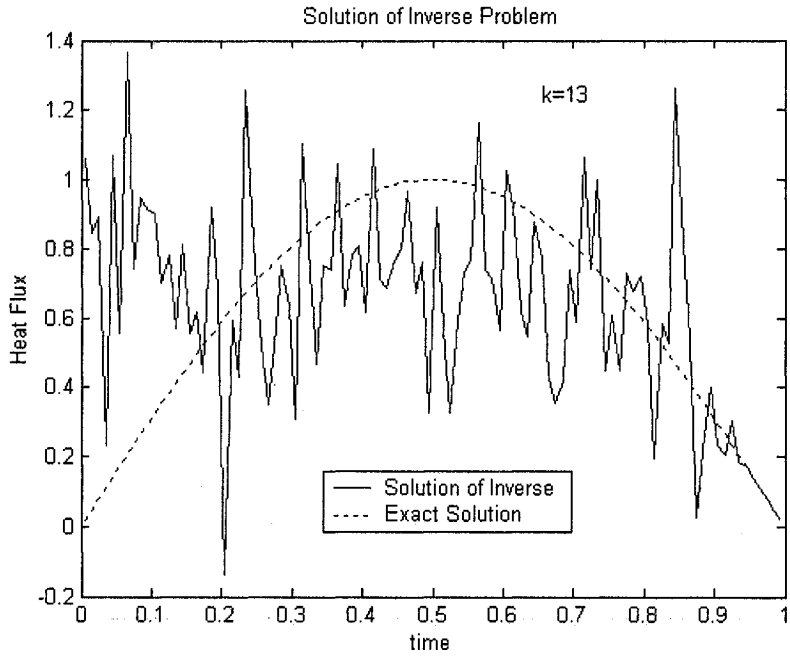

Figure 1.6b: Solution of Inverse Problem, $q(t) = \sin(\pi t)$, k = 13, $i_{max} = 100$

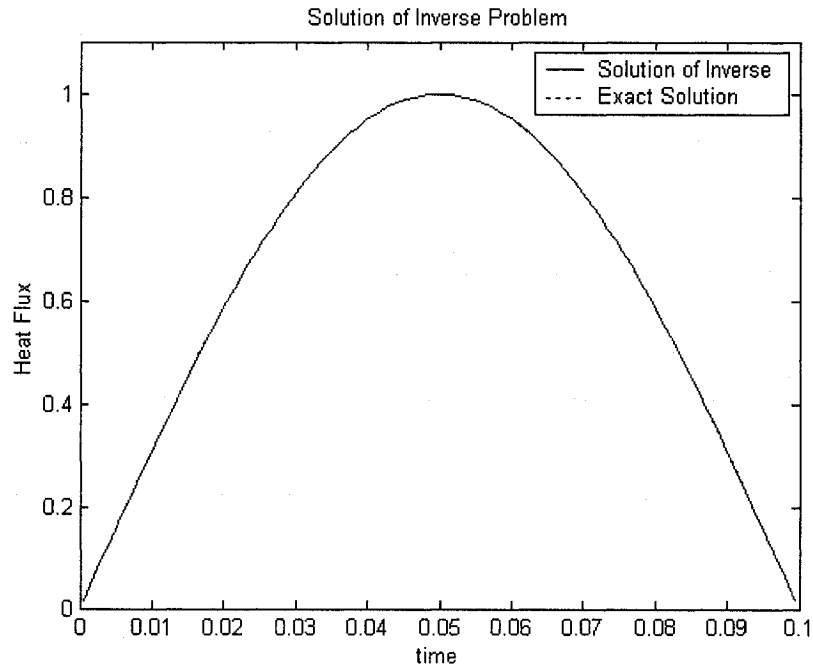

Figure 1.7: Inverse Solution by TSVD, $q(t) = \sin(10\pi t)$, $t_f = 0.1$, k = 20, $i_{max} = 100$

1.6 Modified CGM

The above discussion show that the inverse solution is very difficult to converge to the exact value if the final time is greater than 0.1. Considering that the local minimum points of the error functions may not be unique, only a proper search direction may lead to the unique global minimum (namely the heat flux q that makes the error functional E(q) exactly equal to zero). In fact, a modification of the conjugate direction is found to improve the reconstruction results effectively. This modified CG method [75-78] is based on the assumption that q(t) is a continuously differentiable function defined as

$$q(t) = \int_0^t \frac{dq(t')}{dt'}dt',\ \Delta q(t) = \int_0^t \frac{d\Delta q(t')}{dt'}dt' \tag{1.45}$$

which requires

$$q(t=0) = \Delta q(t=0) = 0 \tag{1.46}$$

Applying the rule of differentiation under the integral sign, we have the identity

$$\frac{d}{dt}\int_{t_f}^{t}\overline{T}(L,t')dt' = \overline{T}(L,t) \tag{1.47}$$

Introducing Eq.(1.47) into Eq.(1.15), we obtain

$$D_{\Delta q}E\left(\frac{dq}{dt}\right) \equiv D_{\Delta q}E(q) = \int_0^{t_f}\left\{\left[\frac{d}{dt}\int_t^{t_f}\overline{T}(L,t')dt'\right]\cdot\Delta q\right\}dt \tag{1.48}$$

Integrating the first term of the right hand side of Eq.(1.48) by parts and rewriting the second term, we get

$$D_{\Delta q}E\left(\frac{dq}{dt}\right) = \left\{\left[\int_t^{t_f}\overline{T}(L,t')dt'\right]\cdot\Delta q\right\}\Bigg|_0^{t_f} - \int_0^{t_f}\frac{d\Delta q}{dt}\left[\int_t^{t_f}\overline{T}(L,t')dt'\right]dt \tag{1.49}$$

Then

$$D_{\Delta q}E\left(\frac{dq}{dt}\right) = \int_0^{t_f}\frac{d\Delta q}{dt}\left[-\int_t^{t_f}\overline{T}(L,t')dt'\right]dt \tag{1.50}$$

By comparing Eq.(1.9) with Eq.(1.50), we have

$$\nabla E\left(\frac{dq}{dt}\right) = -\int_t^{t_f} \overline{T}(L,t')dt' = \int_t^{t_f} \nabla E dt' \tag{1.51}$$

The modified search direction is related to the derivative of the direction of decent R^k by the relation

$$p^k = \int_0^t R^k dt' \tag{1.52}$$

$$R^k = -\nabla E\left(\frac{dq}{dt}\right) + \gamma^k R^{k-1} \tag{1.53}$$

where the conjugate coefficient γ^k is given by Eq. (1.18) and $\nabla E\left(\frac{d\Delta q}{dt}\right)$ takes the place of the gradient of the error functional ∇E:

$$\gamma^k = \frac{\int_0^{t_f}\left[\nabla E^k\left(\frac{dq}{dt}\right) - \nabla E^{k-1}\left(\frac{dq}{dt}\right)\right]\cdot \nabla E^k\left(\frac{dq}{dt}\right)\cdot dx}{\int_0^{t_f}\left[\nabla E^{k-1}\left(\frac{dq}{dt}\right)\right]^2 \cdot dx} \tag{1.54}$$

If we make a modification according to Eq.(1.52), the search direction becomes

$$p^k_{mod}(t) = c_{01}t + c_{02}t^2 + \sum_{n=1}^{\infty}\frac{c_n}{n^2\pi^2}\left[t - \frac{1}{n^2\pi^2}\left(e^{n^2\pi^2(t-t_f)} - e^{-n^2\pi^2 t_f}\right)\right] \tag{1.55}$$

which contains linear and second order components and is thus more adaptable to an arbitrary heat flux than the regular search direction. However, its shortcoming is that $p^k_{mod}(t = 0) = \text{initial guess}$, i.e., the inverse solution must be equal to the initial guess at t = 0.

1.7 Numerical Solutions by CGM and TSVD

1.7.1 Typical Profiles

In this section, we reconstruct some typical profiles during the time interval $0 \le t \le 0.1$. Sine and linear curves are well recovered by CGM and TSVD (see FIG.1.3a, FIG.1.7, FIG.1.8a and FIG.1.8b). However, the iterative CGM may need hundreds of iterations to

arrive at an accurate solution. The process of convergence is slow, and computation time is long. TSVD is a direct regularization method and there exists no iteration process, thus its total calculation time is much shorter. The inverse solutions for the triangular profile are acceptable. Comparing the solutions obtained by TSVD with the solutions obtained by CGM, one can see that the former are better than the latter. It may be due to the fact that the accumulation of numerical errors in the iteration process may affect the accuracy of solutions. As for long pulse heating which is often used in industries, the result is reasonable but its accuracy is not satisfactory. It is obvious that a smooth heat flux q(t) is easier to be recovered than a discontinuous one. The corresponding results are shown in FIG.1.9 and FIG.1.10.

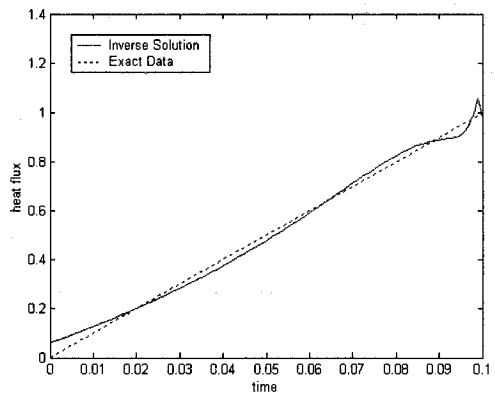

Figure 1.8a: Inverse Solution by CGM,
$q(t) = 10t, \xi = 0$, S(x,t) = 0

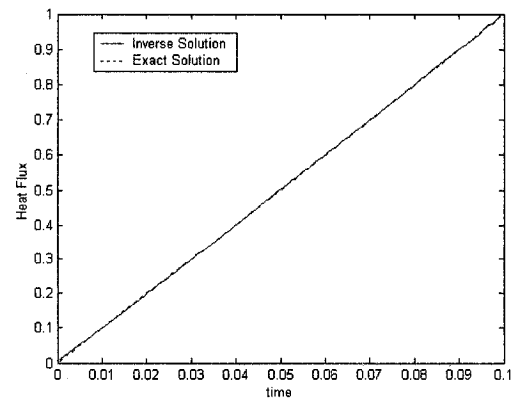

Figure 1.8b: Inverse Solution by TSVD,
$q(t) = 10t, k = 20$, S(x,t) = 0

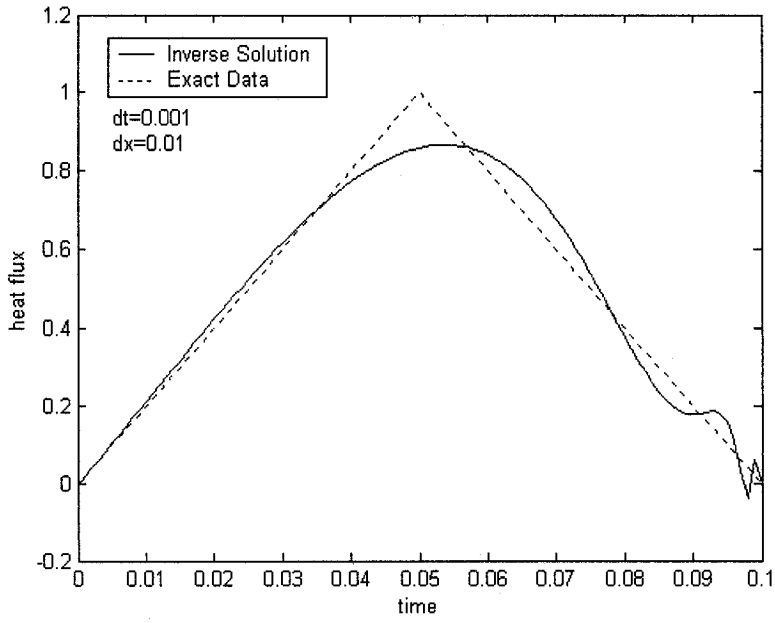

Figure 1.9a: Inverse Solution by CGM, triangular heat flux profile, $\xi = 10^{-7}$, S(x,t) = 0

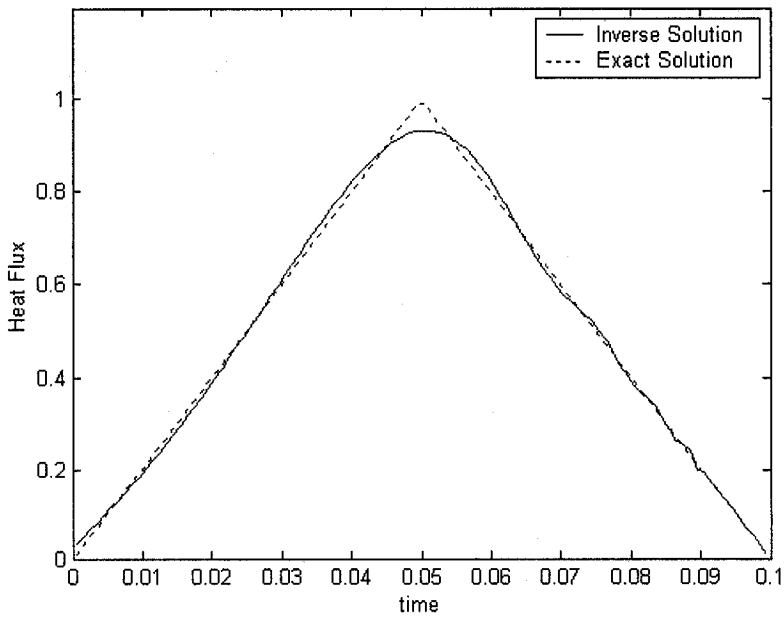

Figure 1.9b: Inverse Solution by TSVD, triangular heat flux profile, k = 20, S(x,t) = 0

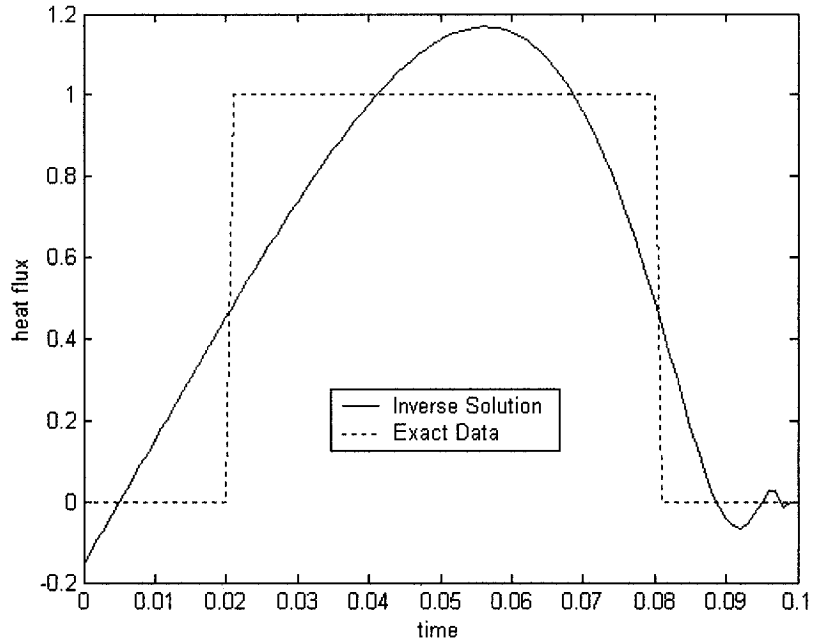

Figure 1.10a: Inverse Solution by CGM, Long pulse heat flux, $\xi = 10^{-7}$, S(x, t)=0

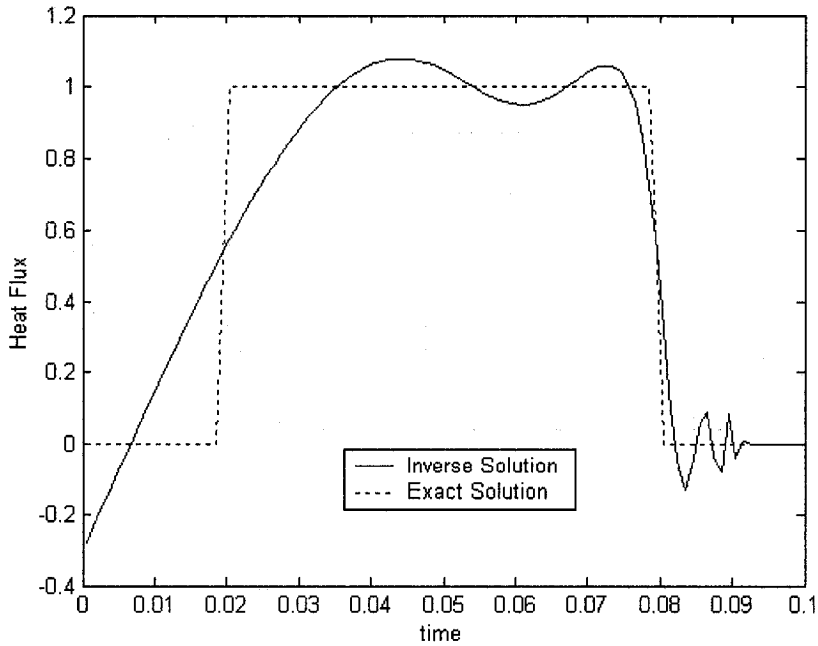

Figure 1.10b: Inverse Solution by TSVD, Long pulse exact heat flux, k = 20, S(x,t) = 0

1.7.2 Effect of Noisy Input Data

In practice, measurement errors can not be avoided. In order to simulate the actual measurements, the noisy data $T_E(1+\sigma\Sigma)$ are used instead of the exact data T_E, where $|\Sigma|<1$ is a uniformly distributed random real number. In ill-posed problems, a slight error in input data may result in a big error in the solution. Comparing FIG.1.11a with FIG.1.11b, it is found that a small error ($\sigma=0.001$) can affect the Picard condition significantly: the decay rate of Fourier coefficient $|U^T T|$ becomes much lower. It makes the problem more ill-posed. Tikhonov regularization is an effective technique to be applied both in CGM and in SVD to stabilize the solutions corrupted by the noisy data. A well-known method of choosing the regularization parameter is the *L-curve criterion* [74, 79]. This method proposes that the optimal regularization parameter that balances the regularization errors and perturbation errors occurs at the "corner" of a plot of solution norm vs. residual norm. Although recently Yagola et al. [80] and some other researchers believed that L-curve method is unreliable even wrong in certain cases, it is found to be applicable in present inverse problems.

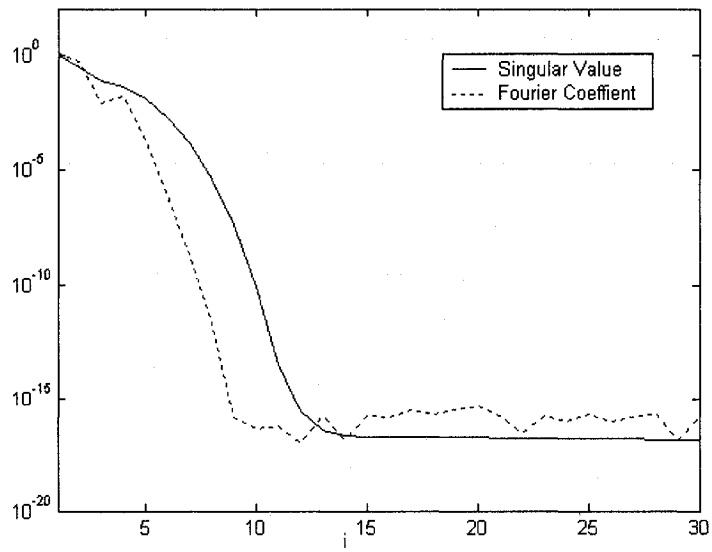

Figure 1.11a: Discrete Picard Condition, $q(t)=\exp[\pi^2(t-t_f)]$,
$t_f=1.0$, $\sigma=0$, $i_{max}=100$

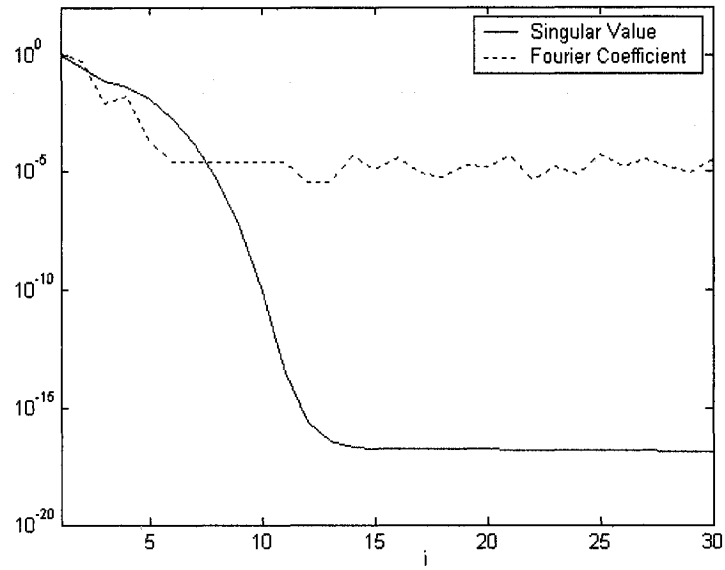

Figure 1.11b: Discrete Picard Condition, $q(t) = \exp[\pi^2(t - t_f)]$,
$t_f = 1.0$, $\sigma = 0.001$, $i_{max} = 100$

Now let us look at the determination of the regularization parameter ξ using the L-curve criterion. FIG.1.12 shows an example of L-curve for SVD algorithm, for supposed exact heat flux $q(t) = 10t$, final time t_f = 0.1 and noise level $\sigma = 0.01$. In Cartesian coordinates, the horizontal direction denotes the residual norm $\|Gq - T_E\|$ and the vertical direction denotes the norm of regularized solution $\|q\|$, we can draw a point for an arbitrary value of ξ. For a set of ξ, we may plot a L-shaped curve. The "corner" point $\xi = 0.001$ is then chosen as the optimal regularization parameter. The corresponding regularized solution shown in FIG.1.13 is very close to the exact data. If ξ is greater or smaller, the reconstructed solution will oscillate or bias the true heat flux. SVD and CGM provide similar solutions even though their regularization parameters are different.

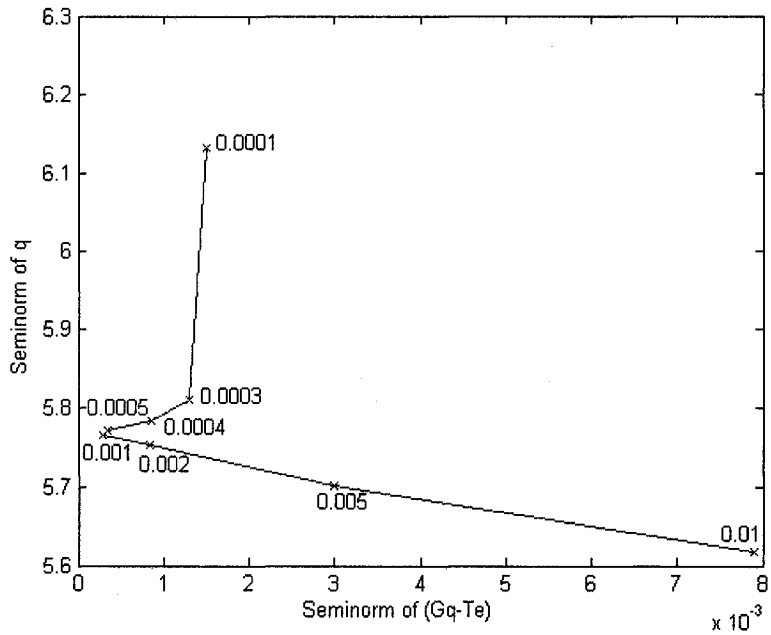

Figure 1.12: L-Curve for SVD, $q(t) = 10t$, Noise level $\sigma = 0.01$

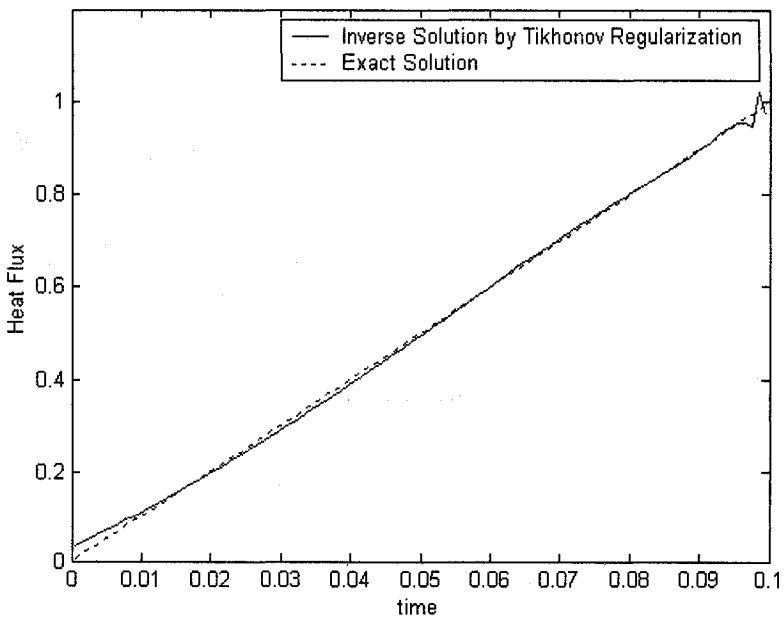

Figure 1.13: Inverse Solution by SVD, $q(t) = 10t$, $\sigma = 0.01$, $\xi = 0.001$

1.7.3 Constrained and Unconstrained Problem

Let's consider the following boundary control problem: the non-dimensional temperature is zero at t = 0, determine the heat flux at active boundary to obtain a temperature distribution as uniform as possible at t_f = 1, supposing T(x, t_f) = 1. Obviously, the exact solution for this problem doesn't exist and the 'optimum' solution is not unique. In engineering practice, the heating process may be limited by several conditions, and we have to deal with a constrained problem.

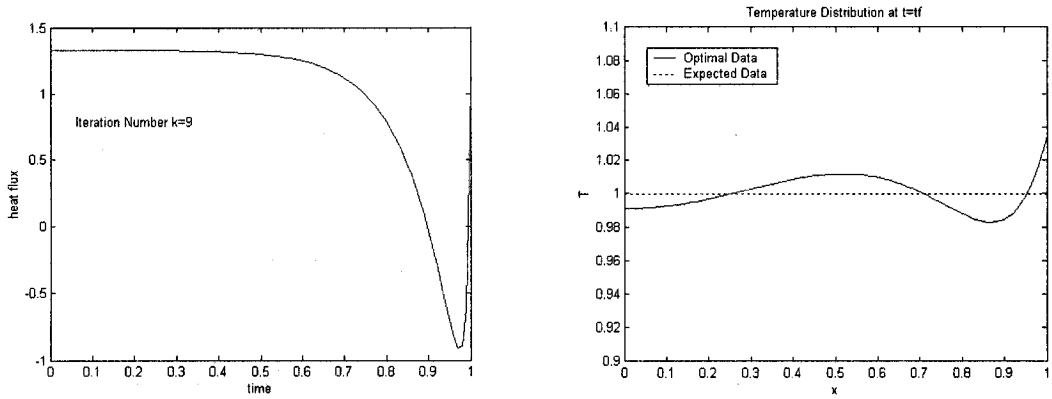

Figure 1.14: Optimal solution for unconstrained problem by regular CGM

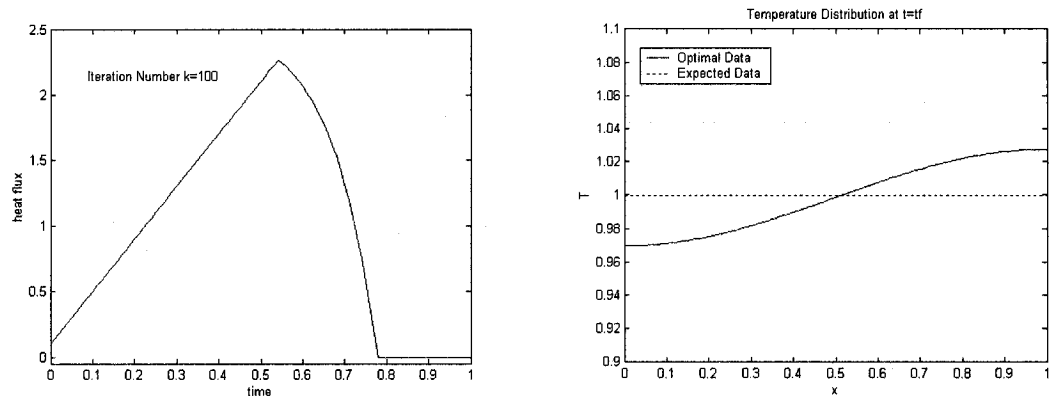

Figure 1.15: Optimal solution for constrained problem by regular CGM

The constraints for boundary heat flux are supposed to be given by $q_{min}(t) = 0$, $q_{max}(t) = 0.1 + 4t$. The optimal solutions for unconstrained and constrained

problem are respectively illustrated in Figs.1.14 and 1.15. For the former, the relative error $E_r = \|T - T_E\| / \|T_E\|$ is about 0.91% after 9^{th} iteration; for the latter, $E_r = 2.04\%$ and the number of iteration increases to 100. This suggests that the constrained problem is harder to solve.

1.8 Numerical Solutions by Modified CGM

1.8.1 Typical Profiles

In this section, we reconstruct some typical profiles using modified CG method. Figs.1.16-1.17 show that linear and sine curves are well recovered by a combination of the modified and regular CGM. We start the iteration process with the modified CGM until a reasonable profile of heat flux is attained. Afterwards, the regular CGM is employed to accelerate the convergence. The estimation by the modified CGM is treated as the initial guess value. It is found that the accuracy of the solution is not affected too much by the final time. The inverse solutions shown in Fig.1.18 and Fig.1.19 with the triangular and trapezoidal profiles are acceptable but their accuracies are not good.

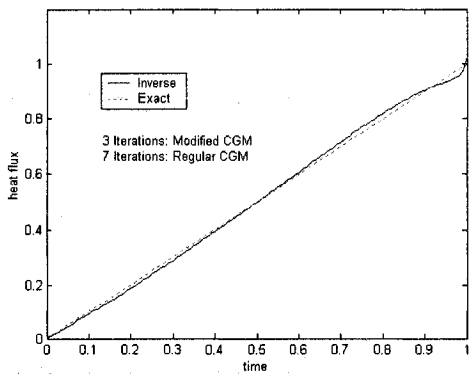

Figure 1.16: Inverse solution by MCGM, Linear heat flux profile

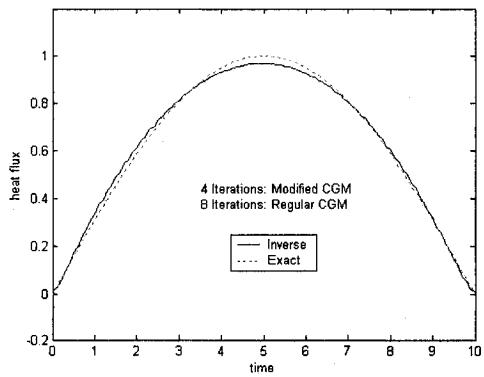

Figure 1.17: Inverse solution by MCGM, sinusoidal heat flux profile

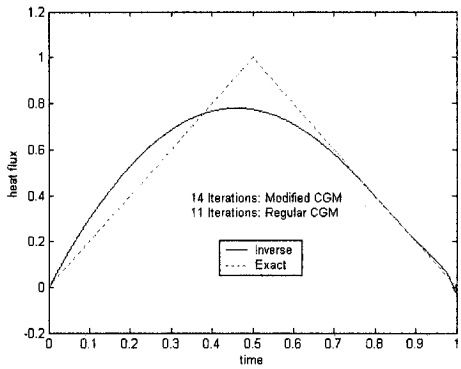

Figure 1.18: Inverse solution by MCGM, triangular heat flux profile

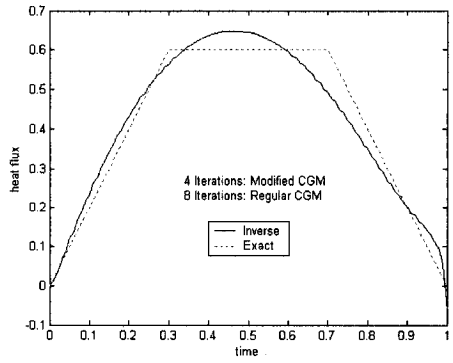

Figure 1.19: Inverse solution by MCGM, trapezoidal heat flux profile

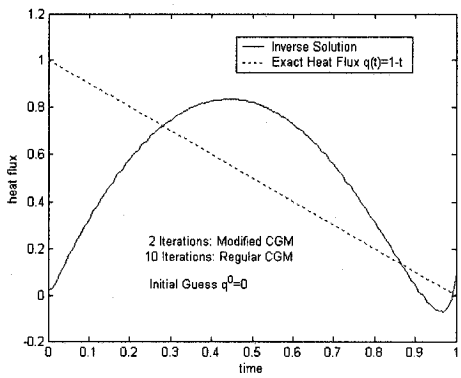

Figure 1.20: Inverse solution by MCGM, q(t) = 1-t, t_f = 1.0, initial guess = 0

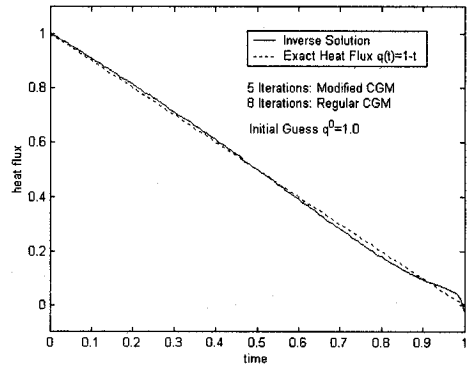

Figure 1.21: Inverse solution by MCGM, q(t) = 1-t, t_f = 1.0, initial guess = 1.0

The modified CGM is based on the assumption $q(t) = \Delta q(t = 0) = 0$ which makes the search direction $P^k(t = 0) = 0$. If the exact heat flux at t = 0 is not equal to the initial guess value, the inverse solution will deviate from the exact profile because this method cannot find the correct values near the initial time (see Fig.1.20). However, if q(t = 0) is known, this difficulty may be alleviated by setting it as the initial guess (Fig.1.21). In engineering practice, the exact heat flux at t = 0 is not known, but a possible range may be given. The numerical tests show that an acceptable solution can be obtained even with an error of $\pm 20\%$ in the initial guess.

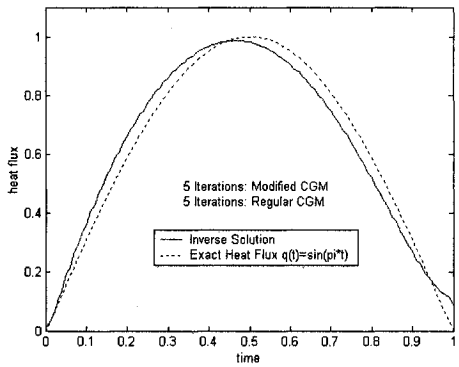

Figure 1.22a: Inverse solution by MCGM, sinusoidal profile

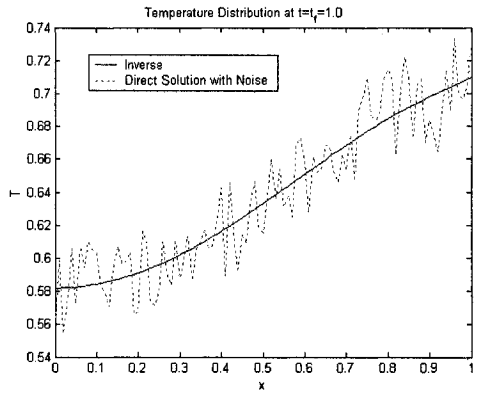

Figure 1.22b: Final temperature distribution with relative error $\sigma = 5\%$

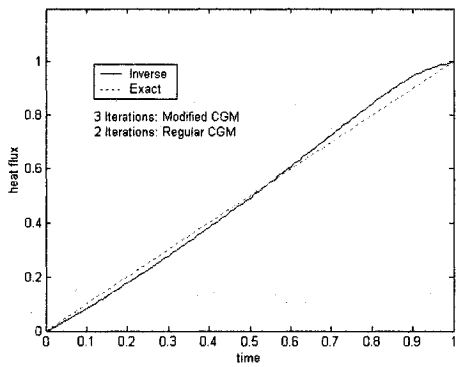

Figure 1.23a: Inverse solution by MCGM, linear profile

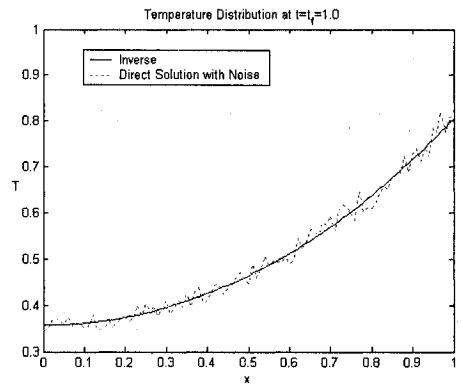

Figure 1.23b: Final temperature distribution with relative error $\sigma = 5\%$

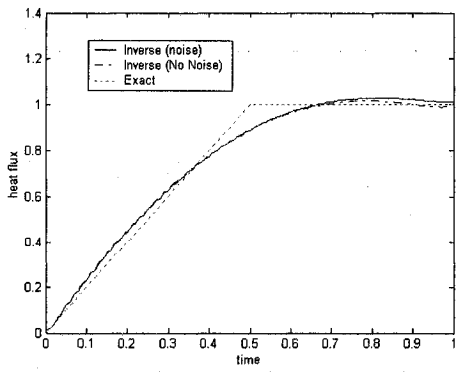

Figure 1.24a: Inverse solution by MCGM, trapezoidal profile

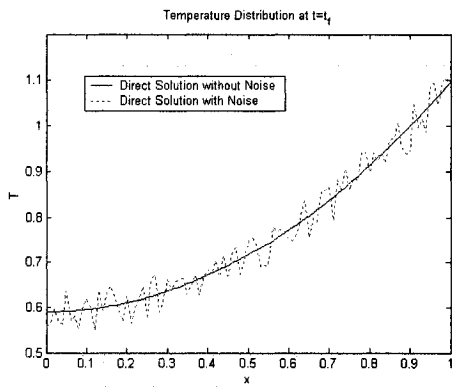

Figure 1.24b: Final temperature distribution with absolute error $\sigma = 5\%$, $T_{max} = 1.2$

1.8.2 Effect of Noisy Input Data

In order to simulate the errors in actual measurements, data with relative errors $T_E(1+\sigma\Sigma)$ or with absolute errors $T_E + T_{max}\sigma\Sigma$ are used instead of the exact value T_E, where $|\Sigma| < 1$ is a uniformly distributed random real number and T_{max} is the maximum range of the measurement device. Since the CGM has self-regularizing power, the Tikhonov regularization is not always necessary, although it may stabilize the solution effectively. In this section, the regularization parameter is set to zero. The numerical tests indicate that a maximum relative error of 5% and a maximum absolute error of $0.05T_{max}$ do not affect the accuracy of the inverse solution significantly (FIG.1.22, FIG.1.23 and FIG.1.24).

1.8.3 Optimal Control Problem

In this section, we resolve the same unconstrained boundary control problem as which has been solved in section 1.7.3, by using modified CGM. The solutions obtained by the regular and modified CGM are respectively illustrated in Fig.1.14 and Fig.1.25. For the former, the relative error $E_r = \|T - T_E\| / \|T_E\|$ is about 0.91% after 9 iterations; for the latter, E_r is only 0.51% after 8 iterations. In addition, to achieve a uniform temperature distribution at the final time, the heat flux at the beginning of heating process should be as high as possible. Suppose the maximum possible heat flux q_{max}=1.75, and set it as the initial guess, the modified CGM gives a better solution with a relative error of 0.28% as shown in Fig.1.26. This suggests that the modified method may provide better solutions than regular CGM.

On the other hand, it is found that the convergence may be very difficult after 8 iterations if the final time is equal to 1.0, i.e., the error functional will not decrease as the iteration number is increased further. If we alternate the search directions, e.g. gradient direction (steepest descent method) and conjugate gradient direction, the

convergence performance will be improved significantly and a better solution can be obtained, where the relative error may decrease further up to 0.05%, can be obtained. As the solution of this optimization problem is not unique, the alternating search direction technique may avoid some "bad" points to reach a better one.

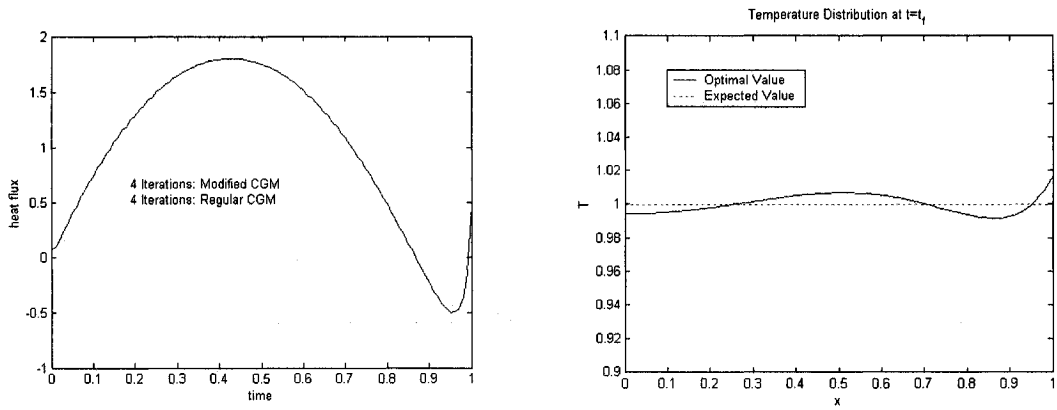

Figure 1.25: Optimal solution by modified CGM, initial guess = 0

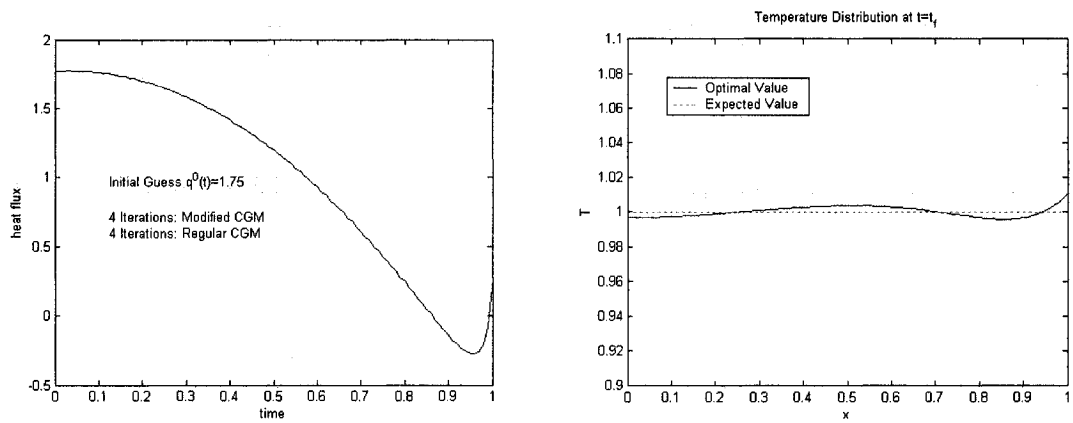

Figure 1.26: Optimal solution by modified CGM, initial guess = 1.75

As expected, the heating process is longer, the final temperature distribution is more uniform. If the final time is infinite, the temperature distribution may be absolutely uniform. However, industrial heating requires as short a heating time as possible to achieve a high production rate. Fig.1.27 presents the relationship between the final time and the relative error. The corner of the L-shaped curve is the optimum point. For regular CGM or modified CGM, the optimum final time is 0.5.

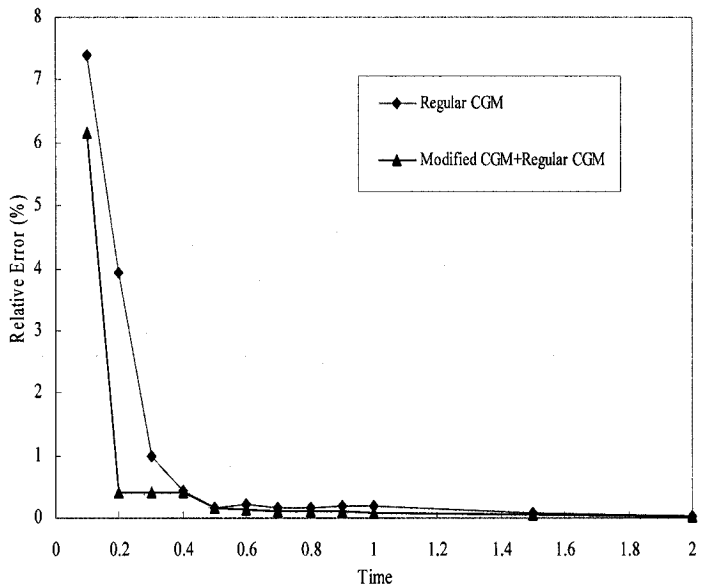

Figure 1.27: Relative error vs dimensionless final time

Now let us consider a real engineering example: control the heating process of an aluminum billet with a diameter of 76mm from 20 °C to 580 °C in 170 seconds, in such way that the final temperature should be as uniform as possible. Because the final temperature is much lower than the melting point of aluminum (660.2 °C), there is no phase change during this process. The thermo-physical properties are assumed to be constants: $k = 233\,W/m\cdot^\circ C$, $\rho = 2640\ kg/m^3$, $c_p = 1030\,J/kg\cdot^\circ C$. The dimensionless time corresponding to 170 seconds is thus about 10. Supposing the ambient temperature $T_\infty = 20^\circ C$ and setting the reference temperature $\Delta T = \frac{Q_{ref} L}{k} = 560^\circ C$, the

dimensionless temperatures 0 and 1 would correspond to 20°C and 580°C , respectively. Both regular CGM and modified CGM may provide an optimal heating strategy (Figs.1.28a and 1.29a). However, the latter scheme is easier to realize than the former because it is smoother and no cooling period is needed. Comparing Fig.1.28b with Fig.1.29b, it is found that modified CGM leads to much better temperature uniformity than regular CGM during the period $8 \le t \le 10$. At the final time t = 10, a relative error E_r of 0.006% and of 0.02% is achieved by modified CGM and regular CGM, respectively. This indicates that the gradually descending profile of heat flux is more effective to eliminate the thermal gradient.

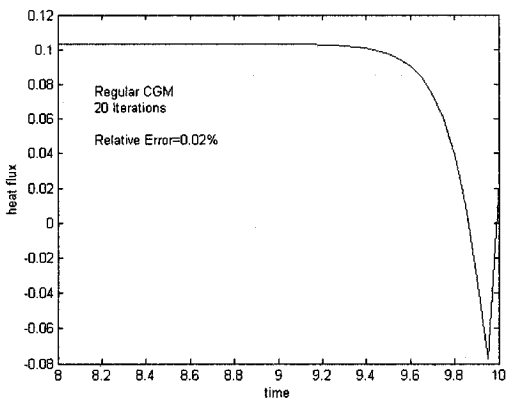

Figure 1.28a: Optimal solution by regular CGM

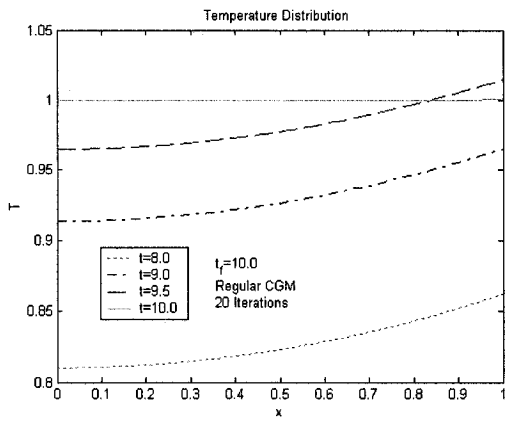

Figure 1.28b: Evolution of temperature distribution, regular CGM

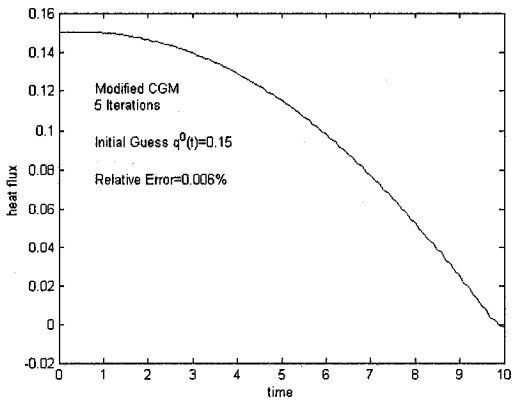

Figure 1.29a: Optimal solution by modified CGM

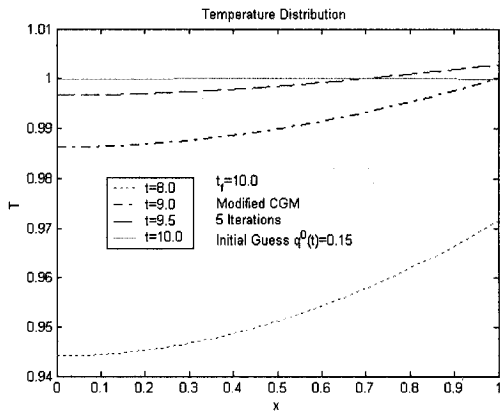

Figure 1.29b: Evolution of temperature distribution, modified CGM

1.9 Influence of Heat Flux Profiles

According to the previous discussion, it seems that we may recover an arbitrary profile of boundary heat flux by using CGM and SVD for a final time around 0.1, and by using modified CGM for an arbitrary final time. In fact, the number of extreme points of heat flux profile is an important factor which may affect the maximum reconstructable time $(t_f)_{max}$. Now let's consider the following profiles of boundary heat flux:

Profile 0: monotonous curve
Profile 1: containing 1 extreme point
Profile 2: containing 2 extreme points
Profile 3: containing 3 extreme points
Profile 4: containing 4 extreme points
Profile 5: containing 5 extreme points

Table 1.4: Influence of Extreme Points

Profile	Example	Regular CGM and SVD	Modified CGM
0	$q(t)=\sin(0.5\pi t/t_f)$	$(t_f)_{max}\approx 0.2$	$(t_f)_{max}>10$
1	$q(t)=\sin(\pi t/t_f)+\cos(\pi t/t_f)-1.0$	$(t_f)_{max}\approx 0.1$	$(t_f)_{max}\approx 1.0$
2	$q(t)=\cos(2\pi t/t_f+0.5\pi)$	$(t_f)_{max}\approx 0.1$	$(t_f)_{max}\approx 0.4$
3	$q(t)=\sin(3\pi t/t_f)$	$(t_f)_{max}\approx 0.1$	$(t_f)_{max}\approx 0.15$
4	$q(t)=\cos(4\pi t/t_f+0.5\pi)$	$(t_f)_{max}\approx 0.065$	$(t_f)_{max}\approx 0.07$
5	$q(t)=\sin(5\pi t/t_f)$	$(t_f)_{max}\approx 0.05$	$(t_f)_{max}\approx 0.05$

From Table 1.4, it is obvious that $(t_f)_{max}$ reduces gradually as the number of extreme point increases. Figs.1.30~1.35 show the inverse solutions obtained by modified CGM with various profiles. This modified method may recover the monotonous profiles for an arbitrary final time. If the exact heat flux contains high frequency components, a reasonable reconstructed solution can be obtained only in a very short time. We must note that the modified CGM is an effective approach which might extend the maximum time of reconstruction much longer if the initial value of heat flux is given.

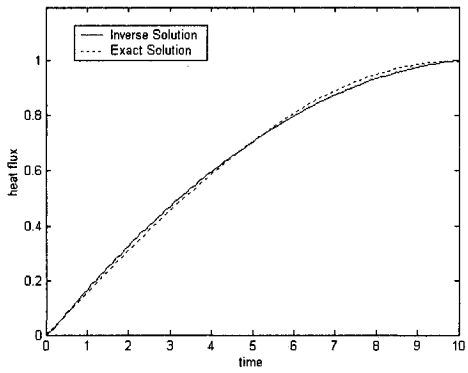

Figure 1.30: Inverse solution by MCGM, $q(t) = \sin(0.05\pi t)$

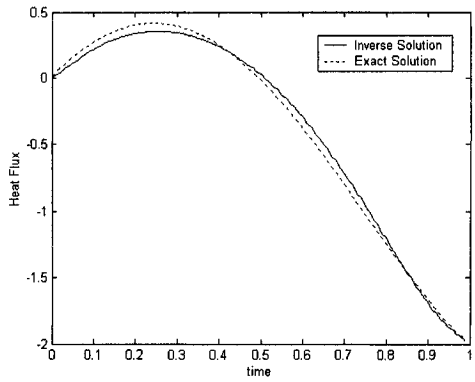

Figure 1.31: Inverse solution by MCGM $q(t) = \sin(\pi t) + \cos(\pi t) - 1.0$

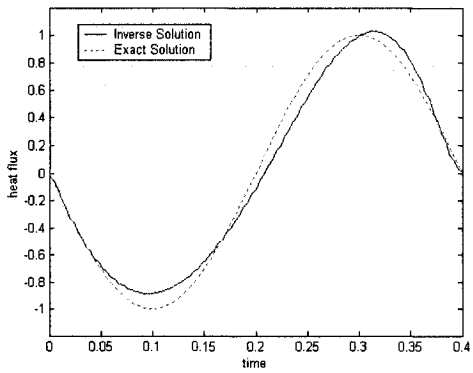

Figure 1.32: Inverse solution by MCGM, $q(t) = \sin(5\pi t)$, t_f=0.4

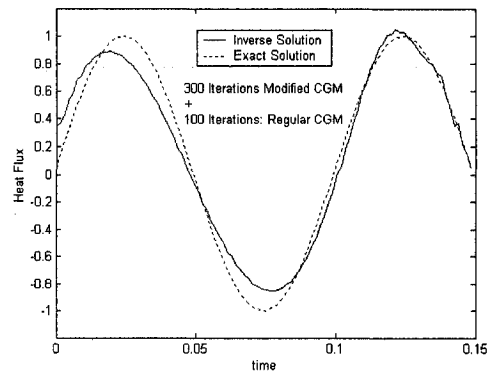

Figure 1.33: Inverse solution by MCGM $q(t) = \sin(20\pi t)$, $t_f = 0.15$

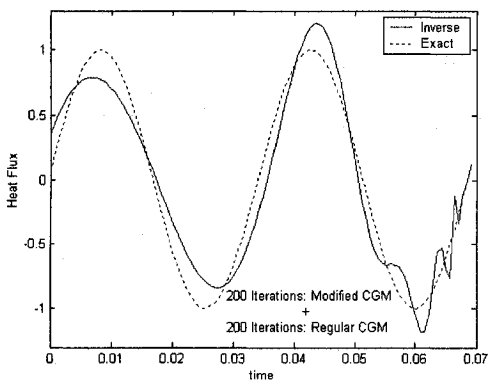

Figure 1.34: Inverse solution by MCGM, $q(t) = \sin(58\pi t)$, $t_f = 0.07$

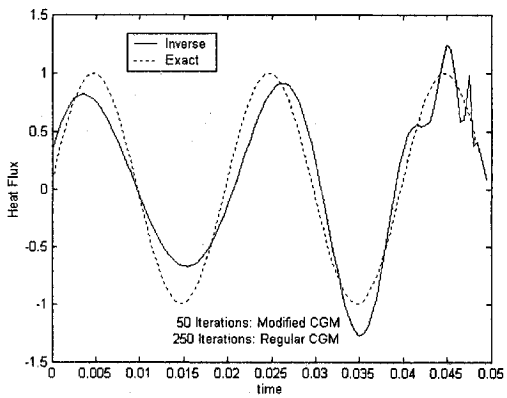

Figure 1.35: Inverse solution by MCGM $q(t) = \sin(100\pi t)$, $t_f = 0.05$

CHAPTER II

INVERSE BOUNDARY HEAT FLUX PROBLEM OF NATURAL CONVECTION IN A POROUS MEDIUM

In order to test the adaptability of CG method, we extend the inverse problem discussed in previous chapter to a two-dimensional system of natural convection in a porous medium.

2.1 Problem Definition and Formulation

Let us consider a two-dimensional inverse natural convection problem in saturated porous medium. The domain geometry and boundary conditions are summarized in Fig.2.1. Ω and C stand respectively the domain surface and the boundaries; C_a is the active boundary (left wall). The right, top and bottom boundaries are assumed to be insulated and the initial temperature field is assumed to be known. Our objective is to determine the unknown heat flux at x = 0 over the time interval $0 \leq t \leq t_f$ from the temperature distribution at the final time of heating process.

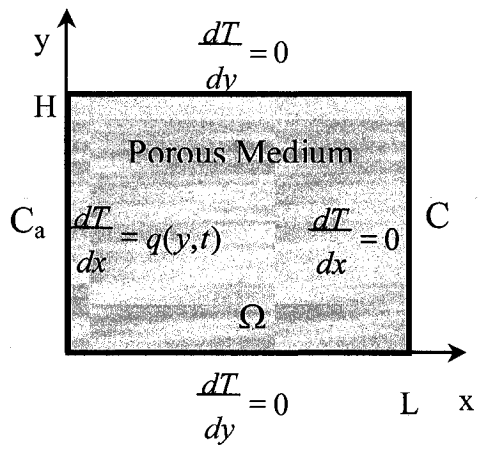

Figure 2.1: Geometry and boundary conditions

Dimensionless equations may be obtained for this problem by scaling length, velocity, temperature, and time defined as

$$T^* = \frac{T - T_0}{\Delta T},\ u^* = \frac{Hu}{\alpha},\ v^* = \frac{Hv}{\alpha}$$
$$x^* = \frac{x}{H},\ y^* = \frac{y}{H},\ t^* = \frac{\alpha t}{\sigma H^2} \tag{2.1}$$

respectively, where all properties are taken as constants evaluated at some reference temperature T_0. Omitting the superscript "*" from now, and substituting Eq.(2.2) into Eq.(2.1), the governing equations for temperature and stream function within the porous medium can then be expressed in conservative form as

$$\frac{\partial T}{\partial t} + \nabla \cdot (\mathbf{u}T - \nabla T) = 0$$
$$\nabla^2 \psi = -Ra \frac{\partial T}{\partial x} \tag{2.2}$$

where $Ra = \beta_T g k H \Delta T / \nu \alpha_T$ is the Rayleigh number. Solving the inverse problem for the unknown heat flux $q(y, t)$ is an iterative process, based on a sequence of approximations $q^1, \ldots q^k$, and so on, from initial guess value q^0. It requires minimizing the error which is defined as

$$E(q) = \frac{1}{2} \int_\Omega [T(x, y, t_f) - T_E(x, y)]^2 \, d\Omega \tag{2.3}$$

where T and T_E stand respectively for the temperature predicted from the approximation for q and the given temperature at the final time. The sequence of approximations for q is generated by conjugate gradient according to $q^{k+1} = q^k + \alpha^k p^k$, where α^k is the step size and p^k is the conjugate search direction, as summarized in the solution algorithm below. The search direction is related to the gradient of E with respect to q, which can not be computed in the usual way without making assumptions about the shape of the function. The gradient of E, as well as the step size α, are obtained instead by solving the adjoint and sensitivity equations.

2.1.1 Sensitivity Equations

Let us again introduce the definition of temperature sensitivity $\tilde{T}$ as the directional derivative of T at q in the direction Δq

$$\tilde{T} = \lim_{\varepsilon \to 0} \frac{T(q + \varepsilon \Delta q) - T(q)}{\varepsilon} \tag{2.4}$$

and similarly for other variable

$$\tilde{\psi} = \lim_{\varepsilon \to 0} \frac{\psi(q + \varepsilon \Delta q) - \psi(q)}{\varepsilon} \tag{2.5}$$

it is straightforward to derive from Eq.(2.2) that the temperature and stream function sensitivities are solutions of the set of equations

$$\begin{aligned} &\frac{\partial \tilde{T}}{\partial t} + \nabla \cdot \left(\mathbf{u}\tilde{T} + \tilde{\mathbf{u}}T \right) = \nabla^2 \tilde{T} \\ &\nabla^2 \tilde{\psi} = -Ra \frac{\partial \tilde{T}}{\partial x} \end{aligned} \tag{2.6}$$

The boundary condition for the stream function sensitivity remains identical with that of the direct problem, namely $\tilde{\psi} = \psi = 0$. It is further shown that the temperature sensitivity must satisfy the homogeneous counterparts of the direct variables boundary condition, except for $\tilde{T}$ at x = 0, where $\left.\frac{\partial \tilde{T}}{\partial x}\right|_{x=0} = \Delta q$. All the sensitivity variables at the initial state are equal to zero, namely $\tilde{T}|_{t=0} = 0$, $\tilde{\psi}|_{t=0} = 0$.

2.1.2 Adjoint Equations

Starting from Eq.(2.3), the directional derivative of E in the direction Δq is defined as

$$D_{\Delta q} E(q) = \int_{\Omega} \tilde{T}(T - T_E) d\Omega \tag{2.7}$$

Introducing the adjoint temperature $\overline{T}$ and stream function $\overline{\psi}$ as Lagrange multipliers

for the sensitivity equations Eq.(2.6) , it is possible to rewrite Eq.(2.7) as

$$D_{\Delta q}E(q) = \int_{\Omega} \tilde{T}\cdot(T - T_E)d\Omega + \int_0^{t_f}\int_{\Omega} \overline{T}\left[\frac{\partial \tilde{T}}{\partial t} + \nabla\cdot\left(\mathbf{u}\tilde{T} + \tilde{\mathbf{u}}T\right) - \nabla^2\tilde{T}\right]d\Omega\, dt$$
$$+ \int_0^{t_f}\int_{\Omega} \overline{\psi}\left(\nabla^2\tilde{\psi} + Ra\frac{\partial \tilde{T}}{\partial x}\right)d\Omega\, dt \qquad (2.8)$$

By using the Green's identities, the divergence theorem, the impermeability condition on the boundary, and the boundary conditions of sensitivity equations, it is shown that Eq.(2.8) above is in fact equivalent to

$$D_{\Delta q}E(q) = \int_{\Omega} \tilde{T}(T - T_E)d\Omega + \int_0^{t_f}\int_{\Omega}\left\{\overline{T}\frac{\partial \tilde{T}}{\partial t} - \tilde{T}\nabla\cdot\left(\mathbf{u}\overline{T} + \nabla\overline{T}\right) - T(\tilde{\mathbf{u}}\cdot\nabla)\overline{T}\right\}d\Omega dt$$
$$+ \int_0^{t_f}\int_{\Omega}\left(\tilde{\psi}\nabla^2\overline{\psi} + Ra\overline{\psi}\frac{\partial \tilde{T}}{\partial x}\right)d\Omega dt - \int_0^{t_f}\int_C \overline{T}\frac{\partial \tilde{T}}{\partial n}dl dt + \int_0^{t_f}\int_C \overline{\psi}\frac{\partial \tilde{\psi}}{\partial n}dl dt \qquad (2.9)$$

If one assumes that the adjoint stream function $\overline{\psi}$ and the adjoint flux $\frac{\partial \overline{T}}{\partial n}$ are equal to zero on the boundary C, namely:

$$\overline{\psi}\big|_C = 0, \quad \left.\frac{\partial \overline{T}}{\partial n}\right|_C = 0 \qquad (2.10)$$

then the fourth and fifth terms in right hand side of Eq. (2.9) must satisfy

$$\int_0^{t_f}\int_C \overline{\psi}\frac{\partial \tilde{\psi}}{\partial n}dl dt = 0$$
$$\int_0^{t_f}\int_C \overline{T}\frac{\partial \tilde{T}}{\partial n}dl dt = -\int_0^{t_f}\int_{C_a} \overline{T}\Delta q dl dt \qquad (2.11)$$

Considering the initial condition of sensitivity equations, we also have

$$\int_0^{t_f}\int_\Omega \overline{T}\frac{\partial \widetilde{T}}{\partial t}d\Omega dt = \int_\Omega \left(\overline{T}\widetilde{T}\right)\Big|_{t_f} d\Omega - \int_0^{t_f}\int_\Omega \widetilde{T}\frac{\partial \overline{T}}{\partial t}d\Omega dt$$
$$\int_0^{t_f}\int_\Omega Ra\overline{\psi}\frac{\partial \widetilde{T}}{\partial x}d\Omega dt = -Ra\int_0^{t_f}\int_\Omega \widetilde{T}\frac{\partial \overline{\psi}}{\partial x}d\Omega dt \qquad (2.12)$$

Additional, from the definition of stream function, we have

$$T(\widetilde{\mathbf{u}}\cdot\nabla)\overline{T} = \widetilde{\psi}\frac{\partial(T,\overline{T})}{\partial(x,y)} - \nabla_n \times \left(T\widetilde{\psi}\nabla\overline{T}\right) \qquad (2.13)$$

It follows from Eqs.(2.11-2.13), using Green's theorem and the boundary conditions on the sensitivity stream function, we may rewrite Eq.(2.9) as

$$\begin{aligned} D_{\Delta q}E(q) = &\int_\Omega \widetilde{T}\left[(T-T_E)+\overline{T}\Big|_{t=t_f}\right]d\Omega \\ &+\int_0^{t_f}\int_\Omega\left\{-\widetilde{T}\frac{\partial\overline{T}}{\partial t}-\widetilde{T}\nabla\cdot\left(\mathbf{u}\overline{T}+\nabla\overline{T}\right)-Ra\widetilde{T}\frac{\partial\overline{\psi}}{\partial x}\right\}d\Omega dt \\ &+\int_0^{t_f}\int_\Omega\left(\widetilde{\psi}\nabla^2\overline{\psi}-\widetilde{\psi}\frac{\partial(T,\overline{T})}{\partial(x,y)}\right)d\Omega dt+\int_0^{t_f}\int_{C_a}\overline{T}\Delta q dl dt \end{aligned} \qquad (2.14)$$

If we let the second and third terms above vanish then it follows that the adjoint variables satisfy the set of equations

$$\begin{aligned} &\frac{\partial\overline{T}}{\partial t}+\nabla\cdot\left(\mathbf{u}\overline{T}\right)+\nabla^2\overline{T} = -Ra\frac{\partial\overline{\psi}}{\partial x} \\ &\nabla^2\overline{\psi} = J(T,\overline{T}) \end{aligned} \qquad (2.15)$$

The next step is to assume that the adjoint temperature at $t = t_f$ satisfies the following equality

$$\overline{T}\Big|_{t=t_f} = -\left[T(x,y,t_f)-T_E(x,y)\right] \qquad (2.16)$$

so that a single term finally remains on the right-hand side of Eq.(2.15), namely

$$D_{\Delta q}E(q) = \int_0^{t_f}\int_0^H \overline{T}\Big|_{x=0}\Delta q dy dt \qquad (2.17)$$

The directional derivative of E can be used also to define the gradient ∇E from the formal equality $D_{\Delta q}E(q) = \langle \nabla E | \Delta q \rangle$. Comparing with Eq.(2.17), the conclusion is that

$$\nabla E = \overline{T}(y,t)\Big|_{x=0} \tag{2.18}$$

on the active boundary. This result is valid irrespective of the shape of the domain Ω or the specific form of the boundary conditions. Nevertheless, the computational tests are performed here in a simple square cavity geometry, under the boundary conditions summarized in Fig.2.1, and for which the active boundary is the vertical wall at x = 0. The scalings in Eq.(2.1) are then done with respect to the height of the cavity H.

2.2 Results and discussion

The direct, sensitivity and adjoint problems described earlier are solved by the control volume method with a power-law scheme and implicit time formulation. All the results shown are computed for L = H =1, with a 41 by 41 uniform mesh, the initial conditions used are $T = \psi = 0$ in every case.

2.2.1 The effect of Rayleigh number

Let us first consider the inverse solution obtained for a heat flux profile on the active boundary that is only a function of height, that is q = q(y). In this case the solution algorithm requires a small modification, in that the averaged right-hand side of Eq.(2.18) over heating time range $0 \le t \le t_f$ is used instead as the error gradient. The results obtained for the sine and linear heat flux profiles namely $q(y) = \sin(\pi y)$ or q(y) = y at x = 0, with a time step $\Delta t = \Delta \tau = 0.01$ and final time t_f = 1.0, from the temperature measurements in the cavity, are respectively shown in Fig.2.2 and Fig.2.3. When the Rayleigh number is set to zero, the heat transfer process is pure conduction. It is clear from the plots that the inverse solution procedure can perfectly predict the unknown Fourier boundary condition. Further computations for a mild level of convection at Ra = 10^3 show that satisfactory inverse solutions can also be obtained. However, the

temperature field within the cavity at the final time becomes more and more insensitive to the variation of boundary heat flux along the height as the Rayleigh number increases. This is confirmed by the numerical results shown in Fig.2.4. Comparing Fig.2.4a with Fig.2.4b, it is obvious that the isotherms at the final time at Ra = 10^4 achieved by the uniform heat flux q = 0.64 and by the non-uniform heat flux of sine profile are very close. So when significant convection reaches the level of Ra = 10^4, the inverse solutions are prone to converge to the height averaged value, and more iterations do not improve the accuracy of the solutions.

The other two typical heat fluxes namely triangular and rectangular profiles are also examined, the corresponding numerical results are presented in Fig.2.5 and Fig.2.6. It is found that the CG algorithm might recover the non-smooth even non-continuous heat fluxes with success under a relatively low level of convection. The accuracy of the inverse solution is affected by the Rayleigh number as expected; it will no longer be satisfactory if Ra is greater than 1000 when the dimensionless heating time is equal to 1.0.

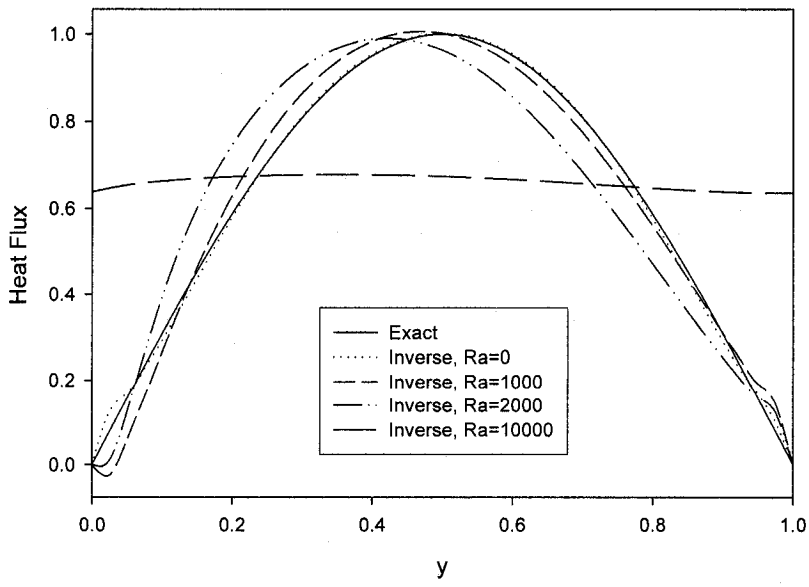

Figure 2.2: Inverse solutions, q = sin(πy), t_f = 1

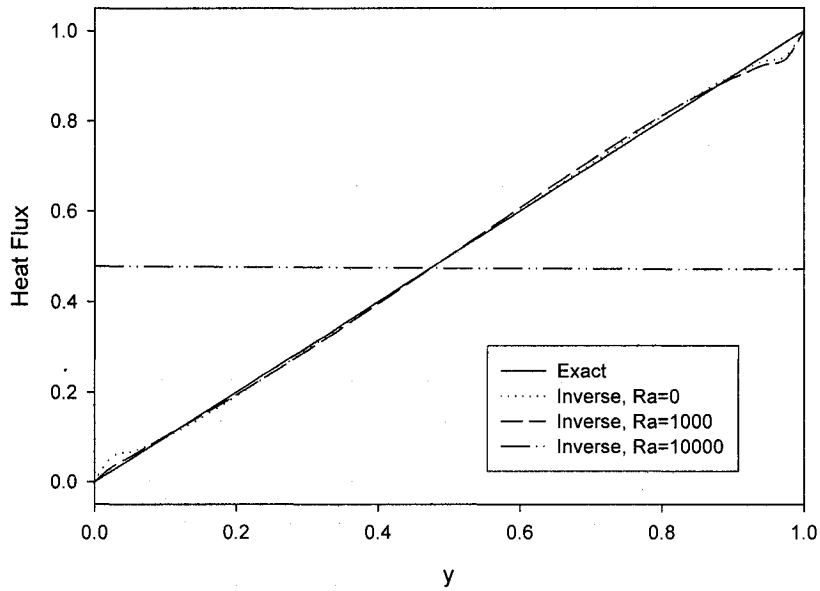

Figure 2.3: Inverse solutions, $q = y$, $t_f = 1$

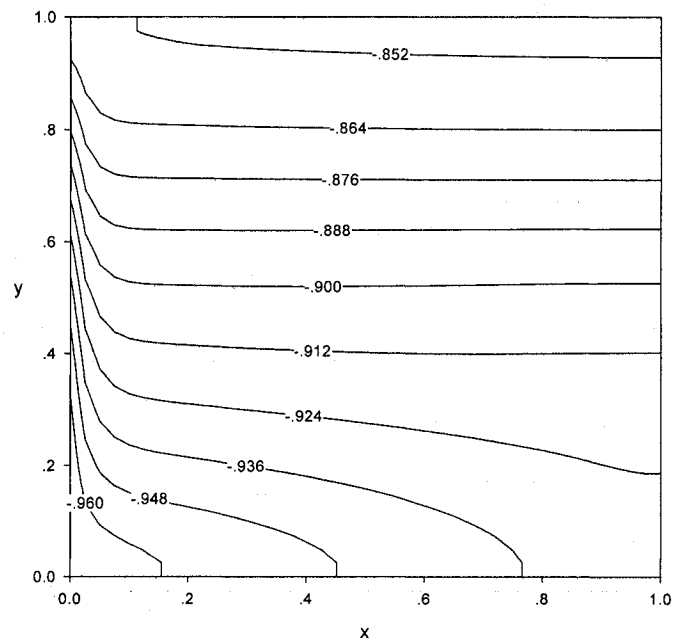

Figure 2.4a: Temperature Distribution at $t = t_f = 1.0$, $q = \sin(\pi y)$, $Ra = 10^4$

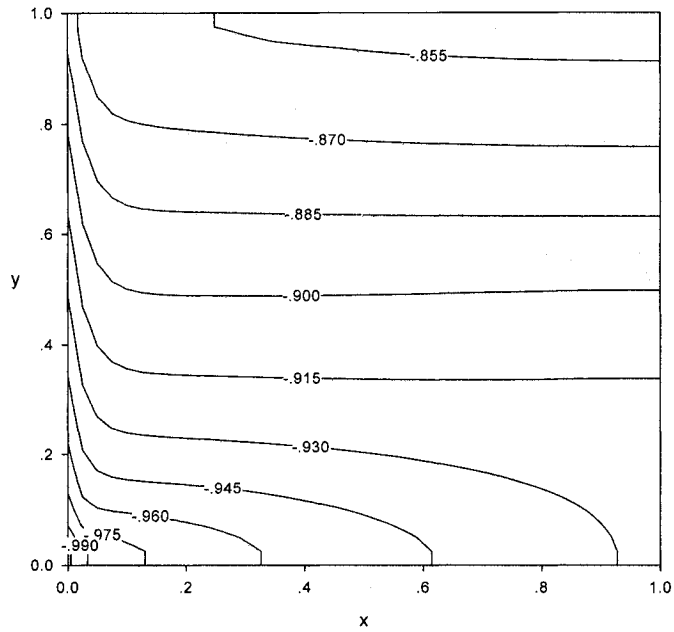

Figure 2.4b: Temperature Distribution at t $=t_f=$ 1.0, q = 0.64, Ra = 10^4

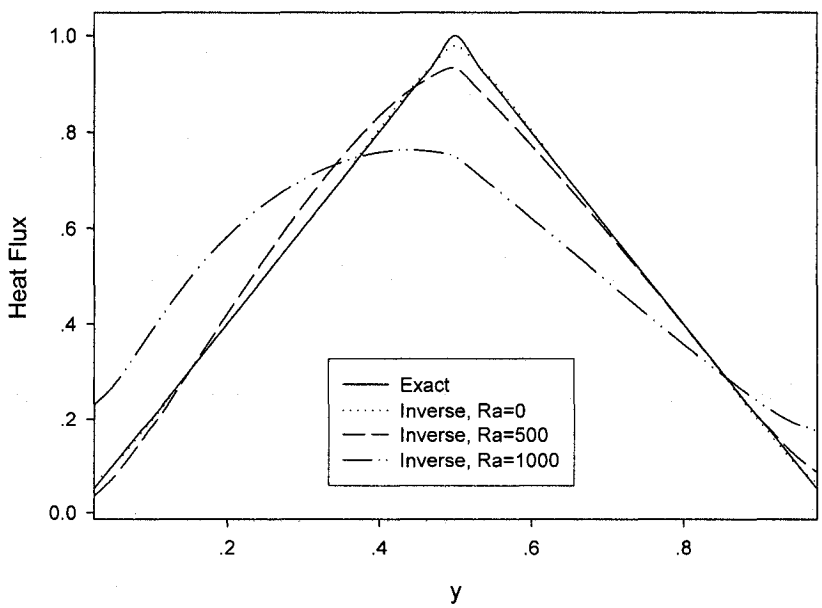

Figure 2.5: Inverse solutions, triangular profile, $t_f = 1$

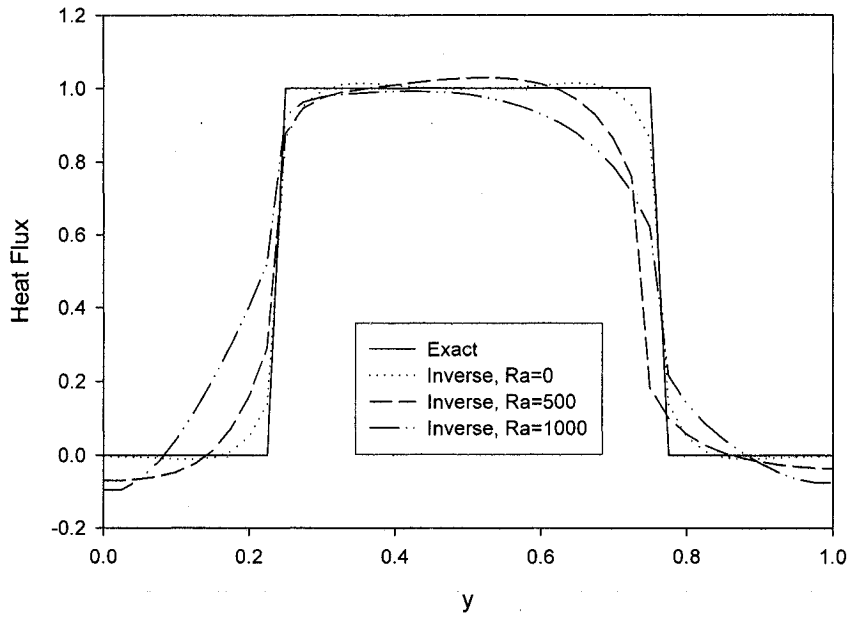

Figure 2.6: Inverse solutions, rectangular profile, $t_f = 1$

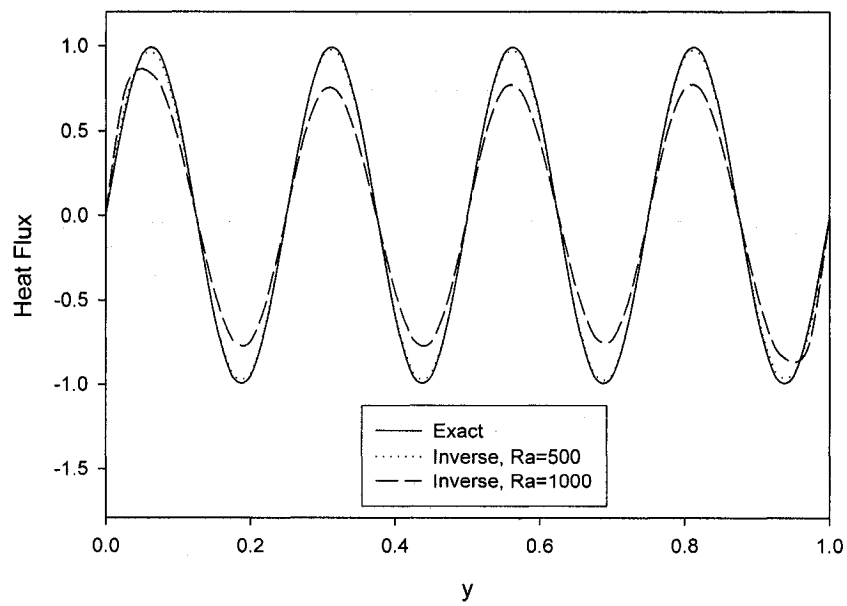

Figure 2.7: Inverse solutions, $q = \sin(8\pi y)$, $t_f = 1$

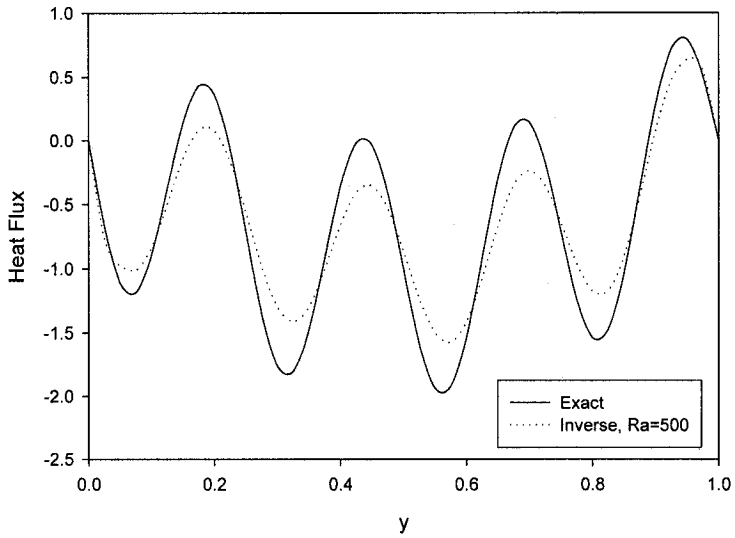

Figure 2.8: Inverse solutions, $q = -\sin(\pi y)-\sin(8\pi y)$, $t_f = 1$

The exact boundary flux which contains high frequency components, for example $q(y) = \sin(8\pi y)$, is also examined in this section. The numerical results shown in Fig.2.7 reveal that the CG method reproduces well the high frequency profile for Rayleigh numbers up to 1000, and 40 ~ 60 iterations (depend on the Rayleigh number) may be necessary. If the flux profile involves two different frequency components, for example $q(y) = -\sin(\pi y)-\sin(8\pi y)$, a reasonable inverse solution shown in Fig.2.8 is obtained after 60 iterations for Ra=500. Because the convergence in this case is much slower, more iterations must be employed to achieve a good accuracy of the inverse solutions.

2.2.2 The influence of final time

According to the discussion in [49, 81], the feasibility of recovering an exact boundary flux essentially depends on the final heating time t_f for this kind of inverse heat conduction problem. In this section, we investigate what happens when the problem is implanted into the system of natural convection in a porous cavity. Let us now suppose that heat flux profile is only a function of time namely $q = q(t)$. Under this situation a small modification for the solution algorithm is needed: the averaged right-hand side of Eq.(2.18) over the active boundary is used as the error gradient. The numerical

experiments suggest that a smaller time step may lead to a better accuracy of the inverse solution, so we set $\Delta t = \Delta\tau = 0.0002$ for the case that heat flux is a function of time. Fig.2.9 gives the solution reconstructed with success for a linear heat flux profile at Ra = 500 with the final time $t_f = 0.1$. However, if the final time is extended to 0.2, the inverse result will lose its accuracy especially in the region $0 \le t < 0.1$, during this period the solution is prone to converge to the time-averaged value regardless of the number of the iterations. The corresponding result is presented in Fig.2.10. If the final time is longer, the time averaged effect will be more obvious and the inverse problem becomes more ill-posed. In fact this phenomenon is the inherent character of this kind of inverse problem. The theoretical analysis and numerical experiments indicate that the final temperature distribution is not sensitive to the variation of heat flux over the range $0 \le t < t_f - 0.1$. Here the dimensionless time 0.1 is not an accurate value but an empirical value which is valid for most cases. The detailed analysis can be found in [81].

In real situations, the case is often encountered where heat flux may be a function of time and position of the boundary. Based on the previous discussion, one may conclude that the boundary flux q(y,t) with non-uniform profile should be successfully recovered within a short heating period at a low Rayleigh number. This is confirmed in Figs.2.11a and 2.11b, in which the exact data and inverse solution for the heat flux at x = 0 corresponding to $q(y,t) = 10\cos(\pi y)t$ are illustrated in the (t,y) plane respectively for Ra = 500 and $t_f = 0.1$. These two contour plots are in perfect agreement except in the region where $t < 0.01$.

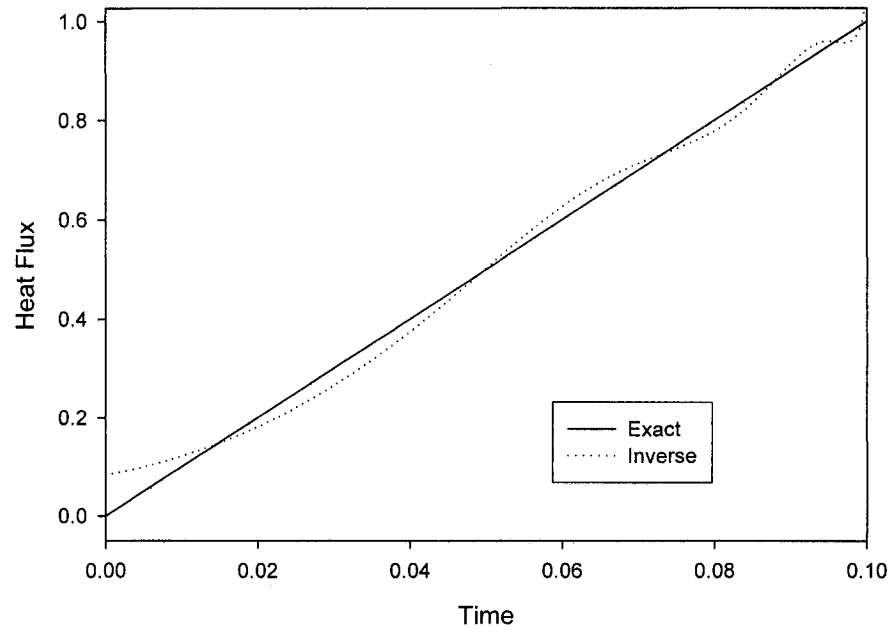

Figure 2.9: Inverse solution, q =10t, Ra = 500, $t_f = 0.1$

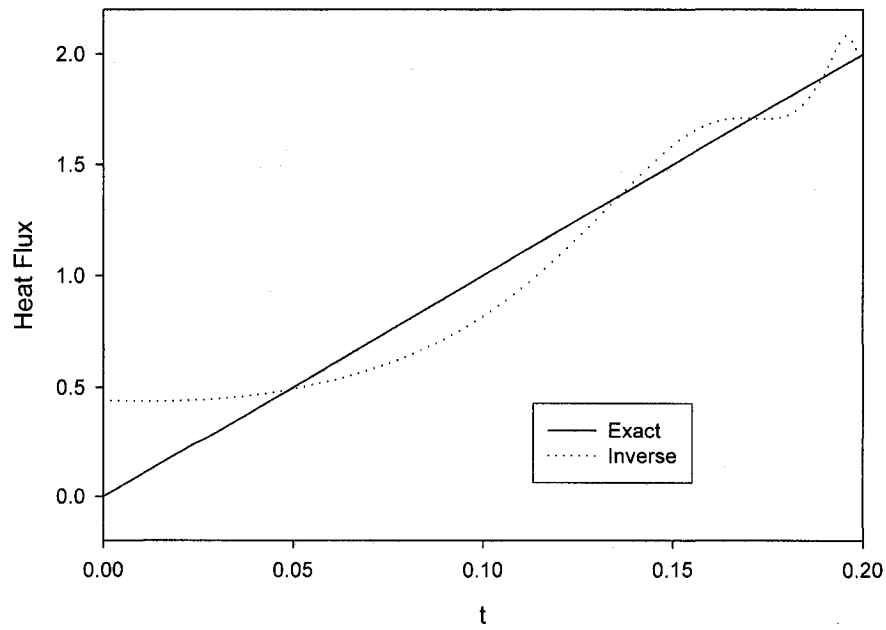

Figure 2.10: Inverse solution, q =10t, Ra = 500, $t_f = 0.2$

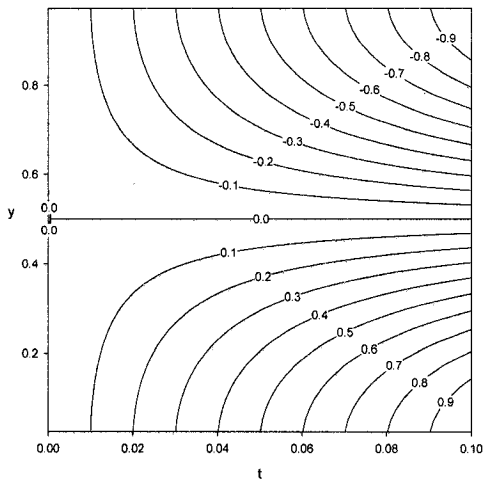

Figure 2.11a:
Exact q(y,t) = 10cos(πy)t

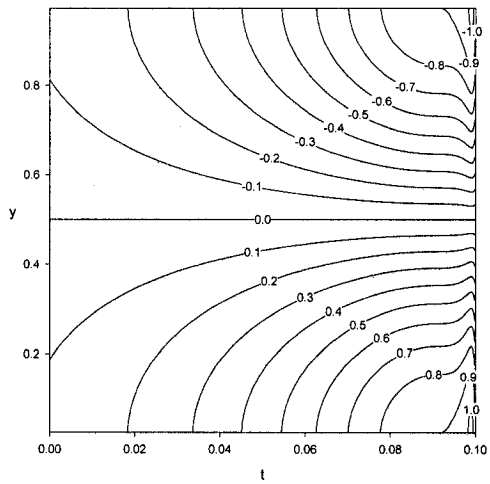

Figure 2.11b:
Inverse Solution, Ra = 500

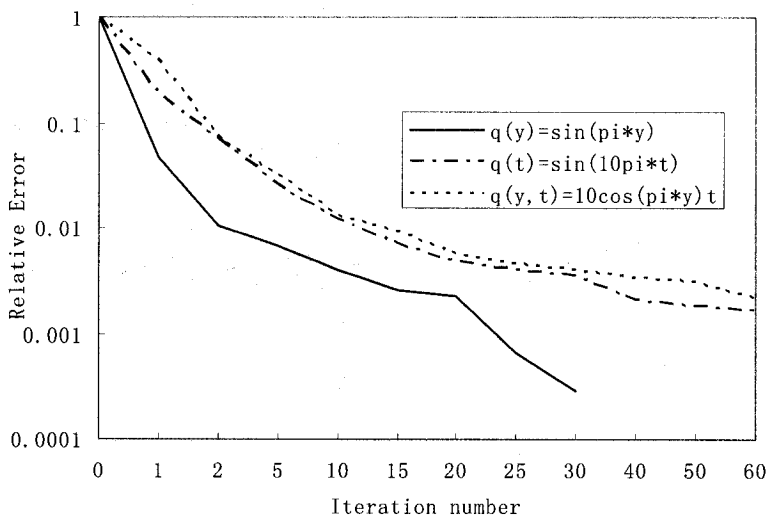

Figure 2.12: Convergence Performance, Ra = 500

It is found that, for time dependent flux q(t), the convergence rate is much slower than for position dependent flux q(y). For instance, the relative error defined as $E_r = \|T - T_E\|/T_E$ reaches 0.39% and 2.53% after 5 iterations for (q(y) = sin(πy), t_f= 1.0) and for (q(t) = sin(10πt), t_f = 0.1) respectively at Ra = 500. The convergence performance for non-uniform profile q = q(y, t) is similar to that for time dependant heat flux. The corresponding comparison is presented in Fig.2.12.

2.2.3 The influence of noisy data

In order to simulate the actual field measurement, the noisy data $T_E(1+\sigma\Sigma)$ is used instead of the exact value T_E, where $|\Sigma|<1$ is a uniformly distributed random real number. The regularization strategy is based on the discrepancy principle of Alifanov, namely by setting the convergence criterion $\varepsilon = \sigma^2$. It might stop the iteration process on time before the high frequency components of the noise start to impair the inverse solution. The predicted linear and cosine flux profiles along y shown in Fig.2.13 and Fig.2.14 respectively for a noise of relative standard deviation $\sigma = 0.05$ are still accurate at Ra = 0. When convection occurs with Ra = 500 and t_f = 1, although the slight oscillations reduce the accuracy, the reasonable reconstructed solutions are also predicted with success for a same level of relative deviation. It is also an illustration of the regularization effect of the conjugate method.

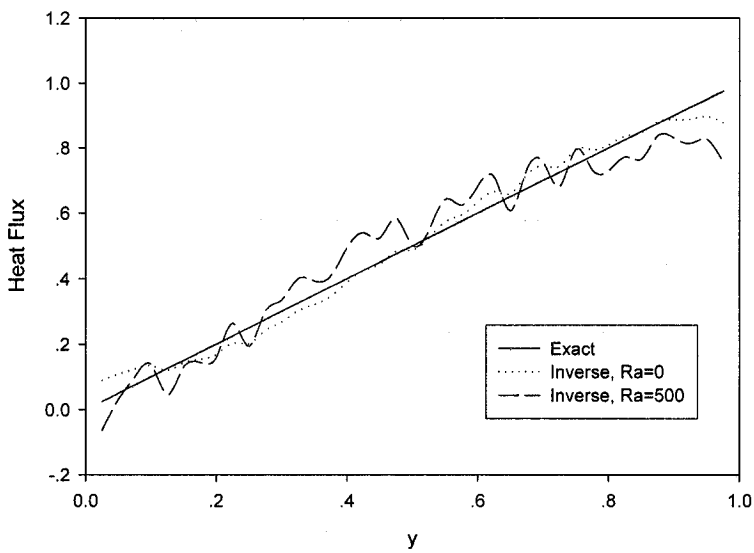

Figure 2.13: Inverse solutions, q(y) = y, $\sigma = 0.05$

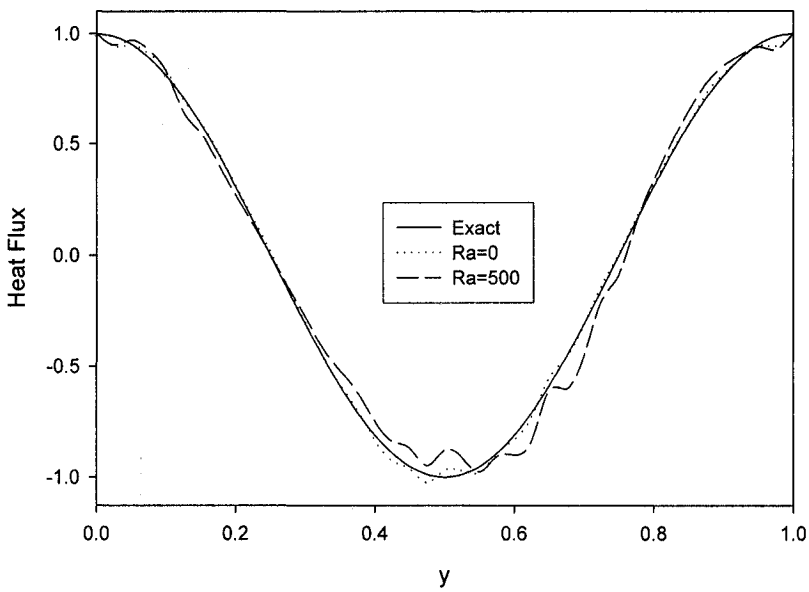

Figure 2.14: Inverse solutions, $q(y) = \cos(2\pi y)$, $\sigma = 0.05$

CHAPTER III
HEAT SOURCE RECONSTRUCTION PROBLEM

As discussed in the introduction chapter, an induction heater may induce an exponential distribution of power density (heat source) along the radius of the cylindrical billet. In general, the heat source is difficult to measure with satisfactory accuracy especially for exponential profiles. However, the temperature field is much easier to measure by thermocouples, infrared imaging thermometers or other devices. In this chapter, we try to recover the real heat source distribution from the temperature measurements by using the inverse technique.

3.1 General Inverse Heat Source Problem

Let us consider a one-dimensional unsteady heat conduction process generated by an inner heat source. This problem is governed by the following dimensionless equation

$$\begin{aligned} &\frac{\partial T}{\partial t} = \frac{\partial^2 T}{\partial x^2} + S(x,t), \quad x \in [0,1];\ t \in [0,t_f] \\ &\left.\frac{\partial T}{\partial x}\right|_{x=0} = q_1(t), \quad \left.\frac{\partial T}{\partial x}\right|_{x=1} = q_2(t) \\ &T(x,0) = f(x) \end{aligned} \tag{3.1}$$

Suppose that all the boundary conditions and initial conditions are known, the purpose of the present inverse problem is to recover the heat source S(x, t) from the measured temperature $T_m(x, t)$. This inverse problem can also be solved by the conjugate gradient method in conjunction with the adjoint equation.

3.1.1 Sensitivity Equation

The sensitivity temperature $\tilde{T}$ is defined as the directional derivative of T at S in the direction ΔS:

$$\tilde{T} = \lim_{\varepsilon \to 0} \frac{T(S + \varepsilon \Delta S) - T(S)}{\varepsilon} \tag{3.2}$$

Starting from Eq. (3.1), we must have

$$\lim_{\varepsilon\to 0}\frac{\partial}{\partial t}\left(\frac{T(S+\varepsilon\Delta S)-T(S)}{\varepsilon}\right)=\lim_{\varepsilon\to 0}\frac{\partial^2}{\partial x^2}\left(\frac{T(S+\varepsilon\Delta S)-T(S)}{\varepsilon}\right)+\lim_{\varepsilon\to 0}\left(\frac{S+\varepsilon\Delta S-S}{\varepsilon}\right)$$

According to the definition of the sensitivity, the previous equation follows the sensitivity equation:

$$\frac{\partial\tilde{T}}{\partial t}=\frac{\partial^2\tilde{T}}{\partial x^2}+\Delta S \tag{3.3}$$

Similarly we have the corresponding initial and boundary conditions of the sensitivity problem:

$$\tilde{T}(x,0)=0,\ \left.\frac{\partial\tilde{T}}{\partial x}\right|_{x=0}=0,\ \left.\frac{\partial\tilde{T}}{\partial x}\right|_{x=1}=0 \tag{3.4}$$

3.1.2 Adjoint Equation

The error functional is defined as follow:

$$E(S)=\frac{1}{2}\int_0^{t_f}\int_0^1\left[T(x,t)-T_m(x,t)\right]^2 dxdt \tag{3.5}$$

where T and T_m respectively stand for the temperature predicted from the approximation for S and measured temperature. According to the definition of the error functional and sensitivity, it is not difficult to derive the following equality:

$$\begin{aligned}
D_{\Delta S}E(S)&=\lim_{\varepsilon\to 0}\frac{E(S+\varepsilon\Delta S)-E(S)}{\varepsilon}\\
&=\frac{1}{2}\lim_{\varepsilon\to 0}\frac{\int_0^{t_f}\int_0^1\left[T(S+\varepsilon\Delta S)-T_m\right]^2 dxdt-\int_0^{t_f}\int_0^1\left[T(S)-T_m\right]^2 dxdt}{\varepsilon}\\
&=\int_0^{t_f}\int_0^1\left\{\tilde{T}(x,t)\cdot\left[T(x,t)-T_m\right]\right\}dxdt\\
&=\int_0^{t_f}\int_0^1\left(\nabla E\cdot\Delta S\right)dxdt
\end{aligned} \tag{3.6}$$

If the adjoint temperature $\bar{T}$ and Eq. (3.3) are respectively treated as Lagrange multiplier and constraint, by using the Lagrange multiplier method we may rewrite

Eq.(3.6) as:

$$D_{\Delta S}E(S) = \int_0^{t_f}\int_0^1 \left\{[T(x,t)-T_m]\cdot\tilde{T}(x,t)\right\}dx + \int_0^{t_f}\int_0^1 \overline{T}\left(\frac{\partial\tilde{T}}{\partial t}-\frac{\partial^2\tilde{T}}{\partial x^2}-\Delta S\right)\cdot dxdt \qquad (3.7)$$

Considering the initial and boundary conditions of sensitivity problem, we must have

$$\begin{aligned} D_{\Delta s}E(S) = &\int_0^{t_f}\int_0^1 [(T-T_m)]\overline{T}\,dxdt - \int_0^{t_f}\int_0^1 \tilde{T}\left(\frac{\partial\overline{T}}{\partial t}+\frac{\partial^2\overline{T}}{\partial x^2}\right)\cdot dxdt + \int_0^{t_f}\int_0^1 \frac{\partial(\overline{T}\tilde{T})}{\partial t}dxdt \\ &+ \int_0^{t_f}\int_0^1 \frac{\partial}{\partial x}\left(\tilde{T}\frac{\partial\overline{T}}{\partial x}\right)\cdot dxdt - \int_0^{t_f}\int_0^1 \overline{T}\Delta S dxdt \end{aligned} \qquad (3.8)$$

If the adjoint temperature satisfies the following adjoint problem

$$\frac{\partial\overline{T}}{\partial t}+\frac{\partial^2\overline{T}}{\partial x^2} = T-T_m \quad \text{or} \quad \frac{\partial\overline{T}}{\partial\tau}=\frac{\partial^2\overline{T}}{\partial x^2}+(T-T_m),\ \tau=t_f-t \qquad (3.9)$$

with the following "initial" and boundary conditions:

$$\begin{aligned} &\left.\frac{\partial\overline{T}}{\partial x}\right|_{x=0} = 0,\ \left.\frac{\partial\overline{T}}{\partial x}\right|_{x=1} = 0 \\ &\overline{T}(x,\tau=0)=0 \end{aligned} \qquad (3.10)$$

then the first, second, third and fourth term of right hand side of Eq. (3.8) vanish, Eq. (3.8) becomes

$$D_{\Delta S}E(S) = -\int_0^{t_f}\int_0^1 \overline{T}\Delta S dxdt \qquad (3.11)$$

Comparing Eq. (11) and Eq. (3.6), we obtain the gradient of the error functional:

$$\nabla E = -\overline{T}(x,t) \qquad (3.12)$$

The overall CGM algorithm is the same as that described in Chapter 2.

3.2 Reconstruction of the Heat Source Distribution

How to determine the distribution of the heat source along the radius of the cylindrical material is an important problem for induction heating, since direct measurement may not be practical. We note that the heat source can be expressed as:

$$S(x,t) = h(t) \cdot g(x,T) \tag{3.13}$$

where g(x, T) denotes the profile of heat source distribution along the radius; h(t) denotes the strength of heat source. It is known that g(x, T) depends on the frequency of the alternating current and the properties of material. If the electromagnetic properties of the material do not change significantly within a range of temperature, i.e. the profile of heat source distribution is independent to the temperature, then Eq.(3.1) becomes

$$\frac{\partial T}{\partial t} = \frac{\partial^2 T}{\partial x^2} + h(t) \cdot g(x), \quad x \in [0,1]; \; t \in [0, t_f] \tag{3.14}$$

Suppose the heating strategy is given, namely h(t) is known, the sensitivity equation (3.3) can be rewritten as:

$$\begin{aligned} &\frac{\partial \tilde{T}}{\partial t} = \frac{\partial^2 \tilde{T}}{\partial x^2} + \Delta g \cdot h(t) \\ &\tilde{T}(x,0) = 0, \left.\frac{\partial \tilde{T}}{\partial x}\right|_{x=0} = 0, \left.\frac{\partial \tilde{T}}{\partial x}\right|_{x=1} = 0 \end{aligned} \tag{3.15}$$

Theoretically speaking, there are two different methods of temperature measurement that may be adopted to recover the heat source distribution g(x).

Method 1: measure the temperature history on the material surface during the interval $0 \le t \le t_f$. If, say, $T(1,t) = T_m(t)$ is known, the inverse problem can be solved by minimizing the error:

$$E(g) = \frac{1}{2} \int_0^{t_f} [T(1,t) - T_m(t)]^2 \, dt \tag{3.16}$$

Based on the above definition of the error functional, the adjoint problem is governed by the following equations:

$$\frac{\partial \overline{T}}{\partial \tau} = \frac{\partial^2 \overline{T}}{\partial x^2},\ \tau = t_f - t$$
$$\left.\frac{\partial \overline{T}}{\partial x}\right|_{x=0} = 0,\quad \left.\frac{\partial \overline{T}}{\partial x}\right|_{x=1} = -\left(T(1,t) - T_m\right) \tag{3.17}$$
$$\overline{T}(x, \tau = 0) = 0$$

Method 2: measure the temperature distribution at the final time $t = t_f$. The heat source distribution g(x) is reconstructed from $T(x,t_f) = T_m(x)$, and the error functional is defined as:

$$E(g) = \frac{1}{2}\int_0^1 \left[T(x,t_f) - T_m(x)\right]^2 dx \tag{3.18}$$

In addition, the adjoint equation accordingly becomes:

$$\frac{\partial \overline{T}}{\partial \tau} = \frac{\partial^2 \overline{T}}{\partial x^2},\ \tau = t_f - t$$
$$\left.\frac{\partial \overline{T}}{\partial x}\right|_{x=0} = 0,\quad \left.\frac{\partial \overline{T}}{\partial x}\right|_{x=1} = 0 \tag{3.19}$$
$$\overline{T}(x, \tau = 0) = -\left(T(x,t_f) - T_m\right)$$

Whether method 1 or method 2 is adopted, the expression of the gradient of the error function is the same:

$$\nabla E = -\int_0^{t_f} \left(\overline{T}(x,t)\cdot h(t)\right) dt \tag{3.20}$$

3.3 Results and Discussion

Let us suppose that the strength of the heat source to be constant and $h(t) \equiv 1.0$. We may measure the temperature following the two different methods mentioned above to recover the heat source distribution g(x).

3.3.1 Results by Method 1

In a real induction heating process, the heat source (power density) distributions along

the radius of the cylinder is normally presented exponential profiles, and most of the power is concentrated in the surface layer. So an exponential profile of g(x) is firstly tested. Although measuring the surface temperature evolution is not difficult, regardless of whether infrared imaging or thermocouples is used, the error mat be considerable. Thus we use noisy data $T_m(1+\sigma\Sigma)$ to simulate the measured temperature, where T_m is the exact temperature value and $|\Sigma|<1$ is a uniformly distributed random real number. Now suppose that the exact $g(x)=\exp(10(x-1.0))$ and the final time $t_f = 0.05$, the surface temperature with 5% noise is presented in Fig.3.1b. It is found that the noisy data just slows down the convergence; the error function does not change beyond the 4^{th} iteration. However, the inverse solution still recovers the exact heat source distribution (see Fig.3.1a) perfectly. The discrepancy principle of Alifanov, Tikonov regularization or the other regularization techniques is not needed in the conjugate gradient algorithm. Generally, the noise does not significantly affect the inverse solution.

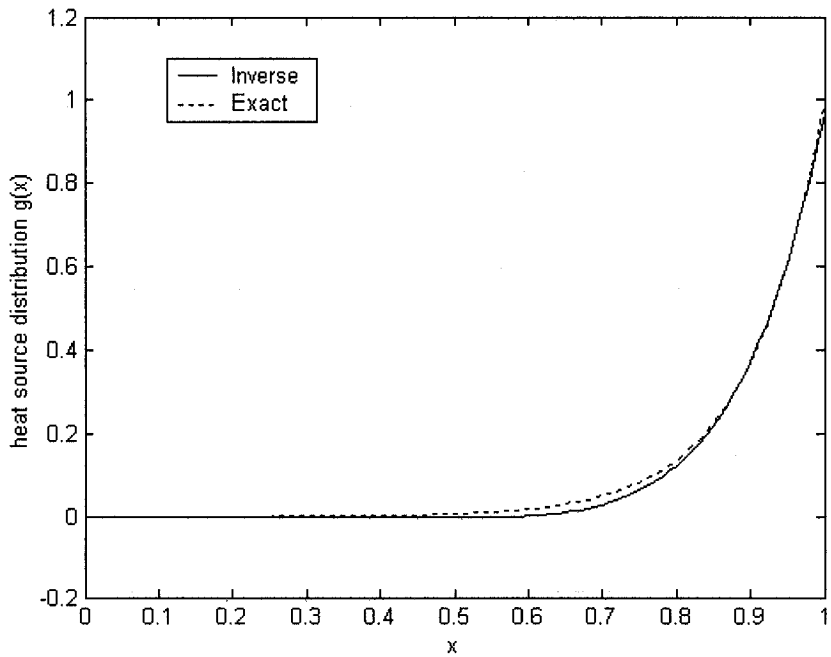

Figure 3.1a: Inverse solution by method 1, $g(x)=\exp(10(x-1.0))$, $t_f = 0.05$

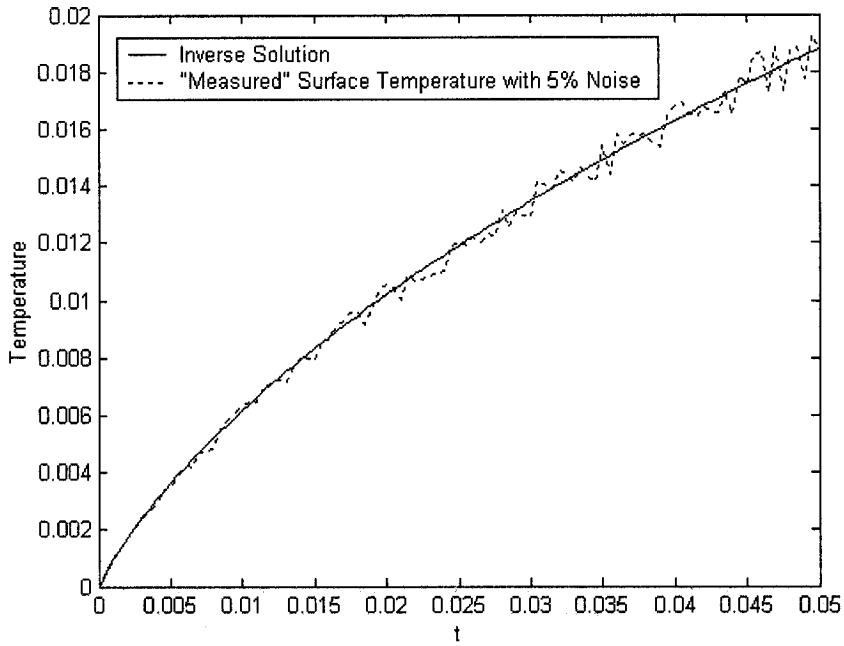

Figure 3.1b: Surface temperature evolution, $\sigma = 0.05$, $t_f = 0.05$

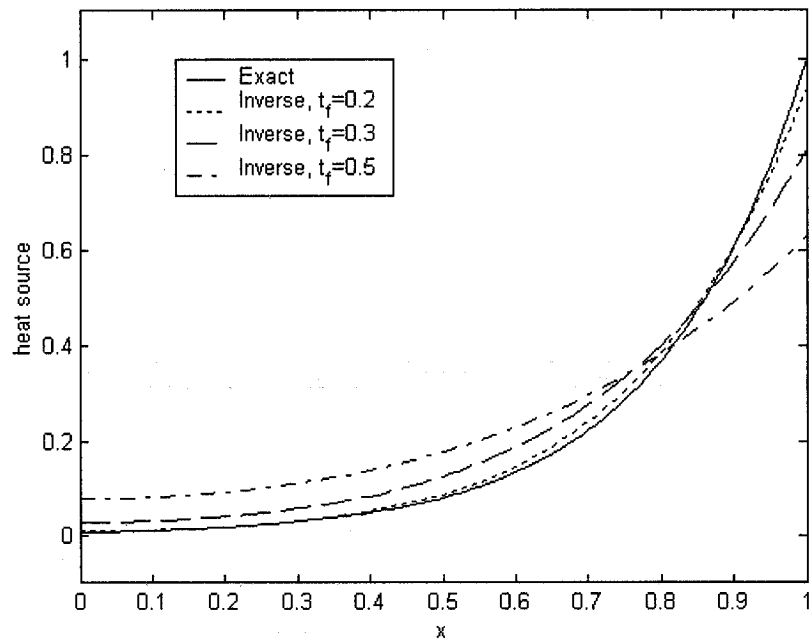

Figure 3.2: Inverse solutions by method 1, $g(x) = \exp(5(x-1.0))$, $\sigma = 0.05$

On the other hand, the final time t_f is found to be an important factor that influences the accuracy of the reconstructed solutions. Fig.3.2 shows a series of inverse solutions corresponding to different final times. Suppose the exact $g(x) = \exp(5(x-1.0))$, the noise level parameter $\sigma = 0.05$, the inverse solution matches the exact data very well if $t_f = 0.2$. As the final time is prolonged, the convergence becomes more and more difficult (the relative error $\|T - T_m\| / \|T_m\|$ stops decreasing at 0.0308, 0.0345 and 0.0513 for t_f= 0.2, 0.3, 0.5 respectively), and then the accuracy of the solution becomes worse and worse. Even the input data without noise is not able to improve the solutions. The numerical tests indicates that the exponential profile can be recovered with success when the dimensionless final time $t_f \leq 0.2$. Nguyen and Bendada [15] considered a similar problem: they recovered the initial temperature field of an A357 cylinder with a diameter of 76mm from the surface temperature history. A ramp profile and a triangular profile were reconstructed with good precision for t_f= 1.6s and 9s respectively. In this problem, the dimensionless time of 0.2 corresponds to the real time of 4.8s.

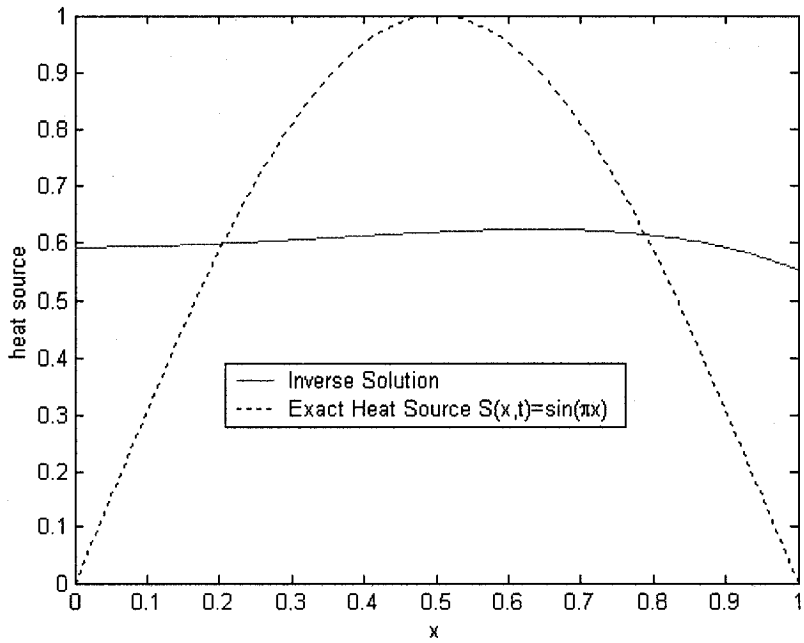

Figure 3.3a: Inverse solutions by method 1, $g(x) = \sin(\pi x)$

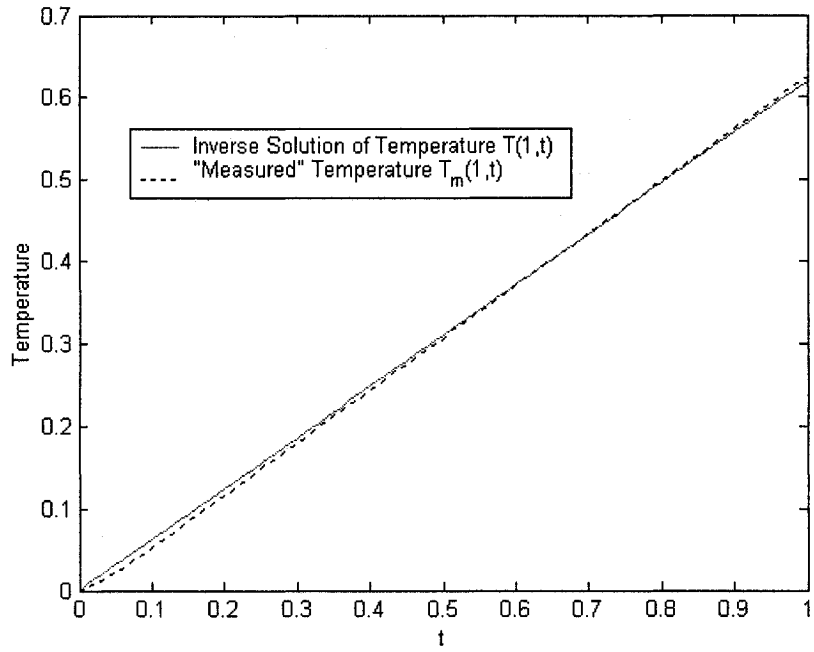

Figure 3.3b: Surface temperature evolution, $g(x) = \sin(\pi x)$

In order to test the algorithm further, a sinusoidal profile of heat source distribution is also examined. It is shown that the inverse solution of heat source is prone to converge to a position-averaged constant (see Fig.3.3a), although the inverse result of surface temperature is identical to the temperature measurements (see Fig.3.3b). Decreasing the final heating time cannot improve the solution considerably. It suggests that numerical solution of this inverse problem might not be unique for arbitrary heat source profiles. In other words, the reconstructed solutions obtained by method 1 may not be reliable for non-exponential profiles.

3.3.2 Results by Method 2

Method 2 requires measuring the temperature distribution at the final time. If the radius of the billet is relatively small, embedding the thermocouples in many locations is not practicable. Furthermore, the drilled holes within the billet may influence the electromagnetic fields, making the experimental model deviate from the real system. To

avoid the limitation to local or pointwise contact measurements, infrared thermography is preferred in this situation. Considering that the billet emissivity is not predictable during induction heating since it is affected by temperature, alloy oxidation, surface texture and alloy grade and other factors, a high emissivity paint (ε=0.94) should be employed to make thermal imaging reliable [15, 20, 68].

To simulate induction heating, the experimental profiles of the heat source distribution are the emphasis of our investigation. Let the exact $g(x) = \exp(5(x-1.0))$, if there is no noise content in the final temperature measurements, the CG method reproduces the heat source distribution with good accuracy after 144 iterations, as depicted in Fig.3.4a. When a 2% random error is added to the input temperature data, the discrepancy principle of Alifanov, namely setting the convergence criterion $\varepsilon = \sigma^2$, may effectively prevent the inverse solution from oscillating. However, we have to point out here that this regularization method also considerably affects the accuracy of the reconstruction, while it stops the iteration process before the oscillation occurs. If the discrepancy principle of Alifanov is not employed, the noise in the input data is not amplified in the output solution, although slight oscillations can not be avoided. However, there are no difficulties to smooth this infected solution by certain numerical techniques, for example least square method. It is found that the smoothed solution is much closer to the exact curve than the results based on the discrepancy principle of Alifanov, as showed in Fig.3.4b.

Besides the exponential curves, the other typical profiles are also examined to make sure that an arbitrary heat source distribution could be recovered with success by method 2. If the final temperature distribution contains no noise (error), then no matter if continuous or non-continuous, smooth or non-smooth, with low frequency or with high frequency, the arbitrary profiles can always be recovered with excellent accuracy. However, one percent noise may make the reconstructed solutions deviate from the exact data depending on the profiles. For sinusoidal and rectangular profiles, this bias is acceptable;

for triangular profile, the inverse solution is reasonable; but for a profile containing high frequency components, the reconstructed solution differs completely from the exact heat source distribution. The corresponding results are shown in Figs.3.5-3.8.

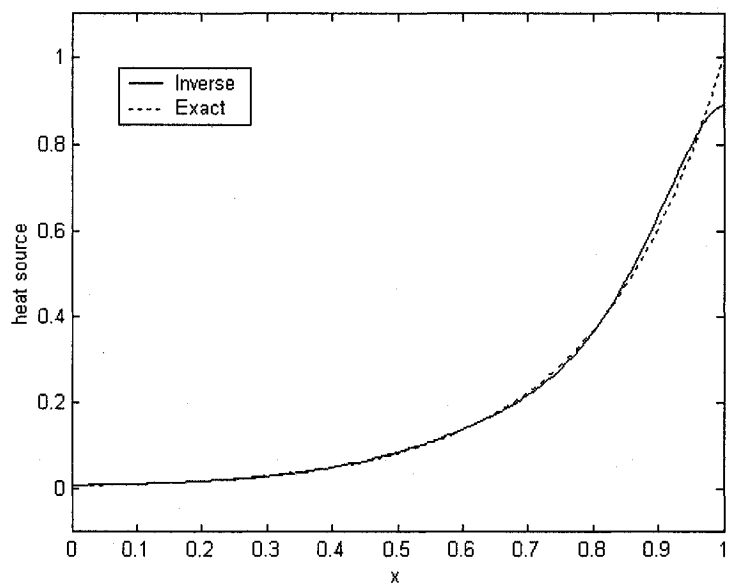

Figure 3.4a: Inverse solution by method 2, $g(x) = \exp(5(x-1.0))$, $\sigma = 0$

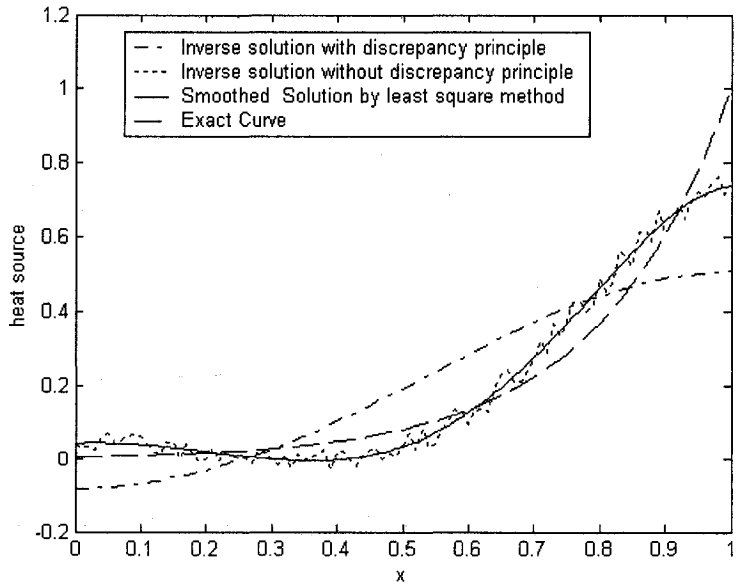

Figure 3.4b: Inverse solutions by method 2, $g(x) = \exp(5(x-1.0))$, $\sigma = 0.02$

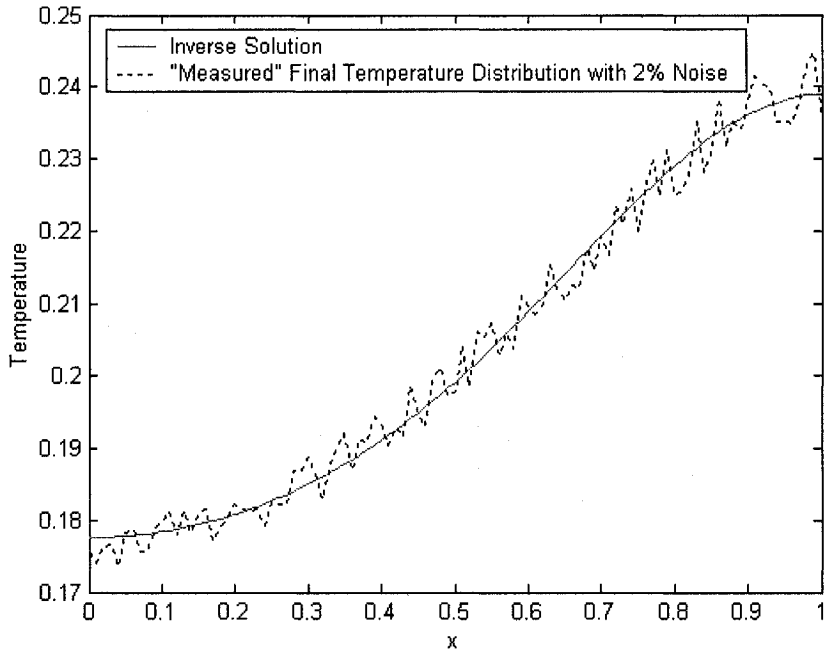

Figure 3.4c: Final temperature distribution, $g(x) = \exp(5(x - 1.0))$

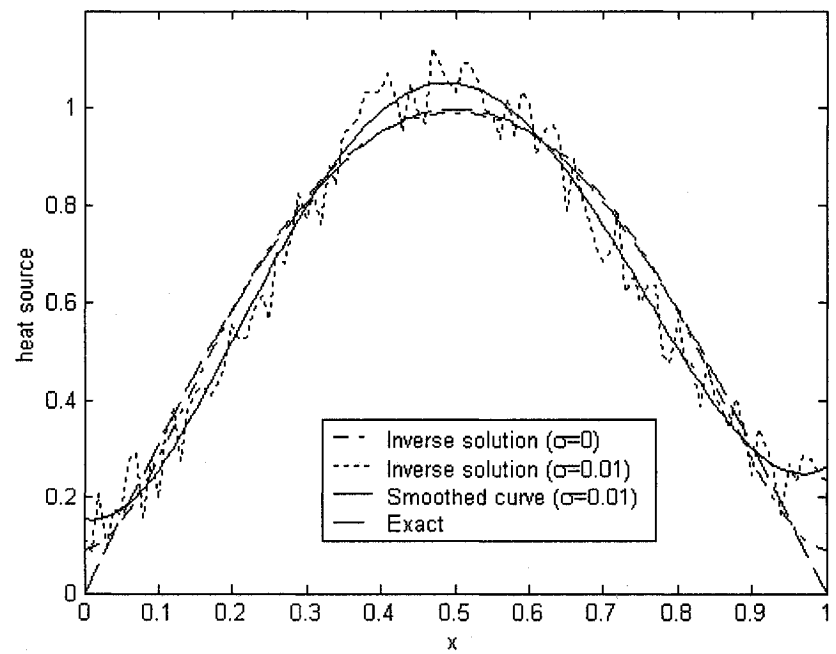

Figure 3.5a: Inverse solutions by method 2, sinusoidal profile

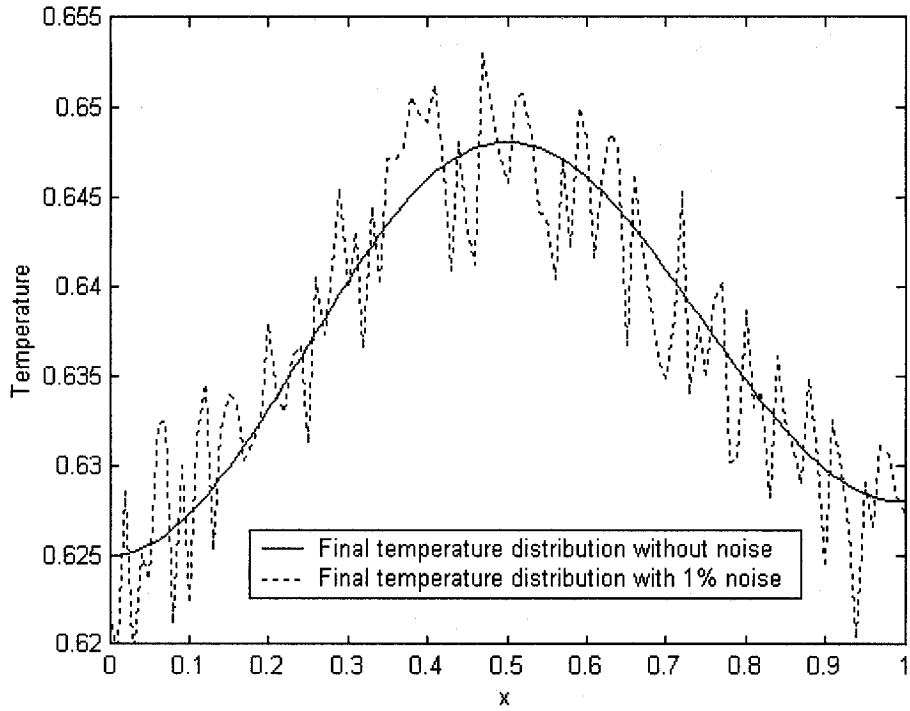

Figure 3.5b: Final temperature distribution, $g(x) = \sin(\pi x)$

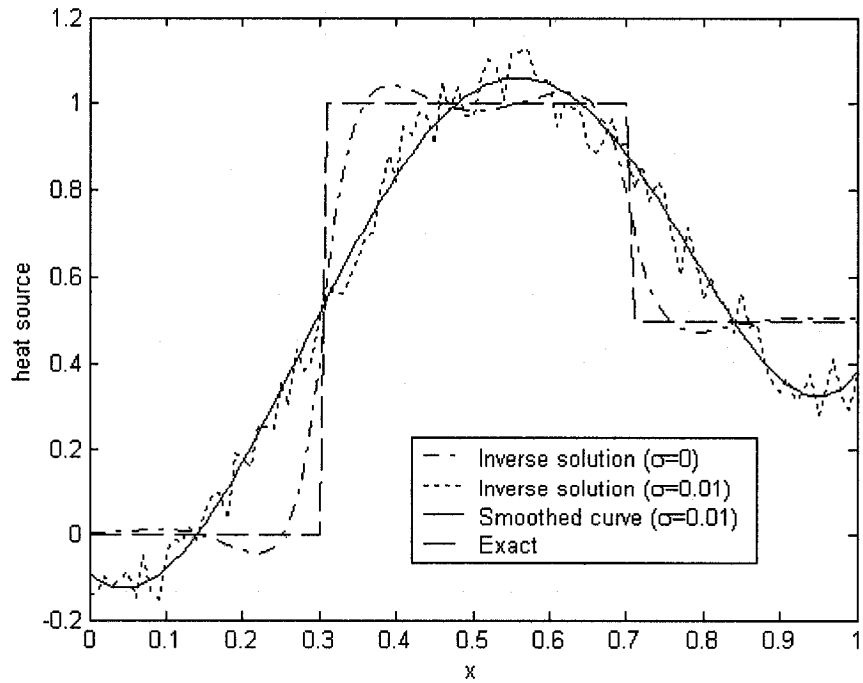

Figure 3.6a: Inverse solutions by method 2, rectangular profile

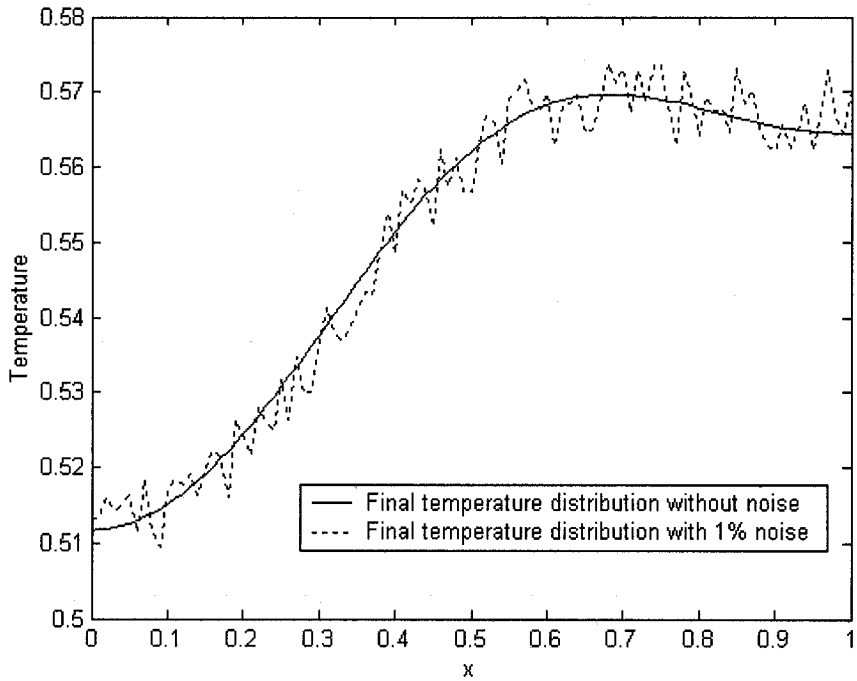

Figure 3.6b: Final temperature distribution, rectangular profile

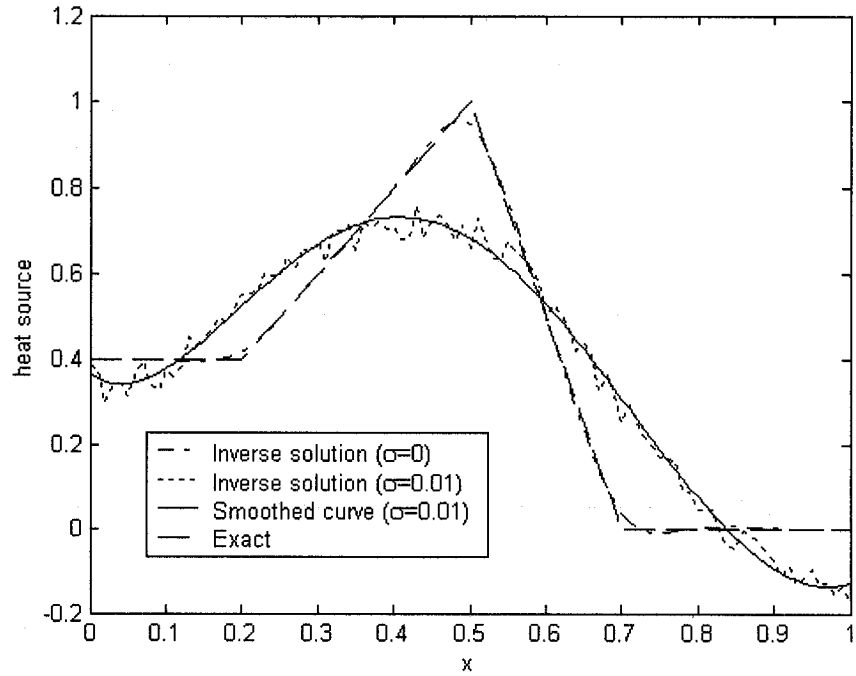

Figure 3.7a: Inverse solutions by method 2, triangular profile

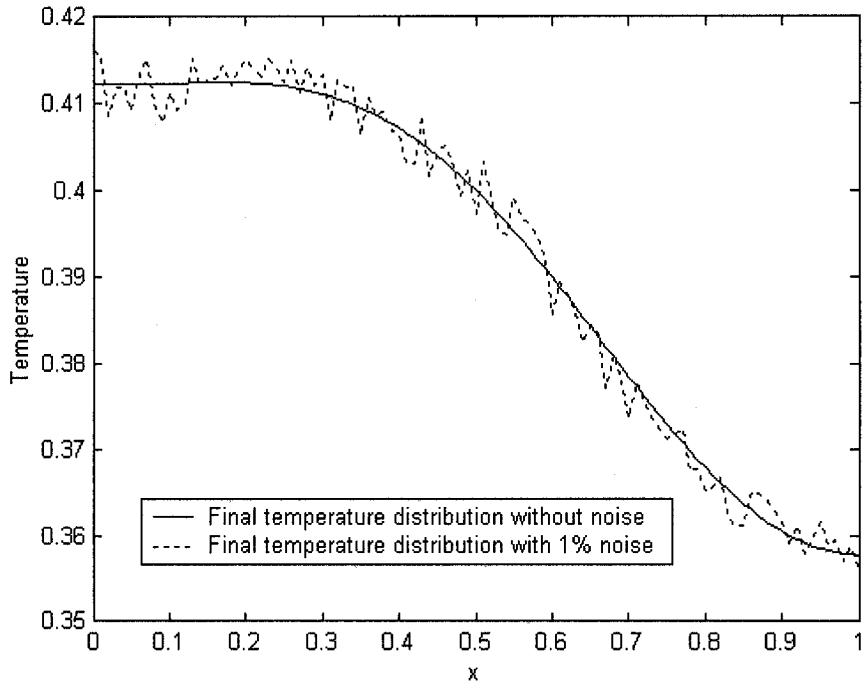

Figure 3.7b: Final temperature distribution, triangular profile

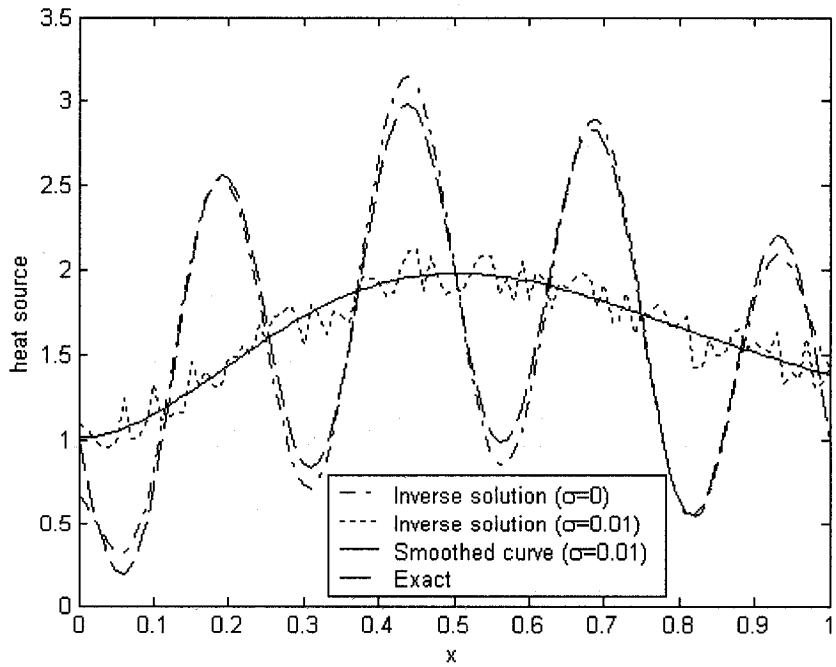

Figure 3.8a: Inverse Solutions by Method 2, $g(x) = \sin(\pi x) - \sin(8\pi x) + 1.0$

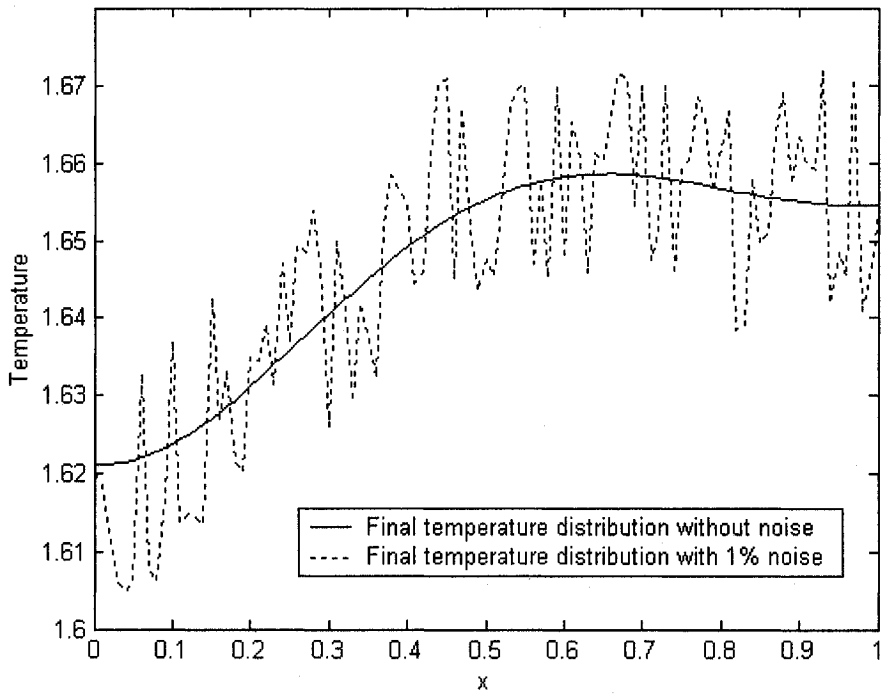

Figure 3.8b: Final temperature distribution, heat source distribution with high frequency components

CHAPTER IV

OPTIMAL CONTROL OF INDUCTION HEATING FOR SEMI-SOLID FORMING

The thixoforming technique requires reheating the feedstock to a semi-solid state with a uniform temperature distribution, a uniform globular microstructure and an optimum liquid fraction. The skin effect of induction heating results in an exponential profile of power density (heat source) distribution within the material as well as an uneven temperature profile from surface to core. In this study, only skin effect is considered and the other two effects, namely end effect and edge effect, are neglected. The conjugate gradient method in conjunction with the adjoint method is used to find an optimal heating/cooling strategy to achieve a uniform temperature distribution along the radius of a cylinder in a relatively short time. It is found that a modified conjugate gradient method may be a more suitable algorithm to solve this optimization problem. The physical and mathematical models take into account the temperature-dependent thermo-physical properties. Radiative and convective heat losses are also considered.

4.1 Problem Description

An aluminum alloy (A356/A357) slug with a diameter of 76mm and a height of 152mm is placed vertically into an induction coil unit (Fig.4.1). The power supply generates an alternating current of 10KHz. In order to obtain a uniform liquid fraction and a good viscosity, the billet temperature should be around 585℃ through the entire cross-section before the material flows into the die cavity under pressure. Due to the skin effect, the temperature is not uniform along the radius of the billet, as $T_{surface}$ is higher than T_{center}. The electromagnetic transverse edge effects are not to be considered because of the cylindrical geometry of the work-piece, and the 'elephant foot' effect is assumed to be controlled. If the induction heater is well designed and there is no coil overhang, then the end effects and the top-to-bottom thermal gradients may be ignored. The physical model can therefore be simplified to a one-dimensional problem.

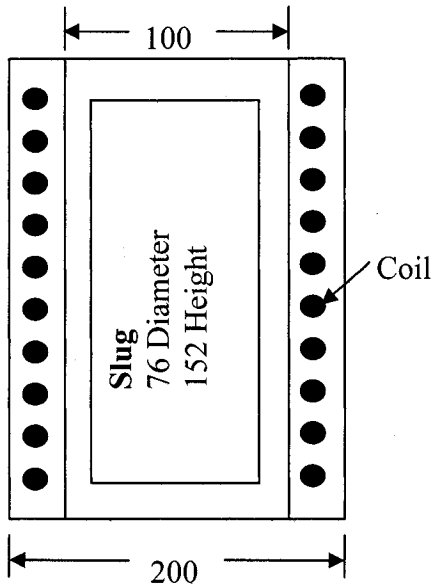

Figure 4.1: Schematic of Induction Heating Coil and Slug

4.2 Mathematical model

Let us consider a metal cylinder cooled by convection and radiation. The initial temperature field and the boundary conditions are known a priori. An internal heat source which is a function of space and time is generated by induction heating. This heat conduction problem is governed by the following non-linear equation:

$$\rho(T)c_p(T)\frac{\partial T}{\partial t} = \frac{1}{r}\frac{\partial}{\partial r}\left(k(T)r\frac{\partial T}{\partial r}\right) + S(r,t) \qquad (4.1)$$

where S(r, t) denotes the inner heat source, ρ is the density, C_p is the specific heat and k is the thermal conductivity. It is assumed that the heat source may be expressed as $S(r,t) = G(t)\cdot H(r)$ and let us define the volumetric heat capacity $C(T) = \rho(T)c_p(T)$. Eq.(4.1) may be rewritten as:

$$C(T)\frac{\partial T}{\partial t} = \frac{1}{r}\frac{\partial}{\partial r}\left(k(T)r\frac{\partial T}{\partial r}\right) + G(t)\cdot H(r) \qquad (4.2)$$

The corresponding boundary and initial conditions are as follows:

$$k\frac{\partial T}{\partial r}\bigg|_{r=0} = 0,\ k\frac{\partial T}{\partial r}\bigg|_{r=R} = p(T) + q(t),\ T(r,0) = f(r) \tag{4.3}$$

where $p(T) = \dfrac{\sigma_b\left(T_s^4 - T_p^4\right)}{\dfrac{1}{\varepsilon_s} + \dfrac{1-\varepsilon_p}{\varepsilon_p}\dfrac{As}{A_p}}$ is the radiative heat flux, q(t) is the convective heat flux and $\sigma_b = 5.67\times10^{-8}\,W/m^2\cdot K^4$ is the Stefan-Boltzmann constant. The subscript 's' refers to the slug surface, while 'p' denotes inner surface of the heater pedestal. We assume that the coil is cooled by air, and that $T_p \equiv T_{ambient}$.

4.3 Heat source distribution

It can be proved from the Maxwell equations that the induced current density decreases exponentially from the periphery of the billet towards the center [82]. The distribution of current density within a cylinder-shaped material is of the form:

$$I(r) = I_0 \cdot e^{-(R-r)/\delta} \tag{4.4}$$

Here I_0 is the maximum eddy current on the surface, R is the material radius. From Joule's law, we may get the radial distribution of power density (heat source) as:

$$S(r) = S_0 \cdot \frac{I^2}{I_0^2} = S_0 \cdot e^{-2(R-r)/\delta} \tag{4.5}$$

Here S_0 denotes the maximum power density (heat source) on the surface and δ is the penetration (skin) depth. The time-dependent heat source may then be expressed as:

$$S(r,t) = G(t) \cdot e^{-2(R-r)/\delta} \tag{4.6}$$

For metallic materials, the skin depth can be expressed in terms of the resistivity, permeability of the material and the current frequency. This yields:

$$\delta = 503.3\sqrt{\frac{\chi}{\mu_r f}} \tag{4.7}$$

The symbol χ stands for the load resistivity (in ohms-meters), μ_r is the load relative magnetic permeability, f is the current frequency (in Hz). For aluminum alloys and copper, $\mu_r \cong 1$. The load resistivity χ is proportional to the temperature. For the

aluminum alloy A357, $\chi = 3.89\times10^{-8} + 1.53\times10^{-10}\mathrm{T}\ (\Omega\cdot\mathrm{m})$. The power density (heat source) distribution for A357 along the radius is shown in Fig.4.2. It is found that the temperature does not influence the heat source distribution significantly within the range $20^{\circ}\mathrm{C}$ to $570^{\circ}\mathrm{C}$. The resistivity can be treated as a constant therefore. However, the current frequency considerably affects the heat source distribution. Generally speaking, the temperature distribution becomes more uniform as the frequency gets smaller.

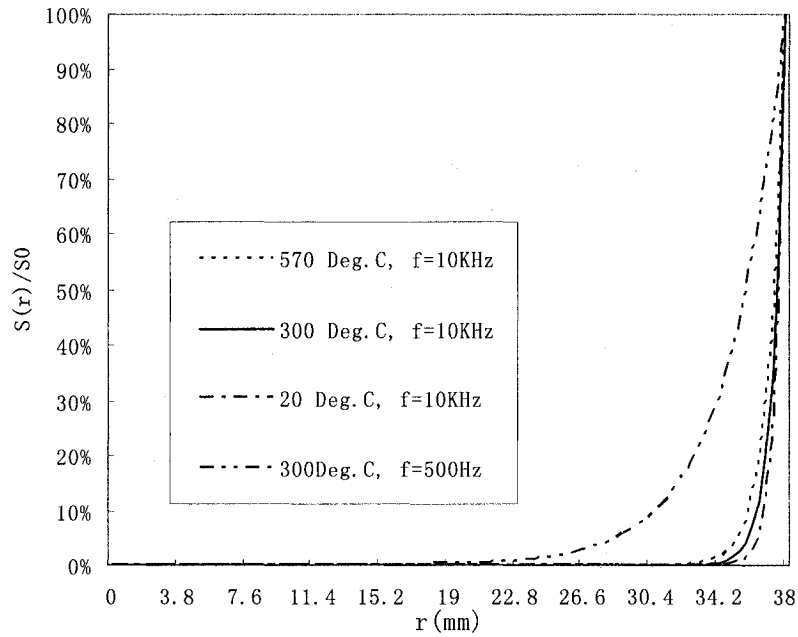

Figure 4.2: Heat Source Distribution of A356

4.4 Phase Change and Apparent Heat Capacity Method

The material heating process in semi-solid state is simulated by applying *apparent heat capacity method* [83-85] that evaluates an effective heat capacity from the rate of change of enthalpy in the mushy range. If the enthalpy in the mushy rigion is defined as:

$$H = \int_{T_{ref}}^{T} \rho(T)c_p(T)dT + \rho_l f_l L \tag{4.8}$$

where T_{ref} is a reference temperature below the melting point, L the latent heat, and f_l

the liquid volume fraction, then the effective heat capacity is defined as:

$$C^*(T) = \frac{dH}{dT} = \rho(T)c_p(T) + \rho_l \frac{\partial f_l}{\partial T} L = f_{w,s}\rho_s c_s + f_{w,l}\rho_l c_l + \rho_l \frac{\partial f_l}{\partial T} L \qquad (4.9)$$

where c_s and c_l are the specific heat heats at solidus and liquidus temperature respectively; $f_{w,s}$ and $f_{w,l}$ are solid and liquid fractions by weight. Similarly, the equivalent thermal conductivity in the mushy region [86] is defined as

$$k^*(T) = k_s f_{w,s} + k_l f_{w,l} \qquad (4.10)$$

Considering that the density of A357 doesn't change too much within the mushy range, we assume that the fraction by weight is equal to the volumetric fraction. Then the conduction problem with phase change is equivalent to the following:

$$C^*(T)\frac{\partial T}{\partial t} = \frac{1}{r}\frac{\partial}{\partial r}\left(k^*(T) r \frac{\partial T}{\partial r}\right) + G(t)\cdot H(r) \qquad (4.11)$$

$$C^*(T) = \begin{cases} C_s(T) & T \le T_s \\ f_s\rho_s c_s + f_l\rho_l c_l + \rho_l \dfrac{\partial f_l}{\partial T} L & T_s < T < T_l \\ C_l(T) & T \ge T_l \end{cases} \qquad (4.12)$$

$$k^*(T) = \begin{cases} k_s(T) & T \le T_s \\ k_s f_s + k_l f_l & T_s < T < T_l \\ k_l(T) & T \ge T_l \end{cases} \qquad (4.13)$$

T_s and T_l are the solidus and liquidus temperature respectively.

Hashemi and Sliepcevich [87] introduced a normal distribution model to express the melting/solidification rate:

$$\frac{df_l}{dT} = (\varepsilon\pi^{-1/2})\exp[-\varepsilon^2(T - T_t)^2] \qquad (4.14)$$

in which $T_t = \frac{T_s + T_l}{2}$; ε is so chosen that $\mathrm{erf}(\varepsilon\Delta T_t) = 1.0 - \lambda$, where $\Delta T_t = \frac{T_l - T_s}{2}$, λ is a sufficiently small positive number. For the aluminum alloy A357, $T_s = 555^\circ C$, $T_l = 615^\circ C$, the melting rate $\frac{df_l}{dT}$ within the mushy region $555 \le T \le 615$ is shown in

Fig.4.3a. Integrating the right hand side of Eq.4.14, the liquid fraction f_l can be determined by employing the Simpson method. It is found that the normal distribution model matches the experimental data provided by IMI (Industrial Material Institute) if ε is set to 0.045 (see Fig.4.3b). By using a general linear least square method, we get an approximation function of the volumetric fraction of liquid:

$$f_l = 1.0068 - 1.1968\frac{(620-T)}{70} + 6.1945\left[\frac{(620-T)}{70}\right]^2 - 23.0084\left[\frac{(620-T)}{70}\right]^3 + 27.5224\left[\frac{(620-T)}{70}\right]^4 - 10.5185\left[\frac{(620-T)}{70}\right]^5 \quad (4.15)$$

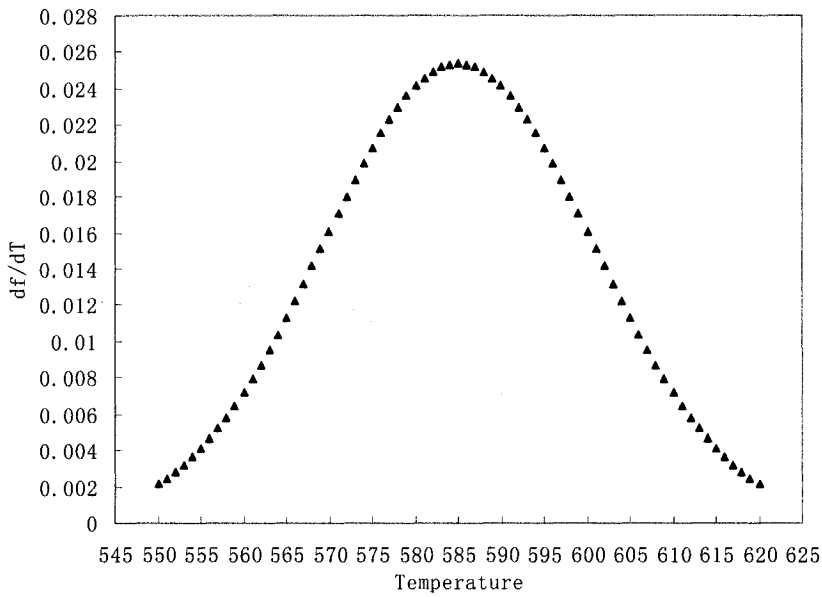

Figure 4.3a: Normal distribution model, A357 alloy, $\varepsilon = 0.045$

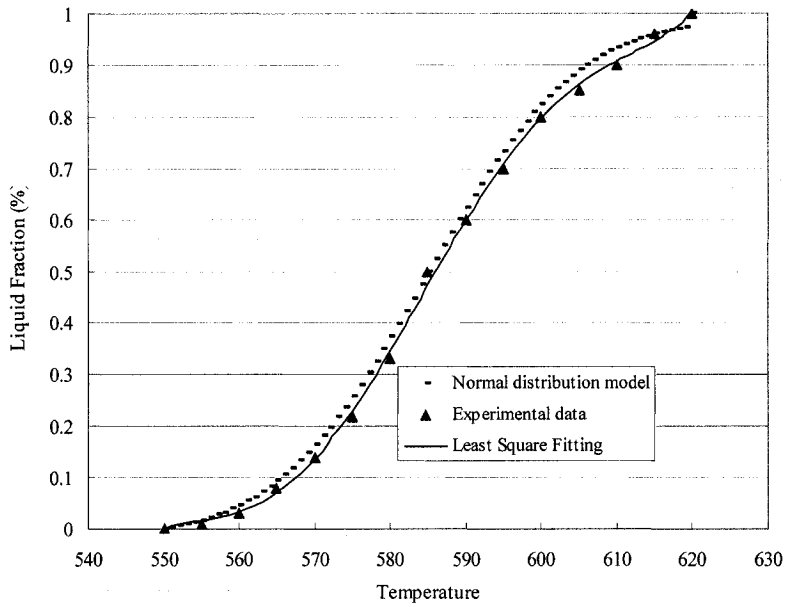

Figure 4.3b: Liquid fraction vs temperature, A357 alloy, $\varepsilon = 0.045$

4.5 Optimal heating control problem

As discussed earlier, the heat source distribution H(r) will be determined by the operating frequency of the induction heater. If the surface cooling flux q(t) is given, our objective is to determine the evolution in time of the heat source G(t) such that the final temperature $T(r,t_f)$ is equal to the targeted value $T_E(r)$. The solution is obtained by minimizing the error functional E:

$$E(G) = \frac{1}{2}\int_0^R [T(r,t_f) - T_E(r)]^2 dr + \frac{\xi}{2}\int_0^{t_f} G^2(t)dt \qquad (4.16)$$

where ξ is the regularization parameter. Among the various optimization techniques, the conjugate gradient method is frequently adopted because of its efficiency and self-regularization character. As with any iterative algorithm, the search direction and step size must be determined. The search direction is related to the gradient of E, which is obtained by solving an adjoint problem, while the optimal step size is determined by solving a sensitivity problem.

4.5.1 Sensitivity equation

In this case, the sensitivity temperature $\tilde{T}$ is defined as the directional derivative of T at G in the direction ΔG:

$$\tilde{T} = \lim_{\varepsilon \to 0} \frac{T(G + \varepsilon \Delta G) - T(G)}{\varepsilon} \tag{4.17}$$

Starting from Eq. (4.2), the sensitivity equation is readily obtained as:

$$\frac{\partial (C\tilde{T})}{\partial t} = \frac{1}{r}\frac{\partial}{\partial r}\left(r \frac{\partial (k\tilde{T})}{\partial r} \right) + \Delta G \cdot H \tag{4.18}$$

Similarly, we can derive the corresponding initial and boundary conditions:

$$\tilde{T}(r,0) = 0, \quad \left.\frac{\partial (k\tilde{T})}{\partial r}\right|_{r=0} = 0, \quad \left.\frac{\partial (k\tilde{T})}{\partial r}\right|_{r=R} = (p' \cdot \tilde{T})\big|_{r=R} \tag{4.19}$$

4.5.2 Adjoint equation

According to the definitions of the error functional and the temperature sensitivity, it is not difficult to derive the following equation:

$$D_{\Delta G} E(G) = \int_0^R \left\{ \tilde{T}(r,t_f) \cdot [T(r,t_f) - T_E] \right\} dr + \xi \int_0^{t_f} (G \cdot \Delta G) dt = \int_0^{t_f} (\nabla E \cdot \Delta G) dt \tag{4.20}$$

If the adjoint temperature $\bar{T}$ and Eq.(4.18) are respectively treated as a Lagrange multiplier and as a constraint, we may rewrite Eq.(4.20) in the form:

$$\begin{aligned} D_{\Delta G} E(G) = & \int_0^R \left\{ [T(r,t_f) - T_E] \cdot \tilde{T}(r,t_f) \right\} dr + \xi \int_0^{t_f} (G \cdot \Delta G) dt \\ & + \int_0^{t_f} \int_0^R \bar{T} \left[r \frac{\partial (C\tilde{T})}{\partial t} - \frac{\partial}{\partial r}\left(r \frac{\partial (k\tilde{T})}{\partial r} \right) - r \cdot \Delta G \cdot H \right] dr dt \end{aligned} \tag{4.21}$$

Considering the initial and boundary conditions of the sensitivity problem, we obtain the following adjoint equation after some algebra:

$$C\frac{\partial \bar{T}}{\partial t} + \frac{k}{r}\frac{\partial}{\partial r}\left(r \frac{\partial \bar{T}}{\partial r} \right) = 0 \text{ or } C\frac{\partial \bar{T}}{\partial \tau} = \frac{k}{r}\frac{\partial}{\partial r}\left(r \frac{\partial \bar{T}}{\partial r} \right), \quad \tau = t_f - t \tag{4.22}$$

$$k\frac{\partial \overline{T}}{\partial r}\bigg|_{r=0} = 0,\ k\frac{\partial \overline{T}}{\partial r}\bigg|_{r=R} = (p'\cdot \overline{T})\big|_{r=R},\ \overline{T}(r,t_f) = -\frac{T(r,t_f)-T_E(r)}{C\cdot r} \tag{4.23}$$

Eq.(4.21) then becomes

$$D_{\Delta G}E(G) = \int_0^{t_f}\left(\xi\cdot G - \int_0^R \overline{T}Hrdr\right)\Delta G dt \tag{4.24}$$

Comparing Eqs.(4.24) and (4.20), it follows that the gradient of the error functional is:

$$\nabla E = \xi\cdot G - \int_0^R \overline{T}(r,t)\cdot H(r)\cdot r\cdot dr \tag{4.25}$$

4.5.3 Regular conjugate gradient method

The iterative formula and the conjugate search direction may be expressed as:

$$G^{k+1} = G^k + \alpha^k P^k \tag{4.26}$$

$$P^k = -\nabla E^k + \beta^k P^{k-1} \tag{4.27}$$

$$\beta^k = \frac{\int_0^{t_f}(\nabla E^k - \nabla E^{k-1})\nabla E^k dt}{\int_0^{t_f}(\nabla E^{k-1})^2 dt} \tag{4.28}$$

The optimal step size may be determined by requiring that the first order derivative of E in the direction of α^k must vanish. It follows that:

$$\alpha^k = -\frac{\int_0^R (T^k - T_E)\tilde{T}^k dr + \xi\int_0^{t_f} G^k P^k dt}{\int_0^R (\tilde{T}^k)^2 dr + \xi\int_0^{t_f}(P^k)^2 dt} \tag{4.29}$$

4.5.4 Modified conjugate gradient method

The works presented in [59, 61, 81] show that the optimal solutions by regular CGM may tend to a (time-averaged) constant and change steeply near the final time. Such a heating/cooling curve is difficult to execute in engineering applications. In fact, a

modification of the conjugate direction is found to be a good way to improve the profile of the optimization solutions [49]. This modified CG method [75-78] is based on the assumption that the objective function G(t) is a continuously differentiable function defined as:

$$G(t) = \int_0^t \frac{dG(t')}{dt'} dt', \; \Delta G(t) = \int_0^t \frac{d\Delta G(t')}{dt'} dt' \tag{4.30}$$

which requires that:

$$G(t=0) = \Delta G(t=0) = 0 \tag{4.31}$$

Differentiating under the integral sign, we get the equality:

$$\frac{d}{dt} \int_{t_f}^{t} \int_0^R \overline{T}(r,t')H(r) r dr dt' = \int_0^R \overline{T}(r,t) H(r) r dr \tag{4.32}$$

Introducing Eq.(4.32) into Eq.(4.20), we obtain:

$$D_{\Delta G} E\left(\frac{dG}{dt}\right) \equiv D_{\Delta G} E(G) = \int_0^{t_f} \left\{ \left[\frac{d}{dt} \int_{t_f}^{t} \int_0^R \overline{T}(r,t')H(r) r dr dt' \right] \cdot \Delta G \right\} dt \tag{4.33}$$

Integrating the first term of the right hand side of Eq.(4.26) by parts and rewriting the second term yields:

$$D_{\Delta G} E\left(\frac{dG}{dt}\right) = \int_0^{t_f} \frac{d\Delta G}{dt} \left[- \int_t^{t_f} \int_0^R \overline{T}(r,t')H(r) r dr dt' \right] dt \tag{4.34}$$

By comparing Eq.(4.27) with Eq.(4.16), we can conclude that:

$$\nabla E\left(\frac{dG}{dt}\right) = - \int_t^{t_f} \int_0^R \overline{T}(r,t')H(r) r dr dt' = \int_t^{t_f} \nabla E dt' \tag{4.35}$$

The modified search direction is related to the derivative of the direction of descent R^k by the relation:

$$p^k = \int_0^t R^k dt' \tag{4.36}$$

$$R^k = -\nabla E\left(\frac{dG}{dt}\right) + \gamma^k R^{k-1} \tag{4.37}$$

The conjugate coefficient γ^k is then given by Eq.(4.28), while the gradient of the error function is replaced by $\nabla E\left(\frac{d\Delta G}{dt}\right)$:

$$\gamma^k = \frac{\int_0^{t_f}\left[\nabla E^k\left(\frac{dG}{dt}\right) - \nabla E^{k-1}\left(\frac{dG}{dt}\right)\right]\cdot \nabla E^k\left(\frac{dG}{dt}\right)\cdot dt}{\int_0^{t_f}\left[\nabla E^{k-1}\left(\frac{dG}{dt}\right)\right]^2 \cdot dt} \tag{4.38}$$

4.6 Optimal cooling control problem

Suppose that the heat source $S(r,t)$ is known. Let us determine the cooling flux $q(t)$ required to achieve a uniform final temperature distribution. The optimization solution is obtained by minimizing the error functional *E*:

$$E(q) = \frac{1}{2}\int_0^R [T(r,t_f) - T_E(r)]^2\, dr + \frac{\xi}{2}\int_0^{t_f} q^2(t)dt \tag{4.39}$$

Following a similar procedure, we obtain the sensitivity and adjoint equations and the gradient of the error functional as follows:

Sensitivity Equation

$$\frac{\partial(C\tilde{T})}{\partial t} = \frac{1}{r}\frac{\partial}{\partial r}\left(r\frac{\partial(k\tilde{T})}{\partial r}\right) \tag{4.40}$$

$$\tilde{T}(r,0) = 0,\ \left.\frac{\partial(k\tilde{T})}{\partial r}\right|_{r=0} = 0,\ \left.\frac{\partial(k\tilde{T})}{\partial r}\right|_{r=R} = (p'\cdot\tilde{T})\big|_{r=R} + \Delta q(t) \tag{4.41}$$

Adjoint Equation

$$C\frac{\partial\bar{T}}{\partial t} + \frac{k}{r}\frac{\partial}{\partial r}\left(r\frac{\partial\bar{T}}{\partial r}\right) = 0 \text{ or } C\frac{\partial\bar{T}}{\partial\tau} = \frac{k}{r}\frac{\partial}{\partial r}\left(r\frac{\partial\bar{T}}{\partial r}\right),\ \tau = t_f - t \tag{4.42}$$

$$\left.k\frac{\partial\bar{T}}{\partial r}\right|_{r=0} = 0,\ \left.k\frac{\partial\bar{T}}{\partial r}\right|_{r=R} = (p'\cdot\bar{T})\big|_{r=R},\ \bar{T}(r,t_f) = -\frac{T(r,t_f) - T_E(r)}{C\cdot r} \tag{4.43}$$

Gradient of the Error Functional

$$\nabla E = \xi q - \overline{T}(R,t) \cdot R \tag{4.44}$$

The overall CG algorithm remains the same as in the previous section.

4.7 Results and discussion

The solution algorithm is tested here for the specific case of A356/A357 aluminum alloy. Table 4.1 shows that the difference between A356 and A357 is slight, the former contains a higher proportion of magnesium. Just about all of this is locked up in solution in the primary alpha phase. For numerical modeling or induction heating purposes, they are treated as the same alloy and the same parameters are employed. The thermo-physical and electromagnetic properties of this light metal alloy are shown in Table 4.2 [15, 82]. The other parameters used for the calculations are presented in Table 4.3. The resistivity of the material should be proportional to the temperature; the surface emissivity of the metal may vary with temperature and oxidation during the heating. However, both parameters are treated as constants here since their variations would only have a minor impact on the final results.

Table 4.1: Chemical composition of A356/A357 alloy

	Al	Si	Mg	Fe	Cu	Mn	Zn	Ti
A356	Bal.	6.5-7.5	0.25-0.45	0.2	0.2	0.1	0.1	0.2
A357	Bal.	6.5-7.5	0.40-0.70	0.2	0.2	0.1	0.1	0.04-0.2

Table 4.2: Thermo-physical and electromagnetic properties of A356/A357

Density (kg/m^3)	-0.208 T(°C)+2680.0
Specific heat ($J/kg\cdot°C$)	0.454 T(°C)+904.6
Thermal Conductivity ($W/m\cdot°C$)	0.04 T(°C)+153.1
Solidus temperature (°C)	555
Liquid temperature (°C)	615

Resistivity ($\Omega \cdot m$)	8.0×10^{-8}
Relative magnetic permeability	1.0
Specific heat of liquid ($J/kg \cdot ^\circ C$)	1300
Thermal conductivity of liquid ($W/m \cdot ^\circ C$)	80
Latent heat (J/kg)	440000

Table 4.3: Parameters in calculations

Current frequency (Hz)	10000
Ambient Temperature ($^\circ C$)	20
Emissivity (Aluminum Alloy)	0.1
Emissivity (Ceramic Pedestal)	0.94
Maximum Input Power (W)	9000
Electrical Efficiency of Induction Heater (%)	80.0

4.7.1 Optimal heating problem

In this section, the forced convection cooling flux is supposed to be known. From Eq.(4.6), the input power may be expressed as:

$$\begin{aligned} P(t) &= \frac{1}{\eta_E}\iiint_V S(x,t)dV = \frac{G(t)}{\eta_E}\int_0^H\int_0^{2\pi}\int_0^R e^{-2(R-r)/\delta} r dr d\theta dz \\ &= \frac{2\pi H}{\eta_E}\left(\frac{\delta R}{2} - \frac{\delta^2}{4} + \frac{\delta^2}{4}e^{-2R/\delta}\right)G(t) \end{aligned} \tag{4.45}$$

It follows that:

$$\frac{P(t)}{P_{max}} = \frac{G(t)}{G_{max}} \tag{4.46}$$

Our purpose is to heat the material up to the targeted temperature as uniformly as possible. If the objective function G(t) is determined, then the optimal heating strategy, namely P(t) is obtained. We note that G(t) should be equal to or greater than zero. This restriction must be taken into account in the optimization problem, which then becomes

a constrained minimization problem. If the maximum power of the induction heater is 9KW and the efficiency of the induction unit equal to 80% when the current frequency is 10KHz, then according to Eq.(4.45), $G_{max} = 2.84 \times 10^8$.

4.7.1.1 Solid phase heating

Firstly, we study an easier problem: the heating process is limited to the solid range and phase change is not considered. In this case, we set the targeted final temperature below the melting point of the alloy.

Model Validation and one-stage heating

Let us validate the present model for the simple one stage heating method. We choose a power level $P(t) = 56.85\%P_{max} = 5116W$ applied to the sample for 240 seconds at a frequency of 10KHz. Because the material is heated with a constant internal heat source, the temperature within the work-piece increases almost linearly (Fig.4.4a). After 240 seconds, the surface temperature is about 553.5℃ while the central temperature just reaches 542.5℃. Fig.4.4b shows a typical surface-to-core temperature profile which is consistent with the experimental data provided by Bendada et al. [68]. This confirms that our mathematical and physical model is reasonable.

The heat transfer in this heating process is the outcome of Joule effect, thermal diffusion and radiative and convective heat loss at the surface. We also note that the exponential heat source distribution doesn't yield an exponential temperature distribution, because of the high thermal conductivity of A356. It is known from heat transfer and electromagnetics that there are at least three ways to reduce the temperature difference: 1) decreasing the frequency of the induction unit; 2) extending the heating process; 3) cooling the surface of the work-piece.

We know from Eq.4.6 and Eq.4.7 that decreasing the current frequency may increase the penetration depth and effectively improve the uniformity of the heat source distribution.

If all conditions except the frequency remain the same, it is found that the maximum temperature difference at the final time is proportional to the logarithm of the frequency (see Fig.4.5). This suggests that the temperature uniformity is not too sensitive to frequency variations. For instance, when the frequency is reduced from 10KHz to 1000Hz and 100Hz, T_{suface}-T_{center} decreases 13.6% and 27.3% respectively.

The driving mechanism of heat conduction is heat diffusion from higher temperature regions to lower temperature regions. Longer heating times allow greater diffusion times and require less heating power that would reduce the thermal gradient effectively. If the induction frequency remains fixed at 10KHz. Fig.4.6 shows the effect of heating duration. As expected, the temperature distribution obviously tends to become uniform as the heating time goes up. When the heating time is extended to 480 seconds, the maximum temperature difference is reduced to 6℃.

Now let us consider a cooling flux of $1.0\times10^5\,W/m^2$ applied to the surface with a compressed air jet during the last 20 seconds of the heating period of 240s, at f = 10KHz as before. In order to compensate for this additional heat loss, the input power has to be increased to 60.65%P_{max}, that is, 5458W. From Fig.4.7a, it is found that the surface temperature does not rise as fast as the central temperature during the last 20 seconds, because that some of the heat accumulated in the surface region is carried away by the jet. As a consequence, the maximum temperature difference at the end of the process is only 2℃, and the maximum temperature is no longer located on the surface (Fig.4.7b). This proves that the optimal heating problem can be solved by determining the optimal cooling strategy. Additionally, surface cooling might effectively prevent the so-called 'elephant foot' effect.

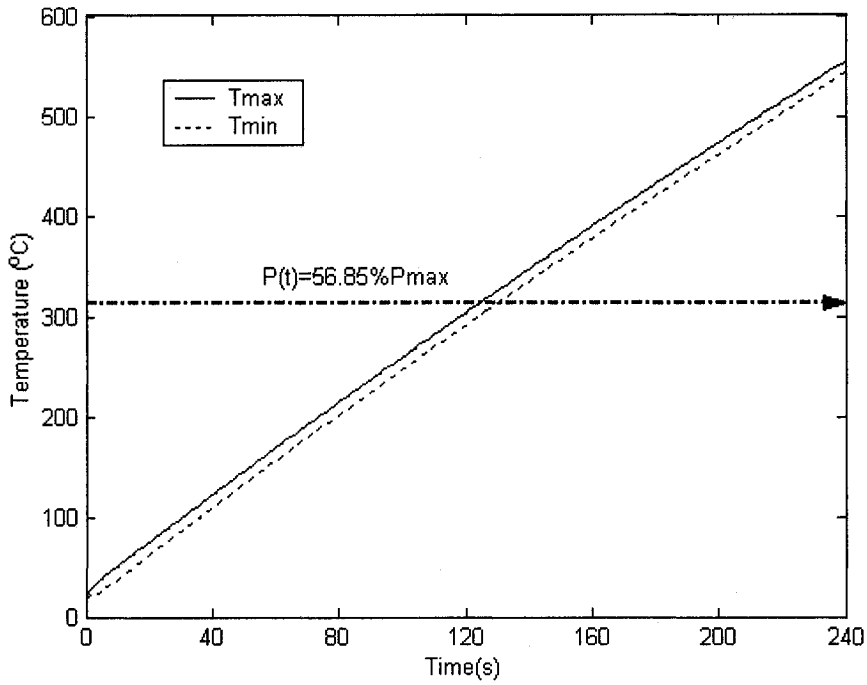

Figure 4.4a: Temperature Evolution, q(t) = 0, f = 10KHz, t_f = 240s

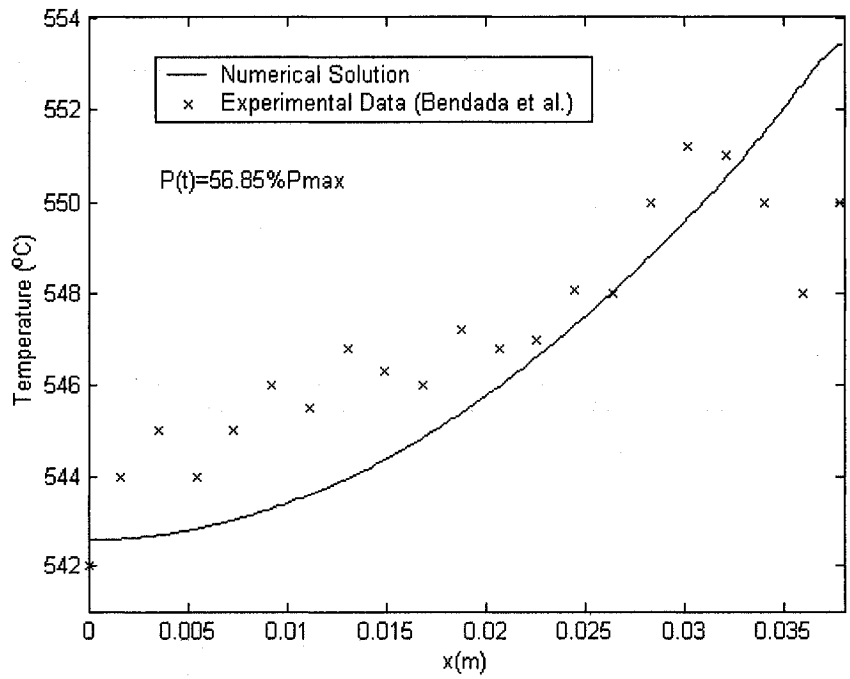

Figure 4.4b: Surface-to-Core temperature profile, q(t) = 0, f = 10KHz, t_f = 240s

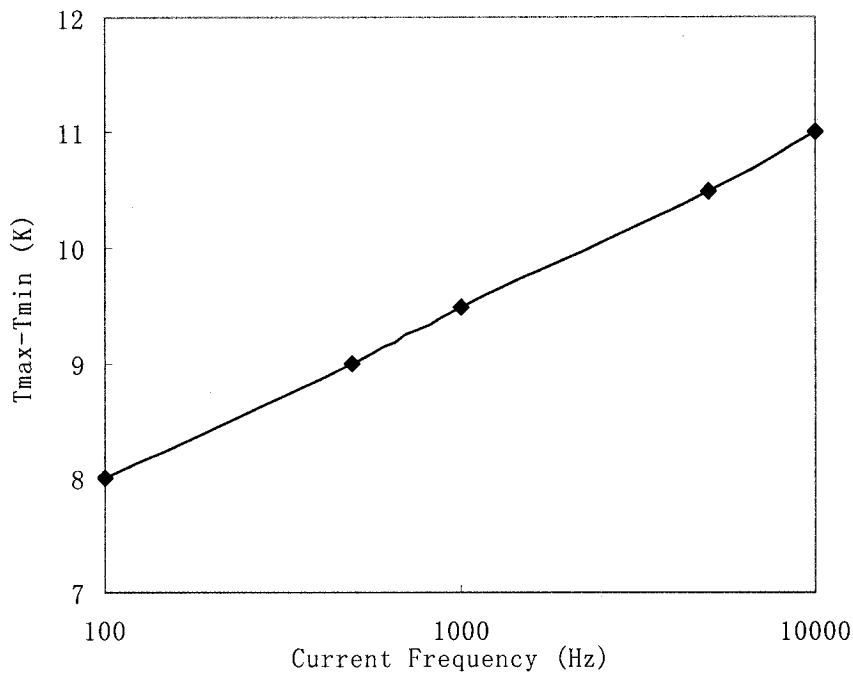

Figure 4.5: Temperature difference vs frequency, q(t) = 0, t_f= 240s

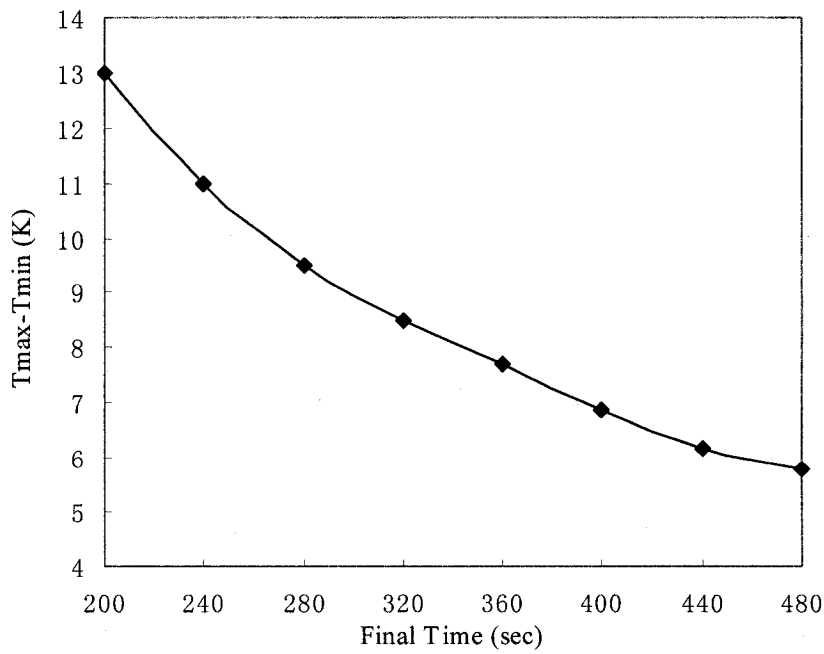

Figure 4.6: Temperature difference vs heating time, q(t) = 0, f = 10KHz

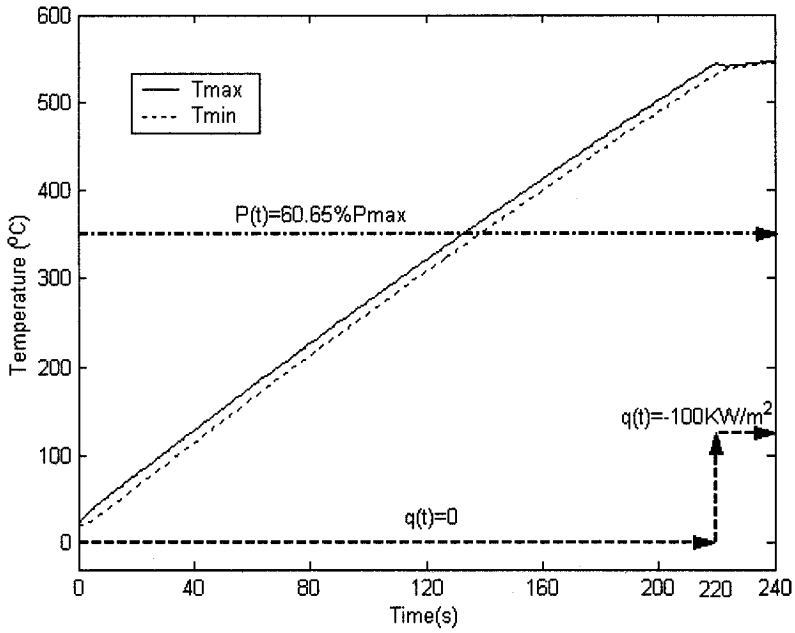

Figure 4.7a: Temperature Evolution, q(t) = -100KW/m^2 (t > 220s), f = 10KHz

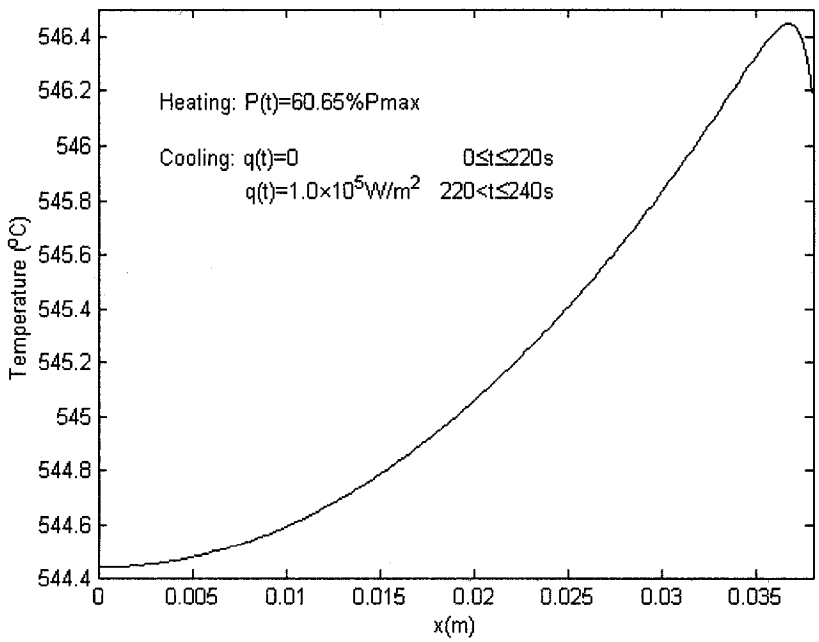

Figure 4.7b: Surface-to-Core temperature profile, q(t) = -100KW/m^2 (t > 220s), t_f = 240s

Optimal Solutions by CGM

In order to achieve a uniform temperature distribution within the work-pieces in the shortest possible heating time, researchers working in the domain of semi-solid forming normally favor multi-step heating strategies. Bendada et al. [68] proposed two empirical two-stage heating strategies: A) start heating at a high-power level for 140s, then switch to a low-power stage during 100s; B) start heating at a high-power level for 205s, then switch to a low-power stage for 35s. We apply these two heating procedures to our model. The high-level powers are then set equal to $91.4\%P_{max}$ and $64.8\%P_{max}$ respectively, while the low-level powers remain at $7.6\%P_{max}$ (Fig.4.8a). Solving the direct problem, the maximum temperature differences at the end of the heating period are found to be 1.6℃ (Fig.4.8b). During the high-power heating stage, the temperature difference between the center and the surface of the sample also remains at a high level: 20℃ for strategy A and 15℃ for strategy B. This suggests that a higher input power may result in a larger temperature difference. This conclusion is also supported by experiments [29]. In the subsequent low-power stage, the temperature differences decrease rapidly because of the sudden drop in the input power. A new heat transfer balance is set up from this moment, and T_{max}-T_{min} remains equal to 1.6℃ until the end of the heating process (Fig.4.8c and Fig.4.8d).

Now let us look at the optimal solutions obtained from the regular CGM. The objective function G(t) must obviously be positive, and this condition has to be accounted for as a constraint in the optimization problem. In order to compare the results with the experimental strategies A and B, tests are performed for a total time of 240s. After 24 iterations starting from a zero initial guess, we obtain a two-stage-like solution (Fig.4.8a). This optimal solution requires that the input power starts from $51\%P_{max}$, then slowly increases to $60\%P_{max}$ and finally rapidly decreases to zero during the last 10 seconds.

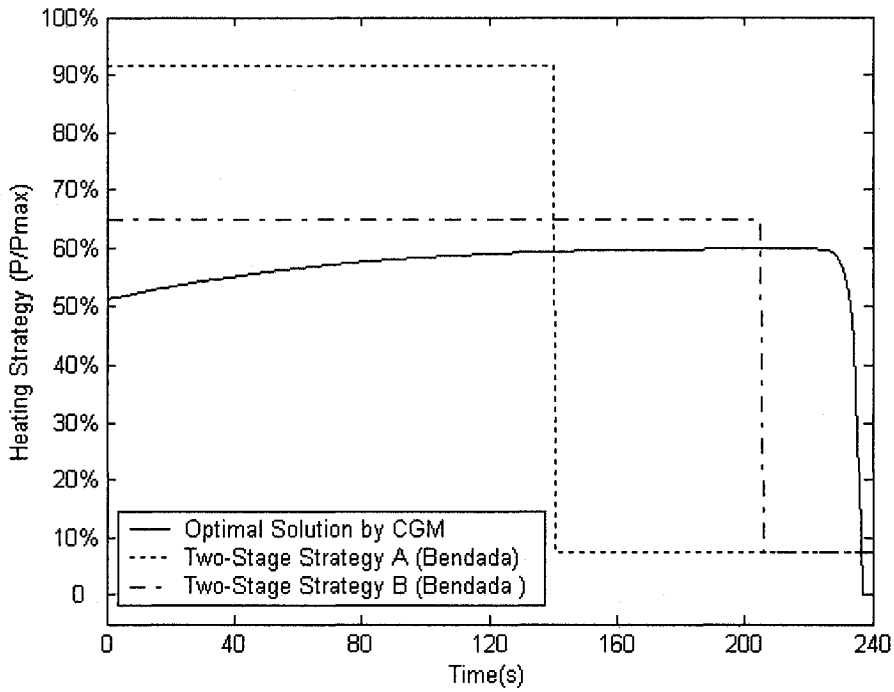

Figure 4.8a: Optimal heating strategy by CGM, initial guess = 0, q(t) = 0, f = 10KHz, t_f = 240s

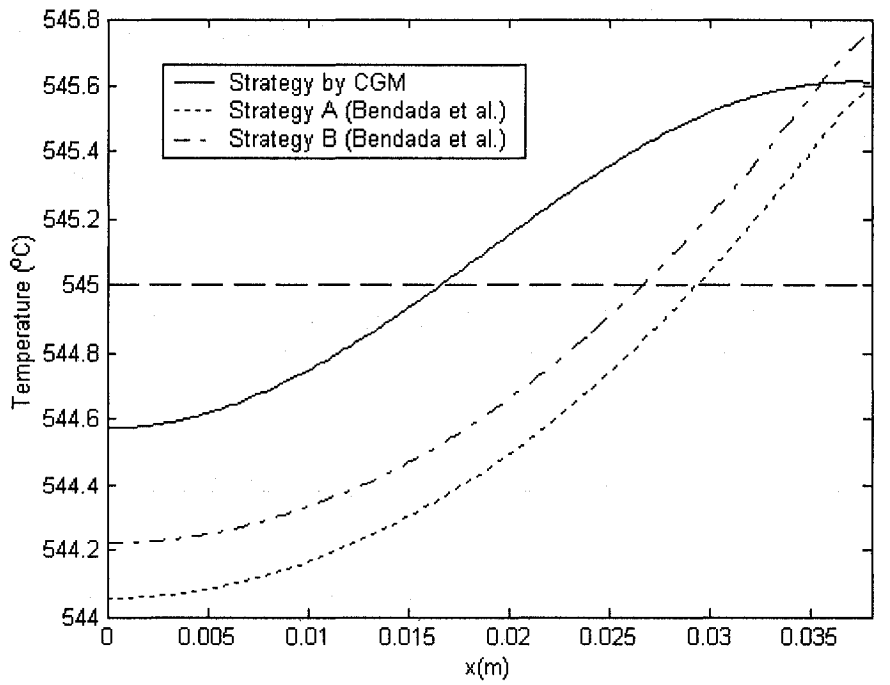

Figure 4.8b: Temperature distribution at final time, q(t) = 0, f = 10KHz, t_f = 240s

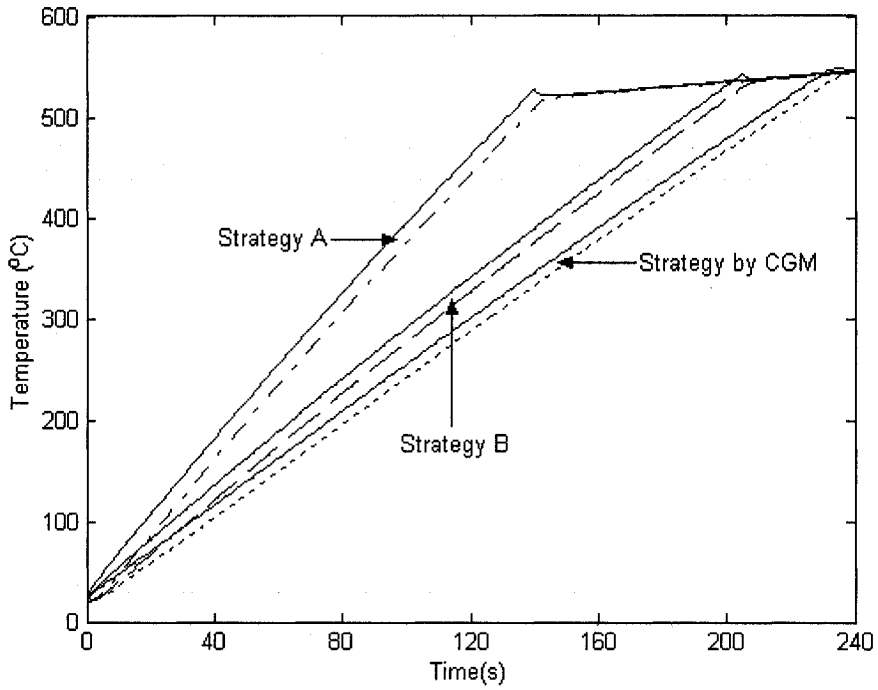

Figure 4.8c: Surface and center temperature evolution, f = 10KHz, t_f = 240s

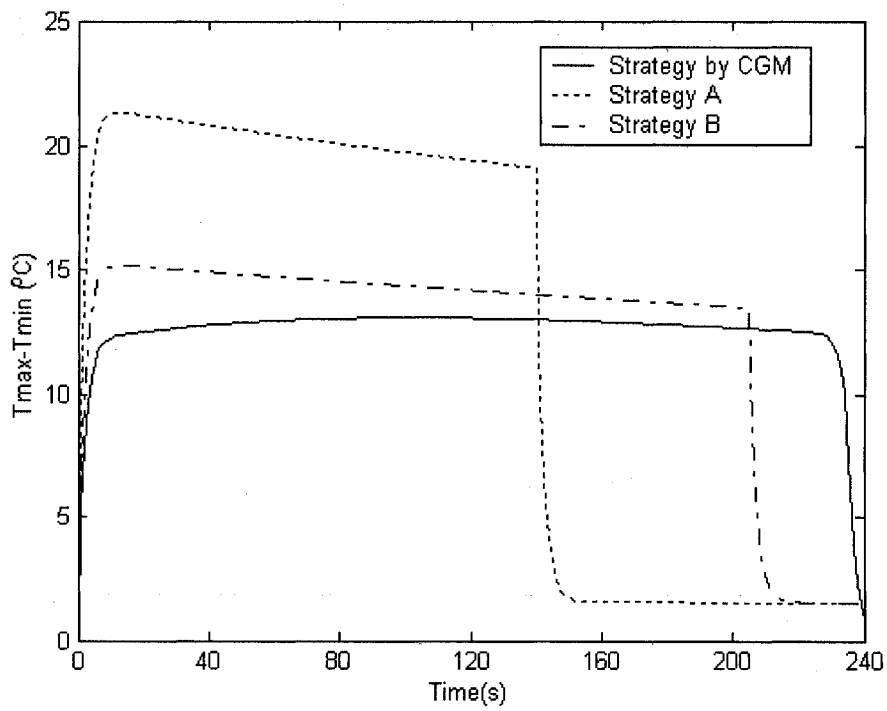

Figure 4.8d: Evolution of maximum temperature difference, f = 10KHz, t_f = 240s

From Fig.4.8b, it is found that the uniformity of the temperature distribution is much better than that obtained from the experimental strategies A and B, and the maximum temperature difference is 1.0℃. The evolution of the temperature on the surface, at the center, and the maximum temperature differences are presented in Fig.4.8c and Fig.4.8d. If we start from the heating strategy B as initial guess, only 7 iterations are needed to obtain the optimal solution shown in Fig.4.9a. This optimal strategy obtained by CGM differs slightly from the initial guess, except during the last 10 seconds, but T_{max}-T_{min} at the final time is considerably reduced from 1.6℃ to 0.22℃ (Fig.4.9b).

Optimal Solutions by Modified CGM

Recently Jiang, Nguyen and Prud'homme [49] found out that a modified CGM is more powerful than the regular CGM to solve this kind of inverse problem. In this study, we shall also use that variant of the algorithm to solve the optimal control problem. The cooling flux is set equal to zero and the frequency is fixed at 10KHz. As discussed previously, the modified CGM is based on the assumption that $G(t) = \Delta G(t = 0) = 0$, which makes the search direction $P^k(t = 0) = 0$. In other words, the optimal solution at t = 0 always remains equals to the initial guess value. The initial guess is very important for the initial solution profile. Both numerical and experimental investigations suggest that the initial input power should be set to a high level. The zero initial guess is then obviously not a good choice.

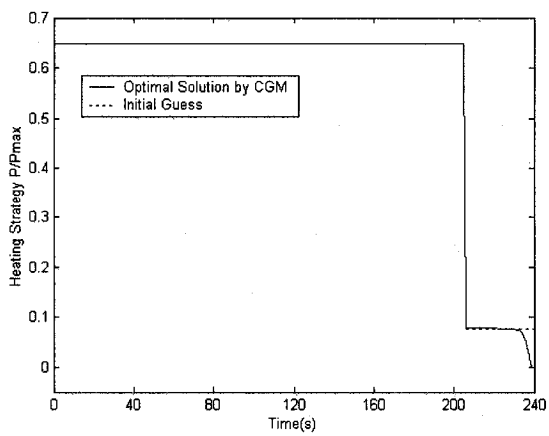

Figure 4.9a: Optimal heating strategy by CGM, initial guess=strategy B, t_f= 240s

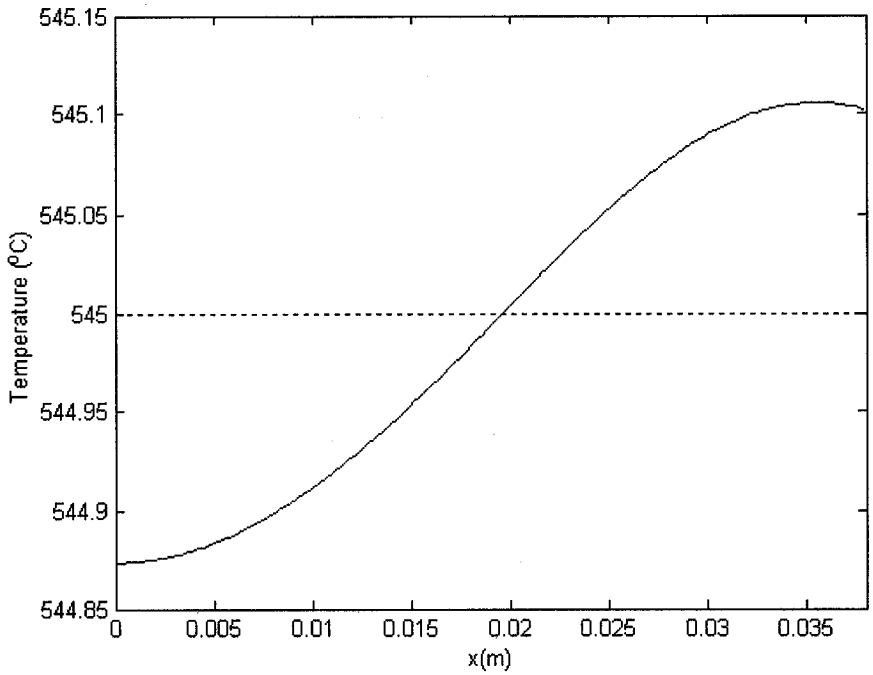

Figure 4.9b: Temperature distribution at final time, q(t) = 0, f = 10KHz, t_f = 240s

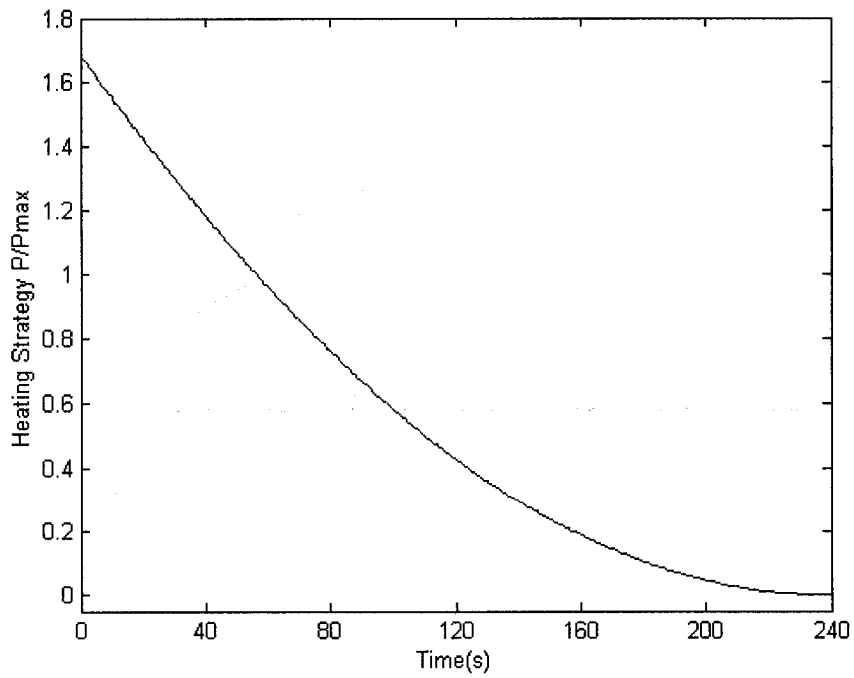

Figure 4.10a: Optimal heating strategy by MCGM, initial guess $G^0 = 168\%G_{max}$

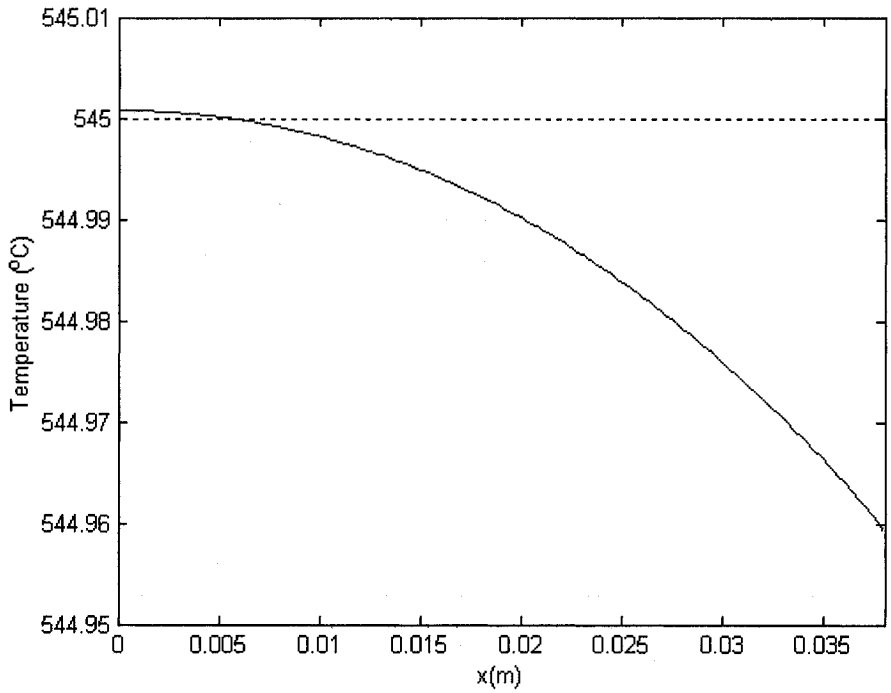

Figure 4.10b: Temperature distribution at final time, q(t) = 0, f = 10KHz, t_f = 240s

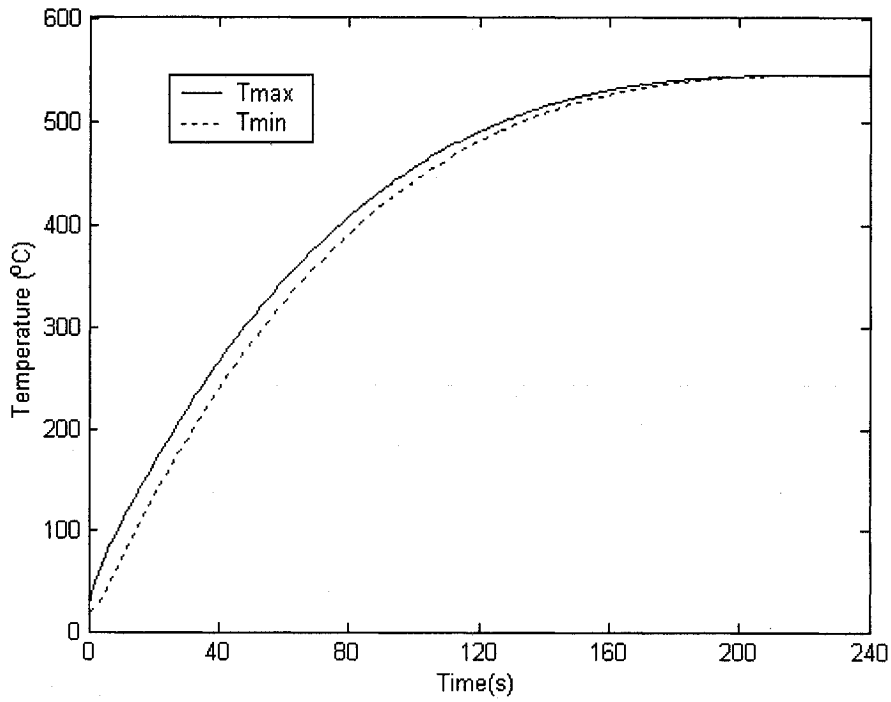

Figure 4.10c: Temperature evolution, q(t) = 0, f = 10KHz, t_f = 240s

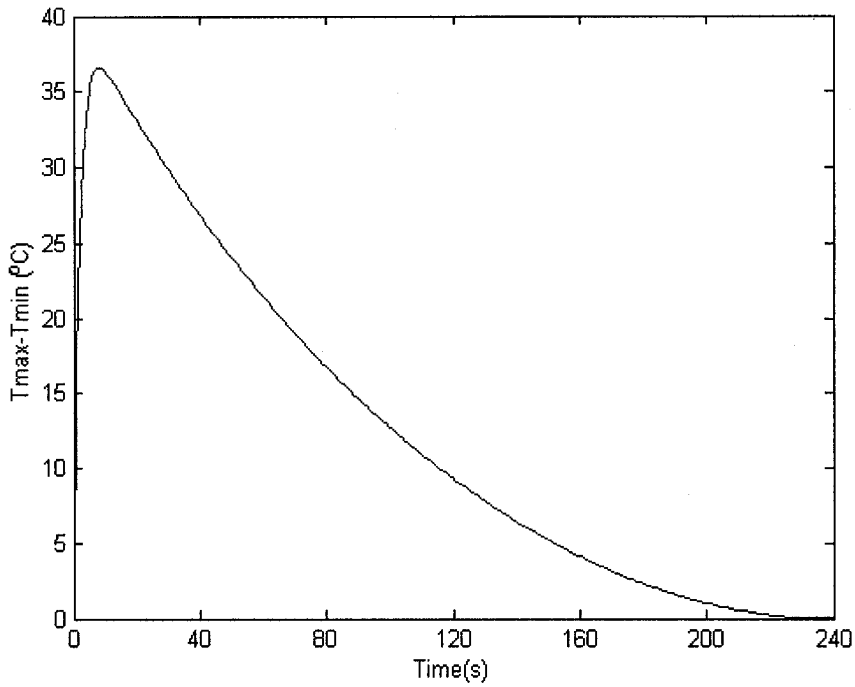

Figure 4.10d: Evolution of maximum temperature difference, q(t) = 0, f = 10KHz, t_f = 240s

When the initial guess G^0 is set to 168%G_{max}, a smooth heating control curve which requires reducing the input power gradually from maximum to zero is predicted from the modified CGM (see Fig.4.10a). The final temperature uniformity is perfectly achieved after 6 iterations: T_{max}-T_{min} is only 0.04℃ (Fig.4.10b). Furthermore, the surface temperature also increases smoothly and the temperature variation rate dT/dt monotonously decreases as the heating time goes up (Fig.4.10c). In the last 40 seconds, dT/dt is very low because the input power is almost zero. Considering the surface radiation heat loss, the surface temperature is even less than that of the center at the final time. There is no risk of surface overheating, meaning that the 'elephant foot' phenomenon is not likely to occur. Comparing Fig.4.10d and Fig.4.10a, it is found that the maximum temperature difference is almost proportional to the input power. This proves again that reducing the heating power to a very low level (even zero) in the last few seconds is the most important condition to achieve the uniformity of the final temperature distribution.

4.7.1.2 Semi-solid heating

In the previous part, the CGM and modified CGM have been successfully applied in optimal control of induction heating for solid-phase metal. However, thixoforming technique requires heating the alloy billet to semi-solid state with uniform liquid fraction. Then phase change has to be considered and the apparent heat capacity method is used to describe the two-phase model. For the A357 alloy, the targeted final temperature is 585℃ which corresponds to a liquid fraction of approximately 50%.

Model validation and four-stage heating

Researchers in Industrial Material Institute (IMI) have found an optimal heating strategy based on a series of reheating experiments aimed to obtain the desired temperature distribution. A single-coil induction heater with 10KHz is chosen to heat the A357 alloy slug with a diameter of 76mm and a height of 152mm. Six K-type thermocouples were embedded in the billet to monitor the temperature curves, beginning from the time when the slug begins to melt to the time just prior to forming.

In order to prevent surface overheating occurring at around 560℃, the input power is reduced to 50% after 240s. However the temperature discrepancies among the points still increase with time, the input power has to be reduced further to 25% and 10% after 375s and 470s. At t = 490s, the power is then cut off and the temperature difference between surface and center is about 1.5℃ at this moment. This four-stage heating strategy shown in Fig.4.11a is undoubtedly a good choice for the specific material (A357) and specific dimensions (76mm diameter).

In order to validate our two-phase heat transfer model based on the apparent heat capacity method, this heating process is simulated numerically, supposing that the surface natural convection coefficient is $10.0\,W/m^2\cdot{}^\circ C$. The corresponding solutions are presented in Fig.4.11b. It is found that the surface temperature agrees well with the experimental data provided by IMI. However, for the coldest temperature located in the

center of billet, the numerical curve deviates from the experimental records after 275s. As we have known, the center area is heated mainly due to the heat diffusion; the effect of heat source there can be ignored. In the mushy region (555℃ < T < 615℃), the liquid fraction increases with temperature, and then the equivalent thermal conductivity will decrease accordingly because the conductivity of the liquid A357 is much lower. Furthermore, more liquid fraction must result in the augmentation of the equivalent heat capacity. Common sense tells us that the temperature increasing rate should be slower and slower with time. Let's observe the experimental data for the time interval between 275 s to 425 s: the central temperature only increases 6.5℃in 150 s; but it raises 11.5℃ in the last 65 s. So it is believed that the numerical solution is more reasonable.

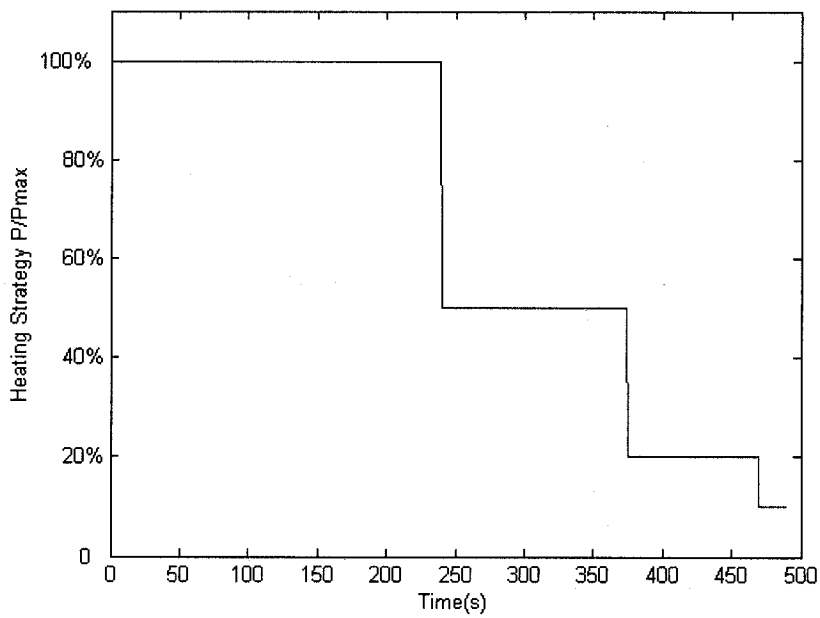

Figure 4.11a: Four-stage heating strategy, maximum power = 5.7KW, η_E = 80%

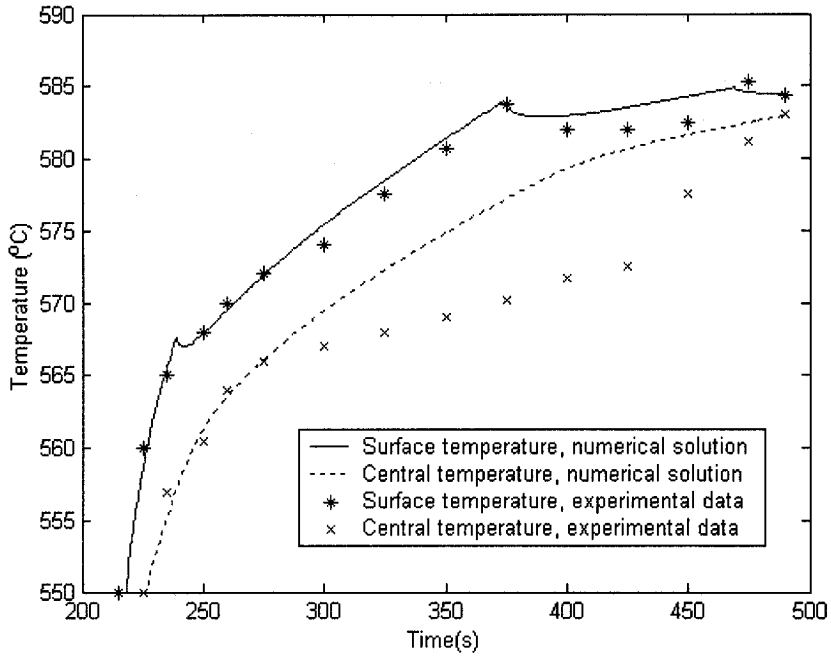

Figure 4.11b: Temperature evolution in the mushy region

Optimal solutions by CGM

Suppose that the input power of an induction heater is 9KW, the total efficiency is 80%, and the working frequency is 10KHz; the billet (76mm diameter, A357 alloy) surface natural convection coefficient is $10.0\,W/m^2\cdot{}^\circ C$. If we apply a one-stage heating mode, for example P(t) = 68%Pmax for a total time of 300s, the maximum temperature difference at the end of heating will be 16℃. Even if we extend the heating time to 490s with input power P(t) = 45%Pmax, a temperature difference of 12℃ still unacceptable.

Now we apply regular the CGM to determine a strategy for heating this material to semi-solid state with uniform temperature distribution (585℃). Obviously, the objective function G(t) should be positive and this constraint must be considered in the optimization problem. The numerical tests are first performed for a total time of 490s. After 30 iterations starting from a zero initial guess, the convergence stops and the optimal solution shown in Fig.4.12a requires that the input power starts from $32.5\%P_{max}$, then slowly increases to $48.5\%P_{max}$ and finally rapidly decreases to zero during the last

10 seconds. Fig.4.12b presents the temperature distribution at the final time, it is found that the uniformity of the temperature distribution is much worse than that obtained from the four-stage strategy mentioned previously, and the maximum temperature difference at the final time is more than 6.0℃. If we reduce the total heating time, the thermal gradient will increase accordingly (Fig.4.13). If the initial guess is zero and t_f= 300s, the maximum temperature at the final time reaches 11℃, that is not acceptable. More iterations do not improve the solution.

From the above discussion, one may conclude that the optimal control strategies obtained by regular CGM from zero initial guess for semi-solid alloy heating are not satisfactory, even if the thermal gradient is deduced. The main reason is probably related to the unreasonable profile of heating curve that requires increasing the input power slowly from beginning then cutting off suddenly in the last few seconds. Both numerical and experimental investigations suggest that an ideal heating curve should decrease the input power gradually with time.

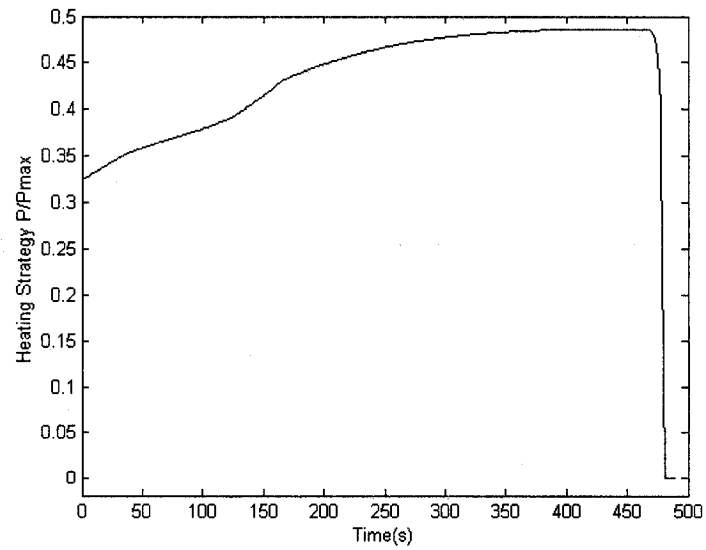

Figure 4.12a: Optimal heating strategy by CGM, initial guess=0,
f = 10KHz, t_f= 490s

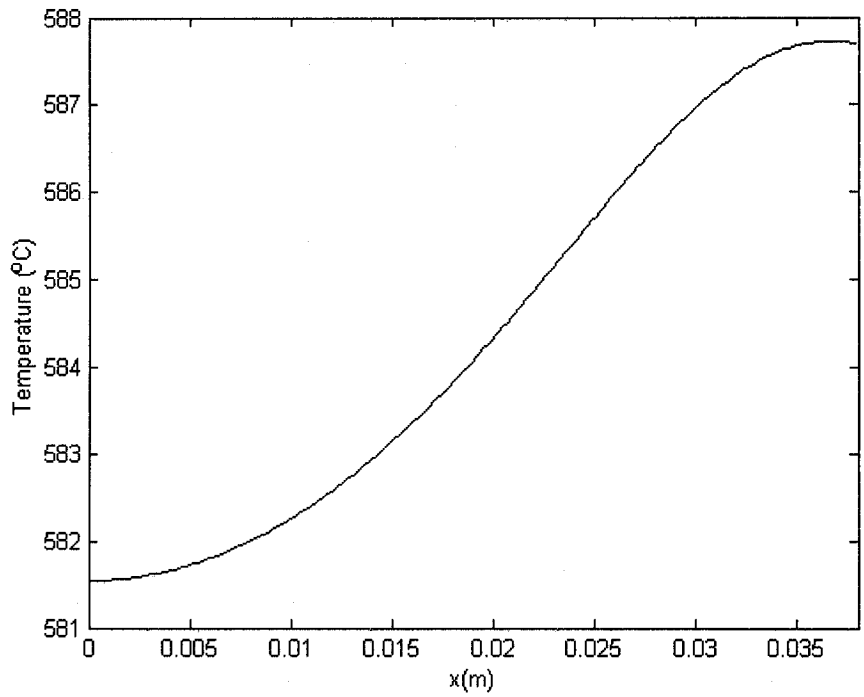

Figure 4.12b: Temperature distribution at final time, f = 10KHz, t_f = 490s

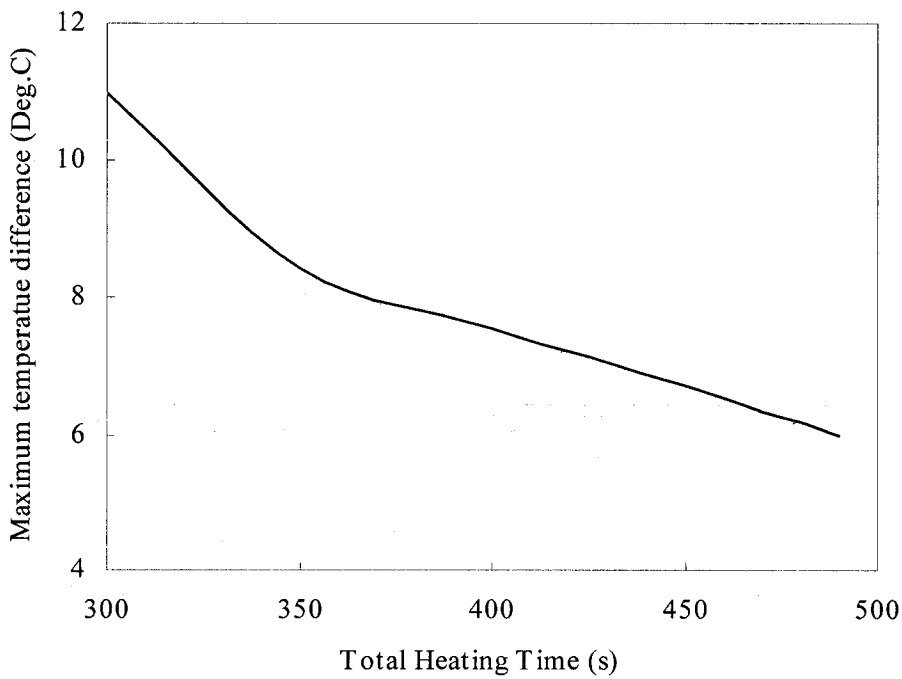

Figure 4.13: Maximum temperature difference at final time, initial guess = 0

In order to improve the profile of optimal solution, we choose a descending curve with $G^0 = 65\%P_{max}\sin(0.5\pi(t_f - t)/t_f)$ as the initial guess for the final time of 490s. Fig.4.14a shows the optimal solution after 13 iterations, which is somewhat close to the four-stage strategy proposed by IMI. Fig.4.14b and Fig.4.14c present the final temperature distribution and the evolution of temperature difference respectively. It is found that the temperature uniformity at the final time is improved considerably: Tmax-Tmin is less than 0.8℃, due to the change of solution profile. We also note that the maximum temperature point is not located on the surface because of the heat loss by natural convection and surface radiation. In addition, the maximum temperature difference decreases with time, and the high values only exist in the solid phase region. It suggests that the surface overheating as well as the 'elephant foot' phenomenon can be effectively prevented.

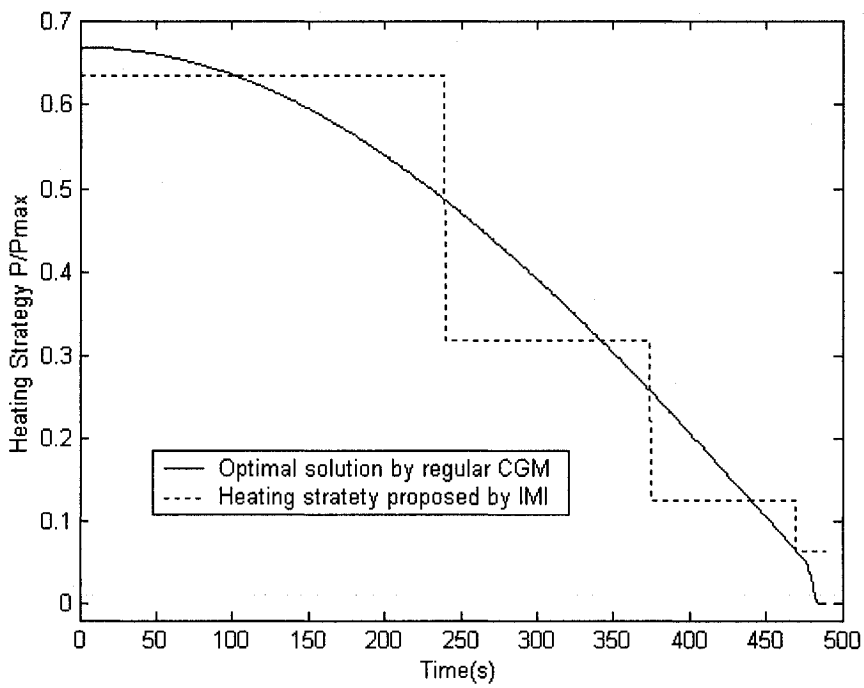

Figure 4.14a: Optimal solution by CGM, t_f= 490s, initial guess $G^0 = 65\%P_{max}\sin(0.5\pi(t_f - t)/t_f)$

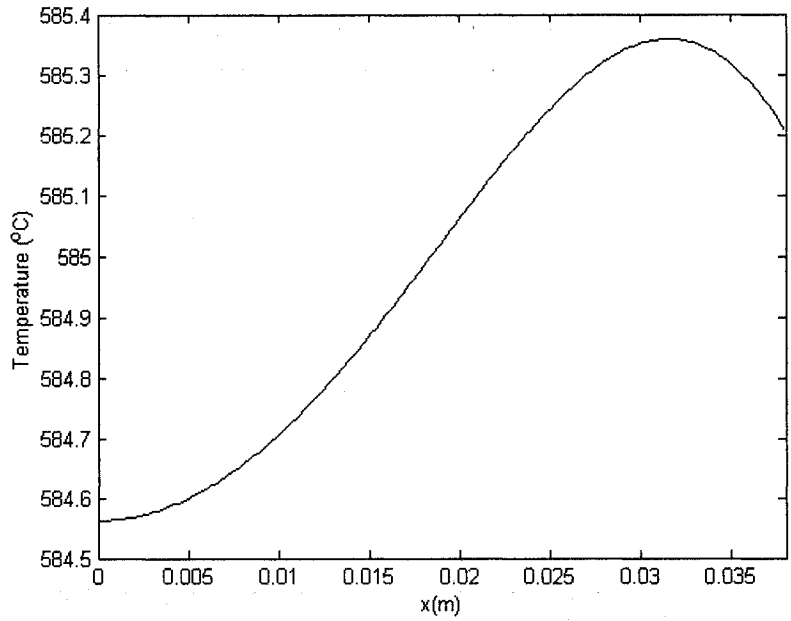

Figure 4.14b: Temperature distribution at final time, t_f= 490s, initial guess $G^0 = 65\%P_{max}\sin(0.5\pi(t_f - t)/t_f)$

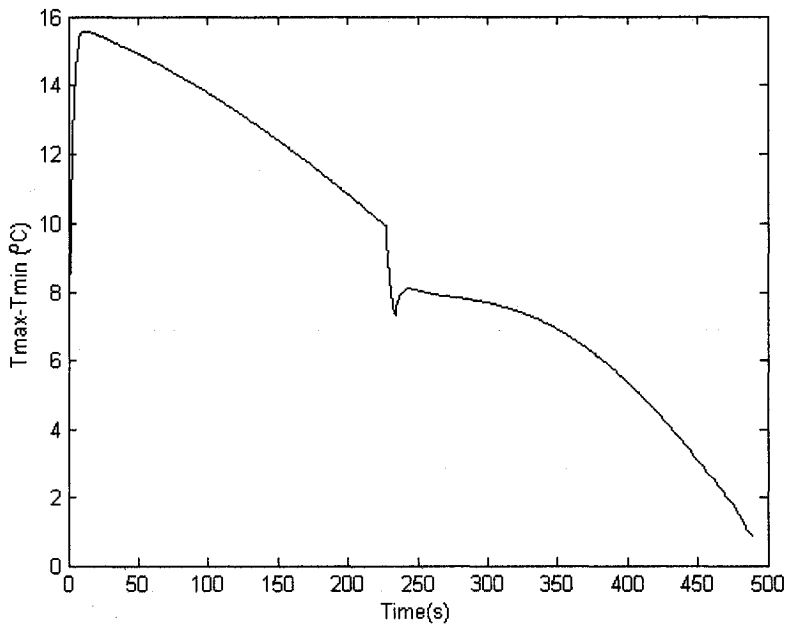

Figure 4.14c: Evolution temperature difference, t_f= 490s, initial guess $G^0 = 65\%P_{max}\sin(0.5\pi(t_f - t)/t_f)$

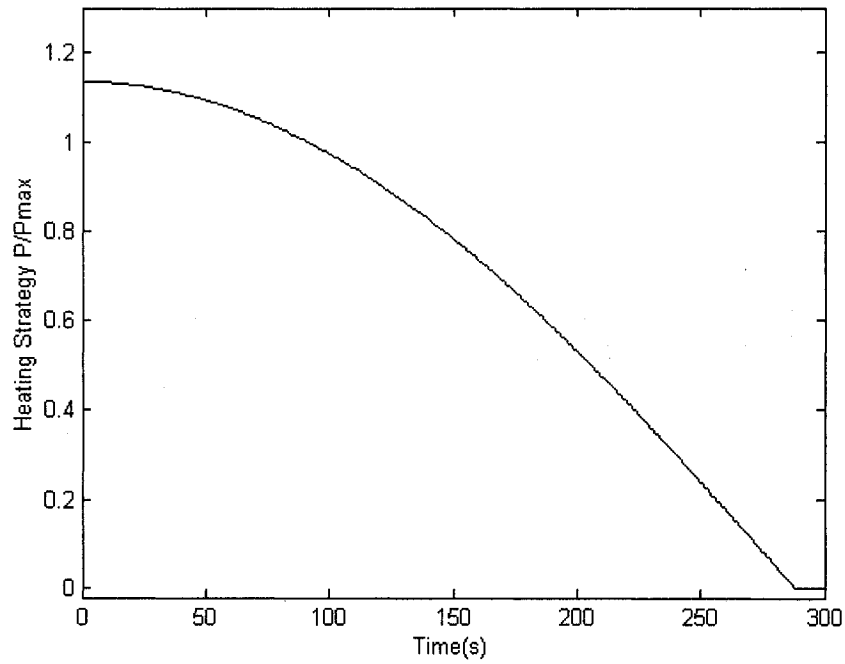

Figure 4.15: Optimal solution by CGM, t_f= 300s, initial guess $G^0 = 120\%P_{max}\sin(0.5\pi(t_f - t)/t_f)$

Considering that the heating process is required to be relatively rapid to maintain the initial globular microstructure, the total time heat treatment should be shortened further. On the other hand, the commercial manufacturing also requires that the heating process should be finished within 5 minutes. Then we have to increase the power capacity of the induction heater to compensate the shorter time. For t_f = 300s, an initial guess $G^0 = 120\%P_{max}\sin(0.5\pi(t_f - t)/t_f)$ is chosen, the corresponding solution of optimal heating control obtained after 25 iterations is presented in Fig.4.15. At the final time, the temperature uniformity is satisfactory: maximum temperature difference is less than 1.3℃.

Optimal solutions by modified CGM

As discussed previously, the modified CG method is a competitive algorithm for present heating control problem. Because that the optimal solution at t = 0 is always equal to the

initial guess value, the initial guess somehow determines the solution profile as well as the convergence of the solution. Just like the regular CGM, the zero initial guess is not a good choice, since it cannot make the error converge to an acceptable level.

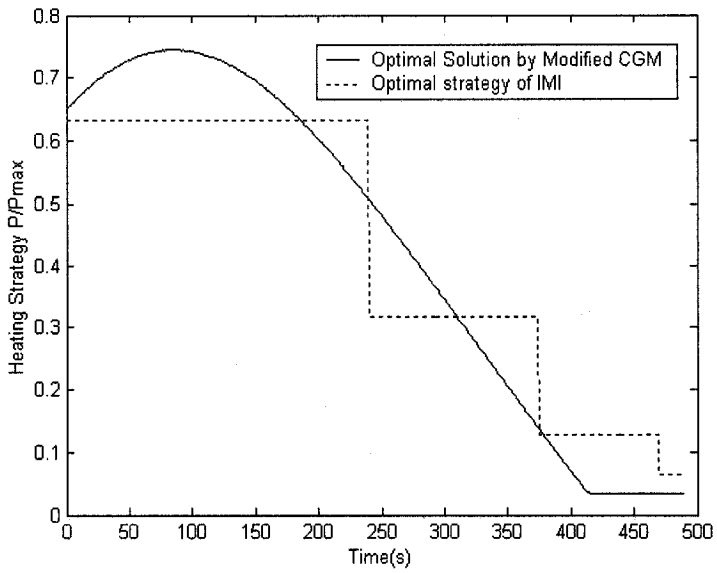

Figure 4.16a: Optimal solution by modified CGM, t_f= 490s, initial guess $G^0 = 65\%P_{max}\sin(0.5\pi(t_f - t)/t_f)$

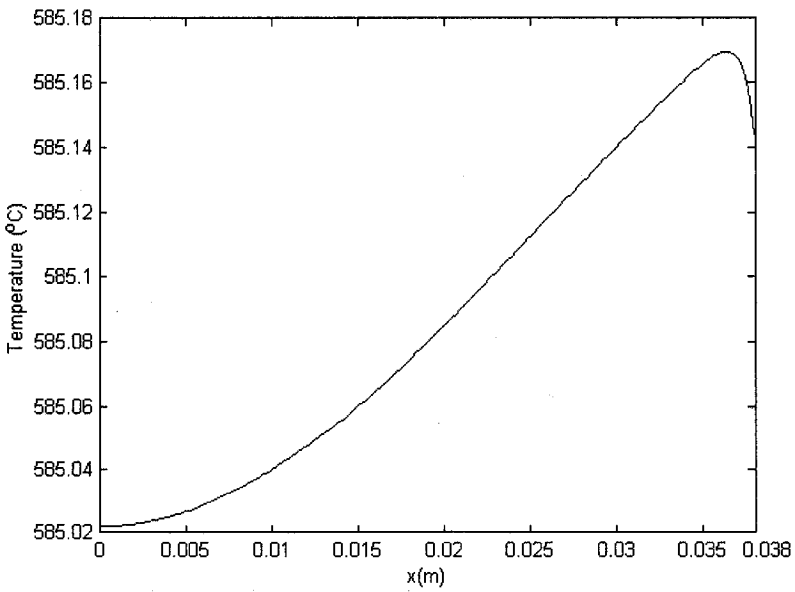

Figure 4.16b: Final temperature distribution, t_f= 490s, initial guess $G^0 = 65\%P_{max}\sin(0.5\pi(t_f - t)/t_f)$

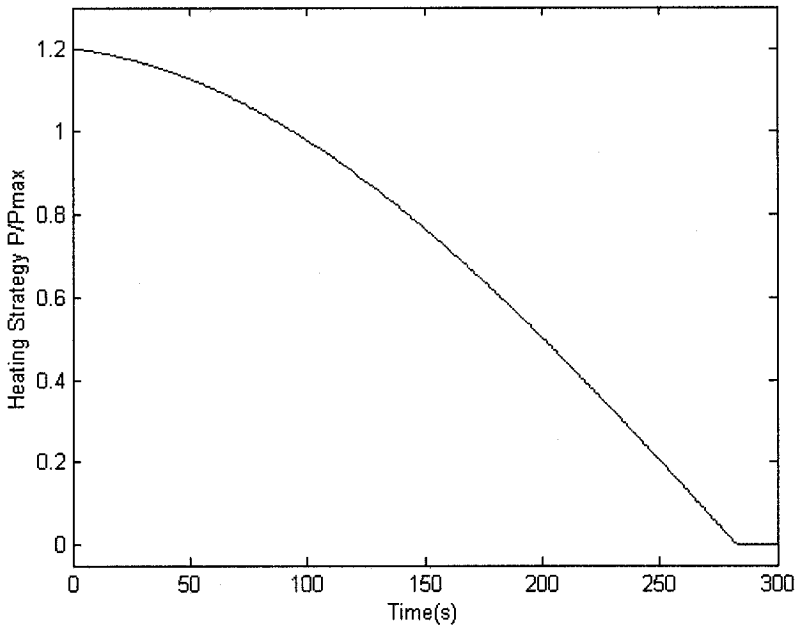

Figure 4.17: Optimal solution by modified CGM, t_f= 300s, initial guess $G^0 = 120\%P_{max}\sin(0.5\pi(t_f - t)/t_f)$

In the previous subsection, we found that a sinusoidal curve might be an ideal profile for the optimal solution. The strength of function G(t) depends on the total heating time, and can be calculated roughly based on the energy conservation ($Q = cm\Delta T$). For $t_f = 490s$ and $t_f = 300s$, we set $G^0 = 0.65P_{max}\sin\left(\frac{\pi(t_f - t)}{2t_f}\right)$ and $G^0 = 1.2P_{max}\sin\left(\frac{\pi(t_f - t)}{2t_f}\right)$ as initial guess respectively. After only 3 iterations, the optimal heating control solutions shown in Fig.4.16a and Fig.4.17 are obtained by utilizing modified CGM. Comparing with the regular CGM, the uniformity of temperature distribution at the final time is greatly improved. For t_f= 490s, the maximum temperature difference is only 0.15℃ (Fig.4.16b)! If the heating process is shortened to 300s, this parameter will increase to 1℃ but is still in satisfactory range.

Based on the above results and discussion, we may conclude that both the regular CGM

and the modified CGM might be appropriate optimization tools to achieve the accurate control of temperature uniformity for semi-solid alloy reheating.

4.7.2 Optimal Cooling Problem

On the other hand, the temperature uniformity at the final heating time also can be controlled via the surface cooling. In this section, the heating procedure is supposed to be known. We apply the CGM to estimate the optimal cooling strategy that might achieve a uniform temperature distribution at the final time. Since the cooling flux q(t) must be equal to or less than zero, this optimal cooling problem also becomes a constrained optimization problem.

4.7.2.1 Cooling in solid phase

Firstly, the heating process is limited to the solid phase region. It is assumed that a A357 alloy slug is heated in an induction unit at a constant power P(t)=56%Pmax namely 5040W, at a current frequency of 10KHz, with a targeted temperature at the final time set to 530℃. If there is no surface cooling, the temperature distribution at the final time is not uniform obviously, the maximum difference being about 12℃.

The regularization parameter ξ is first set to zero. The optimal solution obtained by CGM after 17 iterations exhibits some oscillatory behavior near the final time, although the final temperature uniformity is improved significantly: T_{max}-T_{min} is only 0.2℃. In order to reduce the oscillation, we set $\xi = 10^{-11}$. It turns out that the zeroth Tikhonov regularization might effectively eliminate the oscillatory behavior. However, its side effect is also obvious: the convergence of the solution is affected significantly, the objective error function no longer changes after 6 iterations. In other words, the temperature uniformity becomes worse, T_{max}-T_{min} at the final time increases to 2℃. In fact, those two optimal solutions with and without Tikhonov regularization are quite close to each other. It suggests that the temperature uniformity is very sensitive to the cooling flux especially in the last ten seconds. All the corresponding results are shown in Fig.4.18a and Fig.4.18b.

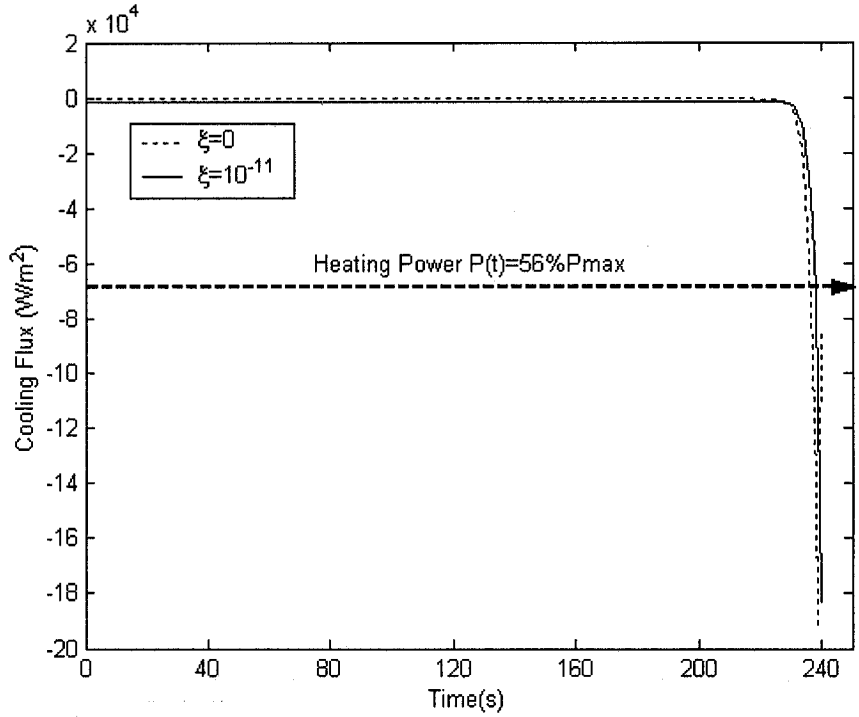

Figure 4.18a: Optimal cooling strategy, f = 10KHz, t_f = 240s

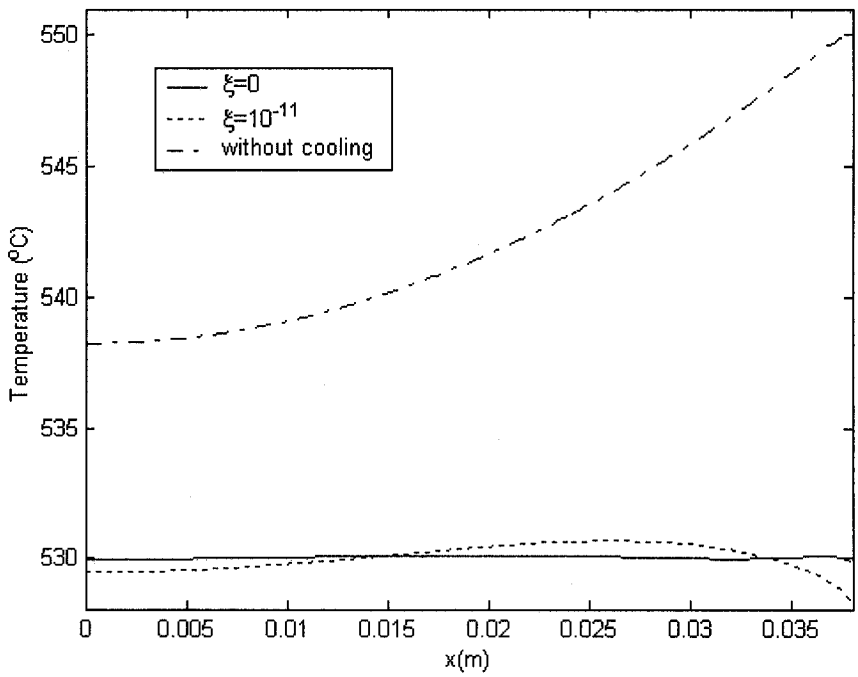

Figure 4.18b:Temperature distribution at final time, f = 10KHz, t_f = 240s

4.7.2.2 Cooling in semi-solid state

The ultimate purpose of this study is related to the optimal control for semi-solid alloy heating, and we have to face the phase change problem. Fortunately, the model of heat transfer in the mushy region described by the apparent heat capacity method has been validated in the previous section. If the A357 alloy slug is heated in an induction heater at a constant power P(t) = 50%Pmax (Pmax = 9KW, $\eta_E = 80\%$) during a period of 490s, at a working frequency of 10KHz, the temperature difference within the billet at the final time will be very high, up to 21.5℃. From Fig.4.19, it is found that the maximum temperature difference increases very fast in the last 90s. According to the discussion in 4.7.1.1, cooling the alloy surface in this period may effectively reduce the non-uniformity of the temperature. We set $q^0 = 0$ for $0 \le t < 400s$ and $q^0 = -1.2 \times 10^5 W/m^2$ for $400s \le t \le 490s$ as initial guess, after 12 iterations, the optimal solution of boundary cooling flux calculated by using CGM is presented in Fig.4.20a. It is a simple control strategy that requires cooling the material surface with a constant flux $-9.75 \times 10^4 W/m^2$ in the last 90s. At the end, the temperature distribution becomes quite uniform: the temperature difference is controlled within 0.5℃ (see Fig.4.20b). On the other hand, the continuous cooling may prevent the surface layer from overheating. This numerical experiment allows us to control the thermal uniformity by using a competitive method via surface cooling.

If the entire heating process of the A357 alloy material is required to be finished in five minutes, and the induction unit produces eighty percent of maximum power during the whole heating period, the non-uniformity of temperature distribution within the billet will become much more serious especially for the last 45 seconds in the mushy region. At the final time $t_f = 300s$, the T_{max}-T_{min} reaches 32.5℃ (see Fig.4.21). Similarly, we set an initial guess $q^0 = 0$ for $0 \le t < 245s$ and $q^0 = -3.0 \times 10^5 W/m^2$ for $255s \le t \le 300s$. After undergoing a series of iterative calculations (15 times), the conjugate gradient method provides us an optimal cooling strategy shown in Fig.4.22a

with success. From Fig.4.22b, we may see that the maximum temperature difference at the final time is significantly reduced to 1.5℃. On the other hand, we also note that some oscillations exist in the optimal solution. It augments the difficulties to execute this cooling instruction subject to the real industrial situation. Fortunately, it is not necessary to strictly follow that curve. Instead, we may impose a constant cooling flux $q(t) = -1.7 \times 10^5 \, W/m^2$ which is a time-average value of optimal solution on the surface in last 45 seconds. The influence on the temperature uniformity can be ignored: Tmax-Tmin is no more than 1.6℃ at the end of heating process.

Summarizing the discussions of this section, we may conclude that a uniformly targeted temperature might be achieved by controlling the input power of the induction unit directly or cooling the surface with proper flux in the appropriate period. In principle, these two methods are equivalent to each other. For the former, an induction unit of greater power capacity is essential; for the latter, more electrical energy must be consumed to compensate the surface cooling.

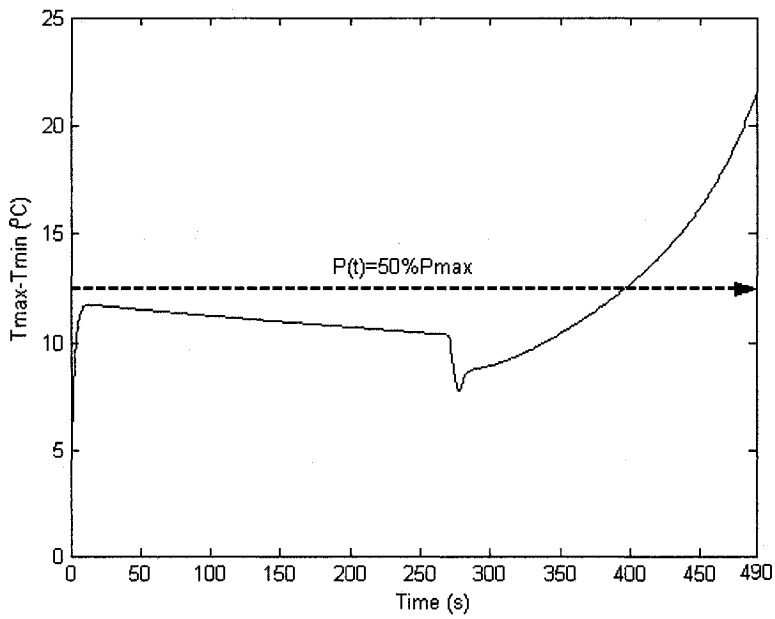

Figure 4.19: Evolution of temperature difference, P(t) = 50%Pmax, t_f= 490s

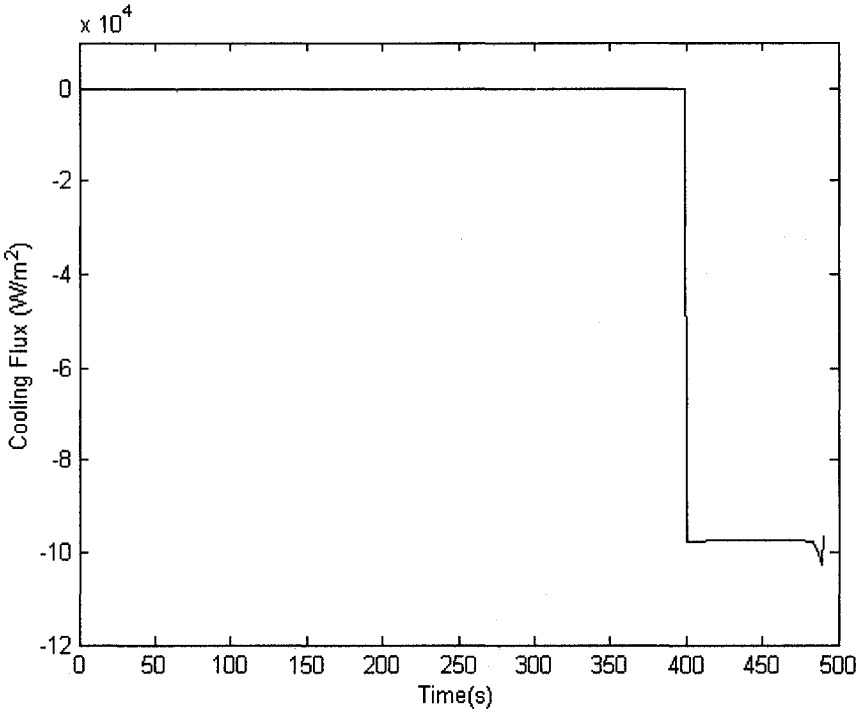

Figure 4.20a: Optimal cooling strategy, P(t) = 50%Pmax, t_f= 490s

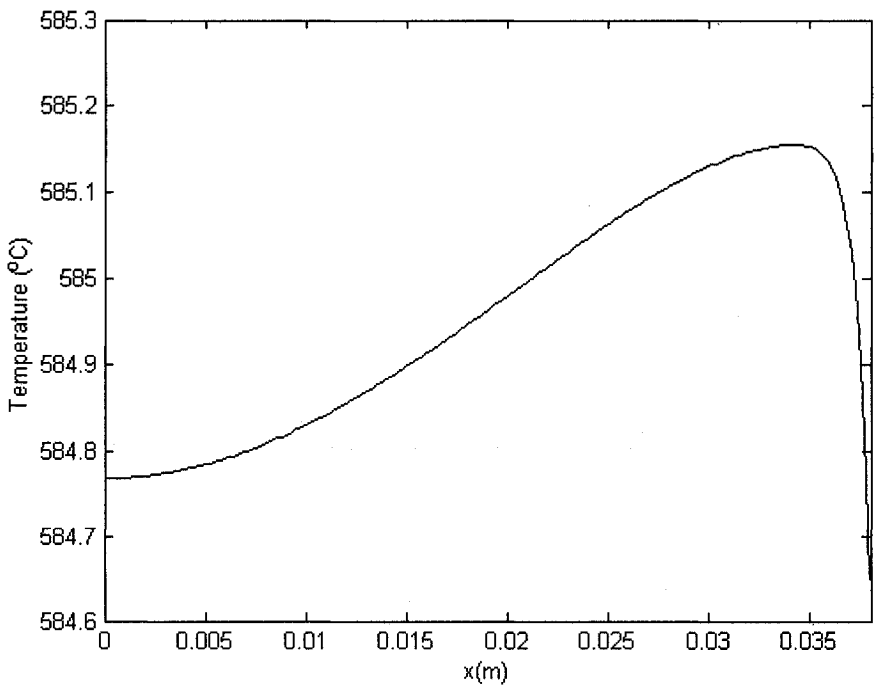

Figure 4.20b: Temperature distribution at the final time, t_f= 490s, P(t) = 50%Pmax

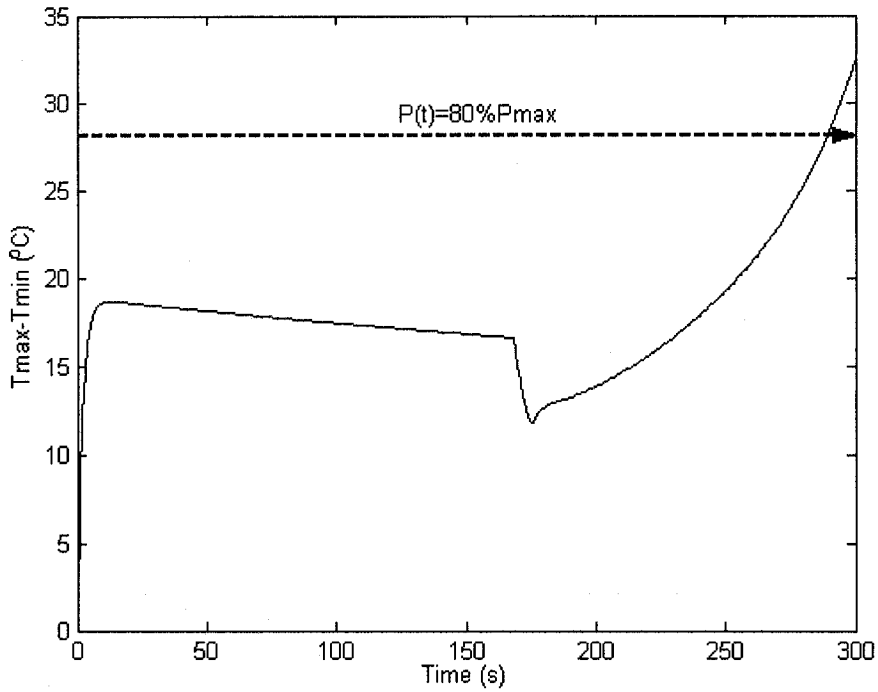

Figure 4.21: Evolution of temperature difference, P(t) = 80%Pmax, t_f= 300s

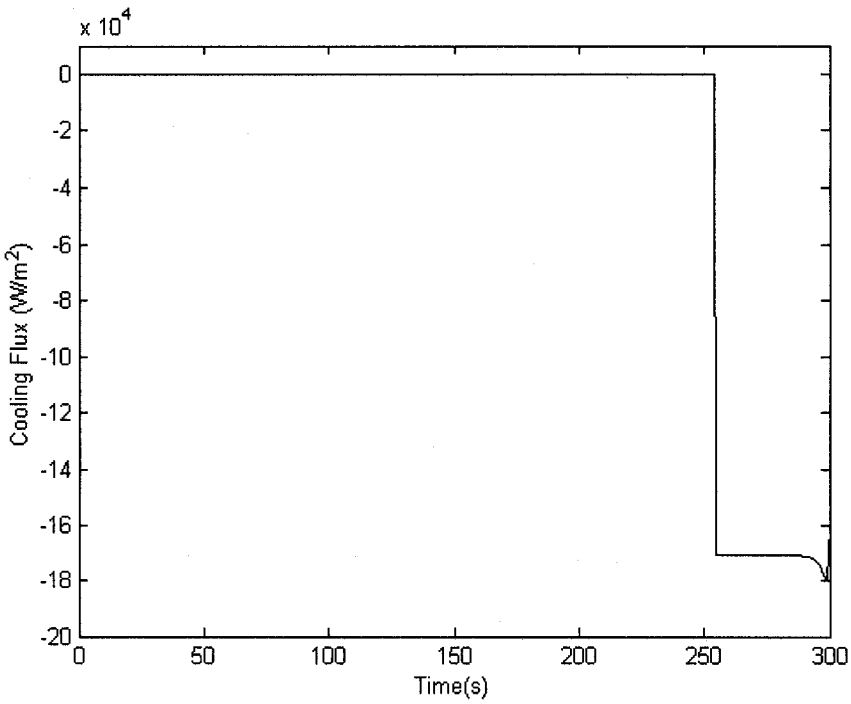

Figure 4.22a: Optimal cooling strategy, P(t) = 80%Pmax, t_f= 300s

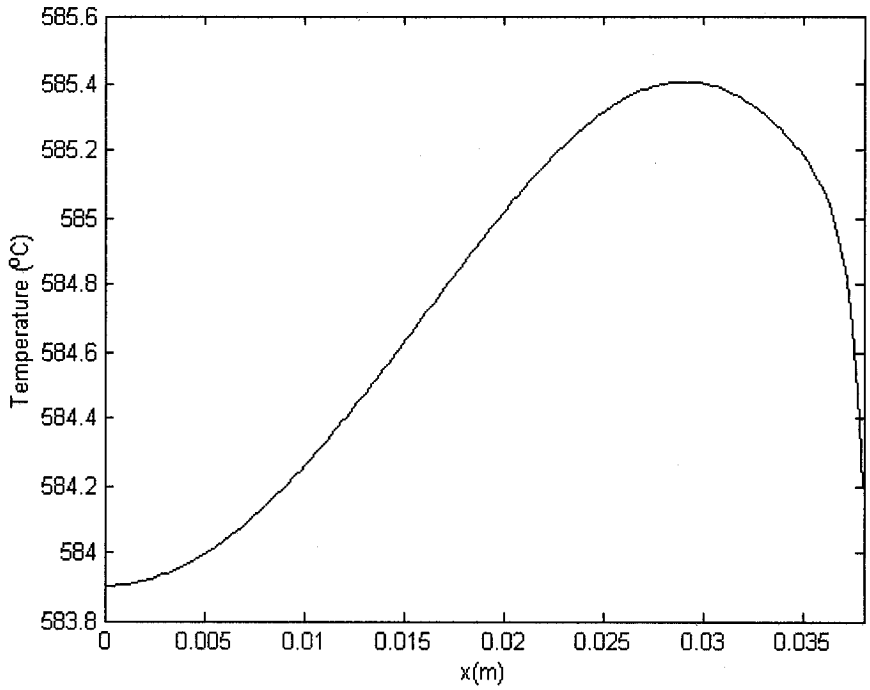

Figure 4.22b: Temperature distribution at the final time, t_f= 300s, P(t) = 80%Pmax

CONCLUSION

The objective of this research is to develop a numerical algorithm to produce optimal heating control strategies for semi-solid alloy forming to achieve a final temperature distribution within the cylinder of metal alloy as uniform as possible by utilizing inverse techniques.

This optimal control problem is essentially an inverse heat transfer problem of the second kind. We start our research by revealing the essential character of this kind of inverse problem by studying a boundary condition problem. It comes out of the present investigation that a continuous boundary heat flux can be recovered from the final temperature distribution only for a non-dimensional final time of the order of 0.1. Both singular value decomposition (SVD) and conjugate gradient (CG) methods might be used to solve this IHCP of the second kind. The SVD method yields better results and requires less computational time. For longer intervals, the conjugate gradient solution is not uniformly valid, unless the flux has a rather specific form. A time-averaging effect is then present. The problem becomes more severely ill-posed as the final time increases, which has been confirmed by the analysis of discrete Picard condition and the singular value decomposition. If the boundary flux is known at $t = 0$, however, a modified conjugate gradient method may be profitably used to reconstruct the heat flux over significantly longer periods of time, as long as the profile is monotonous or has only one or two minima/maxima. If some random noise is present in the temperature measurements, the Tikhonov regularization appears effective to stabilize the inverse solutions obtained by conjugate gradient or singular value decomposition when the regularization parameter is determined according to the L-curve criterion.

The study then goes on further in Chapter II. A formulation of the two-dimensional inverse convection problem of the second kind in a porous medium is presented, leading to an iterative solution algorithm by conjugate gradient with adjoint equations, that is

valid for an arbitrary geometry of the domain. The computations for the determination of unknown boundary heat fluxes from the final temperature distribution are performed in a square cavity. The present method is able to predict steady, non-uniform heat fluxes imposed on the active boundary for Rayleigh numbers up to 1000. For time-dependent profiles, numerous iterations must be expected. The sensitivity of the method drops off significantly for long heating periods, as the final temperature field no longer depends on the earlier part of the flux history. Reasonable solutions may be obtained for a non-dimensional time interval of the order of 0.1, beyond which the inverse solution has a tendency to level off to an average value. Results from noisy input data may be regularized effectively by the CG algorithm and the discrepancy principle.

In order to finally solve the induction heating control problem, we have to first estimate the heat source distribution within the material. It is known that the induction heater may induce an exponential distribution of power density (heat source) along the radius of the cylindrical billet. In general, the heat source is hard to measure with satisfactory accuracy, especially for exponential profiles. However, the temperature measurement is relatively easy to perform by using thermocouples, infrared imaging thermometers or other devices. The source term distribution can be calculated from semi-empirical formula. In Chapter III, however, we determine it by utilizing inverse techniques instead. The conjugate gradient method is applied to recover the heat source distribution in two ways: (1) measure and record the surface temperature history of the material; (2) measure the temperature distribution within the billet at the final time. For exponential profiles, the heat source distributions can be recovered precisely by adopting method (1) even if the temperature measurements contain a relative error up to 5%, but the total experimental time must be limited to 5 seconds; however the reconstructed solutions may not be reliable for non-exponential profiles. On the other hand, the method (2) is adaptable to an arbitrary profile of source term, but hundreds of iterative calculations may be required. In addition, method (2) is much more sensitive to the error contained in the input data, even a low noise level might make the reconstructed solutions deviate

from the exact data depending on the profiles. In general, the relative error of measurements is required to be limited to less than 1%.

In the last chapter, we construct a physical as well as a mathematical model by virtue of the apparent heat capacity method to simulate the induction heating process especially in semi-solid state. The temperature-dependent thermo-physical properties are taken into account, radiative and convective heat losses are also included in the system. This model is proved to be reasonable by comparison of the numerical solutions with experimental data both in solid region and in mushy region. An optimization approach based on the CGM is applied to solve the optimal heating/cooling problem of semi-solid metal forming. The optimal heating strategies estimated by regular CGM achieve more uniform temperature distributions at the final time than the empirical heating methods based on experiments. A modified CGM might be better suited to solve this optimal control problem, because less iterative calculations are needed and better temperature uniformity can be achieved. Furthermore, the smoother heating evolution is much easier to realize in an engineering context. However, a larger power capacity of the induction unit might be required. The optimization of semi-solid alloy heating is more difficult than heating within the solid phase, because that the non-uniformity of temperature in mushy region is much more serious: the maximum temperature difference can be twice of that in the solid phase if a one-stage heating strategy is adopted. The numerical experiments suggest that a monotonously decreasing sinusoid might be an ideal heating profile to achieve the temperature uniformity at the end of heat treatment.

On the other hand, once the heating procedure is fixed, an optimal surface cooling strategy can also be obtained by CGM to eliminate the thermal gradients and the non-uniformities within the final temperature distribution. The surface cooling may result in an equivalent effect as the heating strategy does, but it might be much simpler: just cool the surface with a constant flux in the last dozens of seconds depending on the total time of heat treatment and the beginning time of melting.

In principle, the optimal control problem of induction heating for semi-solid forming has been basically solved. Although only a specific material, size, and current frequency is considered, the mathematical model and optimization algorithm developed in this thesis are adaptable to any kind of metal alloys with any dimensions heated at any frequency.

Based on the present works, we have the following recommendations for the research in the future:

1) All the heating/cooling strategies obtained by optimization algorithm should be validated by experiments;
2) The physical model should be developed further to describe the electromagnetic end effect and/or transverse edgy effect, and the mathematical model should be extended to two-dimensional and/or three-dimensional systems accordingly;
3) Considering the possible bias between the numerical results and real data, a PID unit might be embedded in the control system to modify the predicted heating/cooling strategies.

REFERENCES

1. SPENCER, D.B., MEHRABIAN, R., FLEMINGS, M.C. 1972. «Rheological behavior of Sn-15 Pct Pb in the crystallization range». *Metallurgical. Trans.* 3. 1925-1632.

2. FLEMINGS, M.C., MEHRABIAN, R., and RIEK, R.G. 1975. «Continuous process for forming an alloy containing non-dentritic primary solids». US Patent No.3, 902,544, 1975.

3. FLEMINGS, M.C., MEHRABIAN, R., and SPENCER, D.B. 1976. «Composition and methods for preparing liquid-solid alloys for casting and casting methods employing the liquid-solid alloys». US Patent No.3, 948,650, 1976.

4. FLEMINGS, M.C. 1991. «Behavior of metal alloys in the semi-solid state». *Metall. Trans.* A22. 957-981.

5. YOUNG, K.P. 1995. «SSM casting process: applications and case stories in aluminum and magnesium». *Proc. Conf. on North American Die Casting.* Rosemont, IL: North American Die Casting Association. P.403-410.

6. YOUNG, K.P. 1996. «Recent advances in semi-solid metal (SSM) cast aluminum and magnesium components». *Proc. 4th Int. Conf. on Semi-Solid Processing of Alloys and Composites.* Sheffield: University of Sheffield. P.229-233.

7. LASDAY, S.B. 1995. «Advancements in semi-solid metal processing through modeling and computerized induction heating system». *Industrial Heating.* 28-31.

8. NUSSBAUM, A.I. 1996. «Semi-solid forming of aluminum and magnesium». *Light metal age.* 6-22.

9. BOYLAN, J. 1997. «Semi-solid formed aluminum». *Adv. Mater. Process*. 10. 27-28.

10. MIDSON, S., BRISSING, K. 1997. «Semi-solid casting of aluminum alloys: a status report». *Modern casting*. 41-43.

11. JUNG, H. K., KANG, C.G. 2002. «Induction heating process of an Al-Si aluminum alloy for semi-solid die casting and its resulting microstructure». *Journal of materials processing technology*. 120. 355-364.

12. ONO, Y., ZHENG, C.Q., HAMEL, F.G., CHARRON, R. and LOONG, C.A. 2002. «Experimental investigation on monitoring and control of induction heating process for semi-solid alloys using the heating coil as sensor». *Measurement science and technology*. 13. 1359-1365.

13. KO, D-C, MIN, G-S, KIM, B-M, and CHOI, J-C. 2000. «Finite element analysis for the semi-solid state forming of aluminum alloy considering induction heating». *Journal of materials processing technology*. 100. 95-104.

14. SHEHATA, M.T., KAO, V., ESSADIQI, E., LOONG, C.A. and ZHENG, C-Q. 2002. «Production and die casting of semi-solid magnesium alloy AZ91D». *Light Metals for the Automotive Industry*. Warrendale, PA: Society of Automotive Engineers. P.73-78.

15. NGUYEN, K.T., BENDADA, A. 2000. «An inverse approach for the prediction of the temperature evolution during induction heating of a semi-solid casting billet». *Modeling Simul. Mater. Sci. Eng*. 8. 857-870.

16. MIDSON, S., RUDNEV, V. and GALLIK, R. 1999. «Semi-solid processing of aluminum alloys». *Industrial heating*. 37-41.

17. MIDSON, S., RUDNEV, V. and GALLIK, R. 1998. «The induction heating of semi-solid aluminum alloy». *Proc. 5th Int. Conference on Semi-Solid Processing of Alloys and Composites*. Golden, CO. P.497-504.

18. RUDNEV, V.I. and COOK, R.L. 1995. «Bar end heating». *Forging magazine*. 27-30.

19. NEMKOV, V.S., DEMIDOVICH, V.B., RUDNEV, V.I., and FISHMAN, O. 1992. «The use of end and edge effects for induction heater design». *Proc. of ElectroheatCongress "Electrotech 92"*. Montreal. P.180-188.

20. BENDADA, A., NGUYEN, K.T. and LOONG, C.A. 1999. «Application of infrared imaging in optimizing the induction heating of semi-solid aluminum alloys». *Proc. Int. Symp. On Advanced Sensors for Metals Processing*. Quebec. P.331-342.

21. KAPRANOS, P., GIBSON, R.C., KIRKWOOD, D.H., and SELLARS, C.M. 1996. «Induction heating and partial melting of high melting point thixoformable alloys». *Proc. 4th Int. Conf. on Semi-Solid Processing of Alloys and Composites*. Sheffield: University of Sheffield. P.148-152.

22. KELLER, J. B. 1976. «Inverse problems». *Amer. Math. Monthly*. 83. 107-118.

23. HEINZ, W.E., HANKE, M. and NEUBAUER, A. 1996. *Regularization of Inverse Problems*. Dordrecht: Kluwer Academic Publishers.

24. ALIFANOV, O.M. 1994. *Inverse Heat Transfer Problems*. New York: Springer-Verlag.

25. HADAMARD, J. 1923. *Lecture on Cauchy's Problem in Linear Partial Differential Equations*. New Haven: Yale University Press.

26. HENSEL, E. 1991. *Inverse Theory and Applications for Engineers*. Upper Saddle River: Prentice Hall.

27. TAYLOR, J. and ZIMA, W. 1999. «Solution of inverse heat conduction problems using control volume approach». *Int. J. Heat Mass Transfer*. 42. 1123-1140.

28. YANG, C.Y. 1998. «Solving the two-dimensional inverse heat source problem through the linear least-squares error method». *Int. J. Heat Mass Transfer*. 41:2. 393-398.

29. TARANTOLA, A. and VALETTE, B. 1982. «Generalized Nonlinear Inverse Problems Solved Using the Least-Squares Criterion». *Reviews of Geophysics and Space Physics*. 20:2. 219-232.

30. TIKHONOV, A.N. 1977. *Solution of Ill-Posed Problems*. Halsterd Press.

31. RAMOS, F. and GIOVANNINI, A. 1995. «Resolution of multimentional heat diffusive inverse problem by analytical elements method and principle of maximum entropy». *Int. J. Heat and Mass Transfer*. 38:1. 101-111.

32. HANSEN, P.C. 1994. «Regularization tools for analysis and solution of discrete ill-posed problems». *Numerical Algorithms*. 6. 1-35.

33. BECK, J.V., BLACKWELL and CLAIR, S. 1985. *Inverse Heat Conduction: Ill-posed Problems*. New York: John Wiley and Sons.

34. STOLTZ, G. Jr. 1960. «Numerical solutions to an inverse problem of heat conduction for simple shapes». *Journal of Heat Transfer*. 82. 20-26.

35. MURIO, D. A. 1993. *The Mollification Method and the Numerical Solution of Ill-Posed Problems*. New York: John Wiley and Sons.

36. MARTIN, T. J. and DULIKRAVICH, G. S. 1995. «Finding unknown surface temperatures and heat fluxes in steady heat conduction». *IEEE Transactions on Components, Packaging and Manufacturing Technology*. (CPMT)-Part A. 18:3. 540-545.

37. WOODBURY, K.A. 2003. *Inverse Engineering Handbook*. Boca Raton: CRC Press.

38. KEILIS-BOROK, V.J. and YANOVSKAYA, T.B. 1967. «Inverse problems in seismology (structural review) ». *Geophys. J. R. Astr. Soc.* 13. 223-234.

39. BACKUS, G. and GILBERT, F. 1967. «Numerical applicaton of a formalism for geophysical inverse problem». *Geophys. J. R. Astr. Soc.* 13. 247-276.

40. BACKUS, G. and GILBERT, F. 1968. «The resolving power of gross Earth data». Geophys. J. R. Astr. Soc. 16. 169-205.

41. BACKUS, G. and GILBERT, F. 1970. «Uniqueness in the inversion of inaccurate gross Earth data». *Philos. Trans. R. Soc.* London. 266. 123-192.

42. MOSEGAARD, K. and TARANTOLA, A. 1995. «Monte Carlo sampling of solutions to inverse problems». *J. Geophys. Res.* 100:B7. 12,431-12,447.

43. MOSEGAARD, K. and TARANTOLA, A. 2002. «Probabilistic Approach to Inverse Problems». *International Handbook of Earthquake & Engineering Seismology*. Part A. Academic Press. P. 237-265.

44. TARANTOLA, A. 1987. *Inverse Problem Theory*. New York: Elsevier.

45. HAJI-SHEIKH, A. and BUCKINGHAM, F.P. 1993. «Multidimensional inverse heat conduction using the Monte Carlo method». *ASME J. Heat Transfer*. 115:1. 26-33.

46. GANESA-PILLAI, M. and HAJI-SHEIKH, A. 1998. «Global Estimation of heat transfer in spray cooling using inverse heat conduction». *Proceedings of the 11th International Symposium on Transport Phenomena*. G. J. Hwang, Ed. P.467-473.

47. HAJI-SHEIKH, A. 2003. «Inverse heat conduction using Monte Carlo method». *Inverse Engineering Handbook*. Boca Raton: CRC Press.

48. NGUYEN, T.H. and ZHANG, X.L. 1995. «Back to the Initial State of Convection: A Retrospective Heat Transfer Problem».

49. JIANG, H., NGUYEN, T. H. and PRUD'HOMME, M. 2005. *Inverse Unsteady Heat Conduction Problem of Second Kind.* [Online].Montréal: Ecole Polytechnique de Montréal. 40p. EPM-RT-2005-06.
http://www.polymtl.ca/biblio/epmrt/rapports/rt2005-06.pdf

50. LEZIUS, R. and TRÖLTZSCH, F. 1996. «Theoretical and numerical aspects of controlled cooling of steel profiles». *Progress in Industrial Mathematics at ECMI 94*. Wiley-Tenbner. P.380-388.

51. NGUYEN, T.H., ZHENG, C-Q and LOONG, C.A. 2001. «Induction heating of semi-solid aluminum and magnesium alloys». *2nd International Conference on Computational Heat and Mass Transfer*. Rio de Janeiro, Brazil.

52. CHU, H-S. 2003. «Temperature uniformity of 12-inch silicon wafer during rapid thermal processing». *Journal of the Chinese Society of Mechanical Engineers*. 24:4. 391-406.

53. BUTKOVSKII, A.G. and LERNER, A.Y. 1960. «The optimal control systems with distributed parameter». *Auto. Remote Control*. 21. 472-477.

54. SAKAWA, Y. 1964. «Solution of an optimal control problem in a distributed-parameter system». *IEEE Trans. Auto. Contr.* AC-9:4. 420-426.

55. SAKAWA, Y. 1966. «Optimal control of a certain type of linear distributed-parameter system». *IEEE Trans. Auto. Contr.* AC-11:1. 35-41.

56. CAVIN, R.K. and TANDON, S.C. 1977. «Distributed parameter system optimum control design via finite element discretization». *Automatica*. 13. 611-614.

57. MERIC, R.A. 1979. «Finite element analysis of optimal heating of a slab with temperature dependent thermal conductivity». *Int. Journal Heat and Mass Transfer*. 22. 1347-1353.

58. MERIC, R.A. 1979. «Finite element and conjugate gradient methods for a nonlinear optimal heat transfer control problem». *Int. J. Numer. Meth. Eng.* 14. 1851-1863.

59. KELLEY, C.T. and SACHS, E. W. 1999. «A trust region method for parabolic boundary control problems». *SIAM J. Optimization.* 9:4. 1064-1081.

60. C.H. 2001. «A nonlinear optimal control problem in determining the strength of the optimal boundary heat fluxes». *Numerical Heat Transfer.* Part B. 40. 411-429.

61. HUANG, C.H. and LI, C.Y. 2003. «A three-dimensional optimal control problem in determining the boundary control heat fluxes». *Heat and Mass Transfer.* 39. 589-598.

62. KRENGEL, R., STANDKE, R., TRÖLTZSCH, F. and WEHAGE, H. 1996. *Mathematisches Modell Einer Optimal Gesteuerten Abkühlung von Profilstählen in Kühlstrecken.* Preprint 98-6, TU Chemnitz:Fakultät für Mathematik.

63. TRÖLTZSCH, F. and UNGER, A. 2001. «Fast solution of optimal control problems in the selective cooling of steel». *ZAMM.* 81. 447-456.

64. LANDL, G. and ENGL, H.W. 1995. «Optimization strategies for the cooling of steel strips in hot strip mills». *Inverse Problems in Engineering.* 2. 102-118.

65. ENGL, H.W., LANGTHALER, T. and MANSELLIO, P. 1987. «An inverse problem for a nonlinear heat equation connected with continuous casting of steel». *Optimal Control of Partial Differential Equations.* 67-90.

66. GREVER, W. 1998. «A nonlinear parabolic initial boundary value problem modeling the continuous casting of steel». *ZAMM.* 78-119.

67. LEIBFRITZ, F. and SACHS, E.W. 1994. «Numerical solution of parabolic state constraint control problems using SQP and interior-point-methods». *Large Scale Optimization*. Dordrecht: Kluwer Academic Publishers B.V. 245-258.

68. BENDADA, A., ZHENG, C.Q. and NARDINI, N. 2004. «Investigation of temperature control parameters for inductively heated semi-solid light alloys using infrared imaging and inverse heat conduction». *J. Phys. D: Applied Physics*. 37. 1137-1144.

69. KIM, Y.H., CHOI, J.C., YOON, J.M. and PARK, J.H. 2002. «A study of the optimu reheating process for A356 alloy in semi-solid forging». *Int. J. Adv. Manuf. Technol.* 20. 277-283.

70. JUNG, H.K. and KANG, C.G. 2002. «Induction heating process of an Al-Si aluminum alloy for semi-solid die casting and its resulting microstructure». *Journal of Materials Processing Technology*. 120. 355-364.

71. KANG, C.G., YOUN, S.W. and SEO, P.K. 2005. «Data base construction on mechanical properties of thixoforged aluminum parts and their microstructure evaluation». *Journal of Materials Processing Technology*. 159. 330-337.

72. JAMES, M. H. and DEWYNNE, N. D. 1986. *Heat Conduction*. Oxford London Edinburgh: Blackwell Science Publications.

73. HOFMANN, B. 1986. *Regularization for Applied Inverse and Ill-Posed Problems*. Stuttgart, German: Teubner.

74. HANSON, P.C. 1998. *Rank-Deficient and Discrete Ill-Posed Problems: Numerical Aspects of Linear Inversion*. Philadelphia: SIAM.

75. ALIFANOV, O.M. and MIKHAILOV, V.V. 1978. «Solution of the nonlinear inverse thermal conductivity problem by the iteration method». *Journal of Engineering Physics*. 35. 1501-1506.

76. HUANG, C.H. and ÖZISIK, M.N. 1992. «Inverse problem of determining unknown wall heat flux in laminar flow through a parallel plate duct». *Numerical Heat Transfer*. Part A. 21. 55-70.

77. PARK, H. M. and CHUNG, O. Y. 1999. «An Inverse Natural Convection Problem of Estimating the Strength of a Heat Source». *Int. J. Heat Mass Transfer*. 42. 4259-4273.

78. PARK, H. M. and JUNG, W.S. 2001. «The Karhunen-Loève Galerkin method for the inverse natural convection problems». *Int. J. Heat Mass Transfer*. 44. 155-167.

79. HANSON, P.C. 1992. «Analysis of ill-posed problems by means of L-curve». SIAM Review. 34:4. 561-580.

80. YAGOLA, A.G., LEONOV, A.S. and TITARENKO, V.N. 2002. «Data errors and an error estimation for ill-posed problems». *Inverse Problems in Engineering*. 10:2. 117-129.

81. JIANG, H., NGUYEN, T. H. and PRUD'HOMME, M. 2005. «Control of the boundary heat flux during the heating process of a solid material». *International Communications in Heat and Mass Transfer*. 32:6. 728-738.

82. ORFEUIL, M. 1987. «Electric Process Heating: Technologies, Equipment, Applications». Columbus, Ohio: Battelle Press.

83. MORGAN, K., LEWIS, R.W. and ZIENKIEWICZ, O.C. 1978. «An improved algorithm for heat conduction problems with phase change». *International Journal for Numerical Methods in Engineering*. 12. 1191-1195.

84. SALCUDEAN, M. and ABDULLAH, Z. 1988. «On the numerical modeling of heat transfer during solidification processes». *International Journal for Numerical Methods in Engineering*. 25. 445-473.

85. YAO, M. and CHAIT, A. 1993. «An alternative formulation of the apparent heat capacity method for phase-change problems». *Numerical Heat Transfer, Part B*. 24. 279-300.

86. CIVAN, F. and SLIEPCEVICH, C.M. 1987. «Limitation in the apparent heat capacity formulation for heat transfer with phase change». *Proc. Okla. Acad. Sci.* 67. 83-88.

87. HASHEMI, H.T. and SLIEPCEVICH, C.M. 1967. «Heat transfer with change of phase». *Chem. Eng. Progr., Symp.* 63:79. 34-41.